Fall 12-6-2019

Improving Aquifer Characterization through Integration of Airborne Electromagnetics (AEM) and Well Hydrographs

Jacqueline Polashek
University of Nebraska - Lincoln, jamipolashek@gmail.com

IMPROVING AQUIFER CHARACTERIZATION THROUGH INTEGRATION OF AIRBORNE ELECTROMAGNETICS (AEM) AND WELL HYDROGRAPHS

by

Jacqueline Polashek

A THESIS

Presented to the Faculty of

The Graduate College at the University of Nebraska

In Partial Fulfillment of Requirements

For the Degree of Master of Science

Major: Natural Resource Sciences

Under the Supervision of Professor Jesse Korus

Lincoln, Nebraska

November, 2019

IMPROVING AQUIFER CHARACTERIZATION THROUGH INTEGRATION OF AIRBORNE ELECTROMAGNETICS (AEM) AND WELL HYDROGRAPHS

Jacqueline Polashek, M.S.

University of Nebraska, 2019

Advisor: Jesse Korus

The objective of this study is to evaluate methods of hydrostratigraphic modeling using geophysics and well hydrographs at the eastern edge of the High Plains aquifer (HPA) in Platte and Colfax counties within Nebraska, USA. The HPA is very heterogeneous in the study area, being hosted by architecturally complex glacial sediments and having many irregular hydraulic boundaries. Further, the HPA exhibits local variations between unconfined and confined conditions. Pumping in such bounded aquifers can be unsustainable because of cost increases and lost agricultural productivity. Moreover, the large drawdowns typical of confined aquifers can contribute to well interference during heavy pumping. Mapping the HPA accurately at small (10's of km^2) to medium (100's of km^2) scales is vital to sustainable management.

AEM modeling and well hydrograph interpretation methods were used to characterize the aquifer in the study area. A 2016 airborne electromagnetic (AEM) survey mapped the electrical resistivity of subsurface strata to depths of 300 m. This data was used in the present study to create 3D hydrostratigraphic models using cognitive-layer modeling and voxel-based geostatistical modeling approaches, both with their own advantages and disadvantages. Water-level hydrographs from piezometers near irrigated fields provide the basis for aquifer characterization at each site and for assessing the accuracy of the two AEM modeling approaches, which are applied commonly in

Nebraska and elsewhere. The temporal pattern of water-level drawdown indicated possible boundaries and confinement. The existence of background displacement, size of displacement, and responses of nearby wells led to aquifer interpretations. Little correlation existed between the hydrograph interpretations and both of the modeling approaches, but the voxel model did show boundaries near many of the irrigation wells with bounded hydrograph signatures.

Overall, the simple modeling approaches failed to adequately convert resistivity to accurate interpretations of subsurface stratigraphy, rendering both types of hydrostratigraphic models largely invalid here. Nevertheless, the results of this study lead to important future work recommendations: (1) modeling and quantifying uncertainty using more sophisticated methods, (2) applying different modeling approaches in different areas to fit hydrologic data, and (3) using hydrograph data and pumping tests to validate the results of hydrostratigraphic modeling.

DEDICATION

This thesis is dedicated to:

My mother and my father, who are my constant sources of all kinds of support. Their own experiences with obtaining their Master's degrees enabled them to have a high level of empathy and advice that is very much appreciated.

My friends/colleagues who have offered input with technical writing, presentations, coursework, and advice and accountability in regards to wellness while in graduate school.

AUTHOR'S ACKNOWLEDGEMENTS

I would like to express appreciation to my advisor Professor Jesse Korus, who has helped improve my research and writing skills throughout my program. His guidance with coursework, software usage and project formulation was invaluable to this thesis. I thank my committee members, Professors Troy Gilmore and Matt Joeckel, for their support in this research and multidisciplinary point of views.

I received assistance with data collection from Lower Platte North Natural Resources District and from research assistants. I'd like to thank Daryl Anderson and Russell Oaklund at Lower Platte North NRD for their help in the study area. Another thank you to Levi McKercher and Amber Fertig, who aided in gathering other existing data for this project.

This thesis would not have been possible without the financial assistance of the following:

1. Graduate student support from the Daugherty Water for Food Global Institute
2. A grant from the Water Sustainability Fund, administered by the Lower Platte South Natural Resources District
3. Funding from the Nebraska Department of Natural Resources

TABLE OF CONTENTS Page #

CHAPTER 1. INTRODUCTION

1.1 OVERVIEW

Groundwater is a natural resource that provides drinking water, irrigation for farming, and flow to many streams upon which humans and ecosystems depend. The extent and availability of groundwater varies around the world (Driscoll, 1986), and in many areas, demand exceeds supply (Steward et al., 2013). Irrigation accounts for 90% of global consumptive water uses and therefore contributes greatly to imbalances between water supply and water demand (Siebert et al., 2010; Steward et al., 2013). The variability of supplies and demands from competing uses makes aquifer exploration, mapping, and characterization paramount to managing groundwater and preserving its quality and quantity for future generations.

The inadequate or incorrect characterization of an aquifer can lead to a variety of problems. Overestimation of the groundwater supply (Famiglietti, 2014; Fienen & Arshad, 2016), coupled with unregulated pumping (Aeschbach-Hertig & Gleeson, 2012; Famiglietti, 2014; Fienen & Arshad, 2016; B. R. Scanlon et al., 2012), can lead to overdevelopment and depletion of aquifer storage. It may also cause a reduction of groundwater seepage to surface water bodies. This may lead to water conflicts between political boundaries (Famiglietti, 2014; Fienen & Arshad, 2016; Srinivasan et al., 2012). It can also contribute to degradation of groundwater quality (Fienen & Arshad, 2016; Foster & Chilton, 2003; Scanlon, et al., 2007). Pumping-induced drawdown during irrigation may result in interference between neighboring wells. Over longer periods, the drawdown of

the static water level may result in reduced well yields (Butler et al., 2013; Foster et al., 2015; Scanlon et al., 2007).

The effects of pumping on groundwater levels depends largely on the properties of the aquifer. Confined and unconfined aquifers respond differently to pumping. In a confined aquifer, pumping can result in rapid drawdown over large areas along with potential loss of storage. The amount of water released to a well during pumping can be predicted using the equation (Macfarlane, 1998):

$$V = SA(\Delta h)$$

Where *S* is the storativity, *A* is the surface area above the aquifer that a decline in the hydraulic head affects, and Δh is the decline in hydraulic head. This equation indicates that lower storativity results in greater drawdown and a larger area of extension for the cone of depression in a confined system as opposed to an unconfined system. Furthermore, clay-rich confining units may be subject to compaction upon dewatering, resulting in land subsidence, such as has happened in the Central Valley of California (Knight et al., 2018). Aquifer boundaries also affect the response of water levels to pumping. Recharge boundaries (e.g. hydrologically connected streams) cause the drawdown to be less than expected, whereas impermeable barriers (fine-grained geologic units) increase the magnitude of drawdown.

Understanding how an aquifer responds to pumping is a key to effective management (Balleau, 1988; Famiglietti, 2014). One of the major problems, however, is that many hydrogeological systems are inadequately characterized, making it difficult to predict the potential effects of pumping on water levels (Christensen et al.,

2016). Geological complexities such as faults, variable lithology, and stratigraphic discontinuities may cause variations in the thickness and extent of confining layers, making it difficult to map individual aquifers and the boundaries between them (Paillet & Reese, 2000).

Some of the most complex, heterogeneous sedimentary aquifers are those formed in glacial environments (Benn & Evans, 2014; Eyles & Eyles, 2010). Till is a common glacial deposit consisting of a very poorly sorted admixture of a wide range of grain sizes. Aquifers within till are often affected by confining layers and impermeable barriers. Knowledge of how this complex geology is organized is important in understanding how and where groundwater flows, how to manage it accordingly (Anderson, 1989; Koltermann & Gorelick, 1996), and how to model it (Hall, 1993).

Traditional methods for hydrostratigraphic modeling include borehole logs, geologic cross sections, and aquifer testing (slug tests and pumping tests), which yield reliable information on aquifer properties at the points of measurement (Dawson & Istok, 2002; Domenico & Schwartz, 1998). Mapping hydrostratigraphic units between point measurements is challenging because these methods sample only a small volume of the subsurface and are not cost- or time-effective for characterizing large regions. Hydrostratigraphic modeling benefits from non-invasive methods that detect the geometry and properties of the rock and sediment facies between point measurements. Methods such as geophysics and remote sensing can sample larger volumes of the subsurface and can be rapidly employed over large regions for relatively low cost (Brunner et al., 2007; de Marsily et al., 2005; Vereecken et al., 2005).

Airborne electromagnetics (AEM) is a rapidly emerging geophysical method that finds increasing application in hydrogeologic assessments (Auken et al., 2017). AEM can be used to map electrical resistivity (or, reciprocally, electrical conductivity), identifying major changes in subsurface properties such as the salinity of pore waters or the clay content of soils and sediments (Brunner et al., 2007). Given its ability to rapidly map large areas at relatively low cost, AEM will probably remain the most important method for mapping groundwater for the foreseeable future (Auken et al., 2017). Wherever clay content is the main control on the conductivity structure of subsurface materials, geologic units can be mapped in 3D to show the continuity of hydrostratigraphic units and the connectivity of the aquifer. AEM has proven particularly useful in mapping complex glacial geology in Nordic Europe, Canada, and the north-central US (Sørense & Auken, 2004).

The relationship between AEM resistivity and lithology is non-unique and non-universal, so converting the resistivity-depth model into a hydrostratigraphic framework is an interpretive process. Various approaches, ranging from the simple to the computationally complex, have been applied in these conversions. Cognitive-layer modeling and voxel-based geostatistical modeling approaches are simple, straightforward, accessible to most geologists, and widely employed. Each method has advantages and disadvantages. Methods that are relatively rapid and easily accessible through commercial software are more likely to be adopted for regional hydrogeological characterization because these approaches can be understood and applied by most hydrogeologists. Notwithstanding, few studies have addressed whether or not these methods can produce

accurate models of the subsurface in settings with complex glacial geology. All the more, it is unclear whether these simple approaches can successfully identify confining units or hydrogeologic boundaries.

1.2 RESEARCH MOTIVATION

The purpose of this research is to compare and evaluate the validity of two basic hydrostratigraphic modeling approaches using AEM: cognitive-layer modeling and voxel-based geostatistical modeling. It is unknown how accurately these modeling approaches yield hydrostratigraphic models representative of the true aquifer characteristics. Groundwater-level hydrographs are informative of aquifer connectivity, aquifer boundaries, and confining layers. Such data can therefore be used as an independent test of hydrostratigraphic model validity.

In February, 2014 Lower Platte North Natural Resource District (LPNNRD) designated the present study area as Special Quantity Subarea #2 (SQS2) because of localized, excessive drawdown and well interference during periods of heavy pumping. The specific hydrogeologic conditions in SQS2 remained uncharacterized, however. Therefore, this study evaluates (1) hydrostratigraphic model results from cognitive and voxel-based methods, (2) analyses and interpretations of well hydrograph data, and (3) an evaluation of hydrostratigraphic modeling effectiveness within the SQS2 area. This area contains localized confined and unconfined aquifers that are bounded by impermeable units.

CHAPTER 2. REVIEW OF AEM AND WELL PUMPING TEST METHODS

2.1 GEOPHYSICAL TECHNIQUES

Near-surface geophysical methods have been commonly used to help describe groundwater and its processes in more detail and over larger areas than can be achieved with traditional methods such as drilling. These hydrogeophysical methods include remote sensing, airborne surveys, electric and magnetic surveys, high temporal resolution measurements, seismics, ground-based gravimetry, and magnetic resonance sounding (Robinson et al., 2008; Vereecken et al., 2005). These ground-based and airborne methods are non-invasive and therefore can be applied more readily than drilling, but ground-truth data from boreholes is necessary to match the geophysical properties to geological and hydrogeological observations (Vereecken et al., 2005). Hydrogeophysical methods collect data at different scales; high-resolution methods generally cover small areas while coarse-resolution methods can be applied over large areas. One main advantage to these methods is that they produce data that can help hydrogeologists correlate between boreholes and develop more robust 2D and 3D models of the subsurface.

Airborne electromagnetic (AEM) surveys have been used for mining and petroleum exploration since the 1950s (Sørense & Auken, 2004), but over the past decade these surveys are being increasingly used for hydrological applications and to map groundwater resources (Auken et al., 2017; Robinson et al., 2008; Sørense & Auken, 2004). The helicopter suspends a wire transmitter loop that emits electromagnetic (EM) waves, which penetrate the ground, producing eddy currents in the subsurface. These eddy currents generate a secondary EM signal that is read by a receiver, creating a sounding of the

apparent resistivity (Aqua Geo Frameworks, 2017; Auken et al., 2017). GPS coordinates, elevation, and inclination are recorded for each sounding. The helicopter flies between 15 and 20 km/hr at an altitude of about 50 meters (Sørense & Auken, 2004). An AEM survey is usually flown in a closely spaced grid pattern so as to collect enough data for a 3D characterization of the survey domain. AEM soundings are highly affected by noise due to electrical coupling with infrastructure, such as power lines, railroads, and pipelines (Aqua Geo Frameworks, 2017). AEM does not directly map the geology or the groundwater, but rather, it provides a measure of the subsurface electrical resistivity structure through geophysical inversion (Auken et al., 2017). Inversion produces a resistivity-depth model that can be related to hydrogeological properties using one or more modeling approaches, described in the next section.

AEM is particularly useful for mapping salinity because of the high electrical conductivity of groundwater with high ionic concentrations (Cresswell et al., 2004; Cresswell et al., 2007; Dent, 2007; Palamara et al., 2010). AEM is also useful in karst environments for mapping the open, water filled areas where the limestone has dissolved away (Gondwe et al., 2012; Supper et al., 2009). AEM has been used widely in glacial environments to map aquifers and confining units, which is especially helpful in describing the complexity of the hydrogeology (Høyer et al. 2015; He et al. 2014; Jørgensen et al., 2013, 2015; Marker et al., 2017; Christensen et al., 2017). Regardless of the specific hydrogeologic geologic settings in which AEM is applied, independent data such as borehole lithologic logs, other geophysical methods (magnetics, radiometric) or satellite imagery must inform interpretations (Vereecken et al., 2005).

2.2 AEM HYDROSTRATIGRAPHIC MODELING

The resistivity-depth data must be converted into a hydrostratigraphic model in order to make use of the AEM data for mapping confining units and hydrogeologic boundaries. This depends, however, on establishing general relationships between resistivity and lithology for the model area (Brunner et al., 2007). Borehole data such as lithological descriptions and down-hole geophysical logs are particularly useful.

The electrical resistivities of sediments and sedimentary rocks depends primarily on the ionic concentration of their pore waters and their clay-mineral content (Figure 1). If the pore water is generally fresh, then clay-bearing materials can be distinguished from clay-free materials. Pure clays tend to be electrically conductive (i.e., have low resistivity values), whereas clay-free sediments and rocks are electrically resistive (i.e., have low conductivities). Resistivity surveys are widely used to map glacial terrains because they exhibit characteristically sharp contrasts between clay-rich and clay-poor sediments.

There is a considerable degree of overlap between some lithologies (Figure 1) clay and shale are both conductive and typically indistinguishable. Similarly, sand and limestone are both resistive and they may be difficult to distinguish in the absence of independent data (Palacky, 1988). In sedimentary bodies of mixed lithologies—such as thinly interbedded clays and sands—the overall resistivity of the modeled layer will be intermediate between the resistivity values of pure clay and pure sand (Foged et al. 2014).

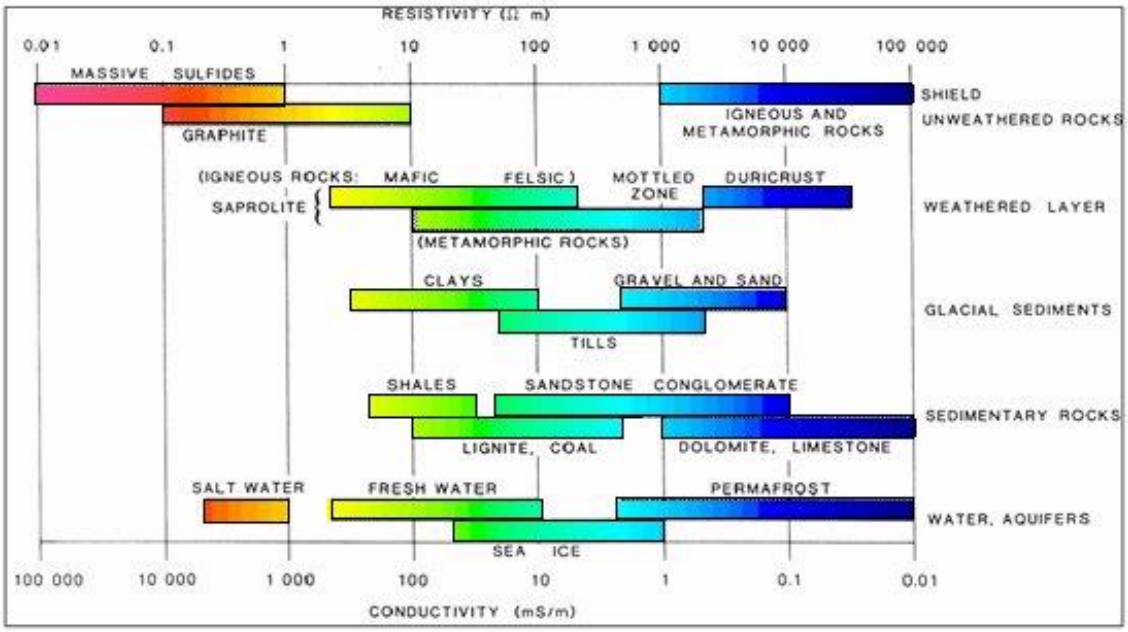

Figure 1 Electrical conductivity/resistivity of geologic material in logarithmic scale (Palacky, 1988)

Both deterministic or probabilistic (stochastic) methods are employed to convert resistivity values to modeled lithology. A deterministic model represents just one of many possible solutions to the dataset. A probabilistic model reflects the inherent uncertainty of the model parameters by incorporating randomness into the model structure (Isaaks & Srivastava, 1989). A probabilistic model has its advantages, considering the wide range of resistivities for any given lithology, but it is usually desirable to incorporate the realism that only tacit geologic knowledge can impart. Therefore, deterministic approaches will likely remain an essential modeling approach for the foreseeable future.

Hydrostratigraphic modeling can be deterministic or probabilistic, or it can employ a combination of both methods. Two simple approaches in common use are (1) cognitive-layer modeling, and (2) voxel-based geostatistical modeling. These methods are described

below, followed by a summary of some of the more sophisticated methods that have recently been developed.

2.2.1. COGNITIVE-LAYER MODELING:

A cognitive- modeling approach can employed for 3D geological modeling by manually digitizing points along multiple profiles and then interpolating those points to surfaces representing layer boundaries. This approach requires the input of a modeler's geologic knowledge to interpret hydrostratigraphic units. The resistivity-lithology relationship is interpreted subjectively through visual comparison to borehole logs along the paths of individual profiles (Figure 2). Test hole lithology and resistivity values are taken into account when interpreting the aquifer top and bottom surfaces. Accordingly, subsurface geology can only be modeled as horizontal layers. The outcome is one interpretation of many possible outcomes, which makes it a deterministic modeling approach.

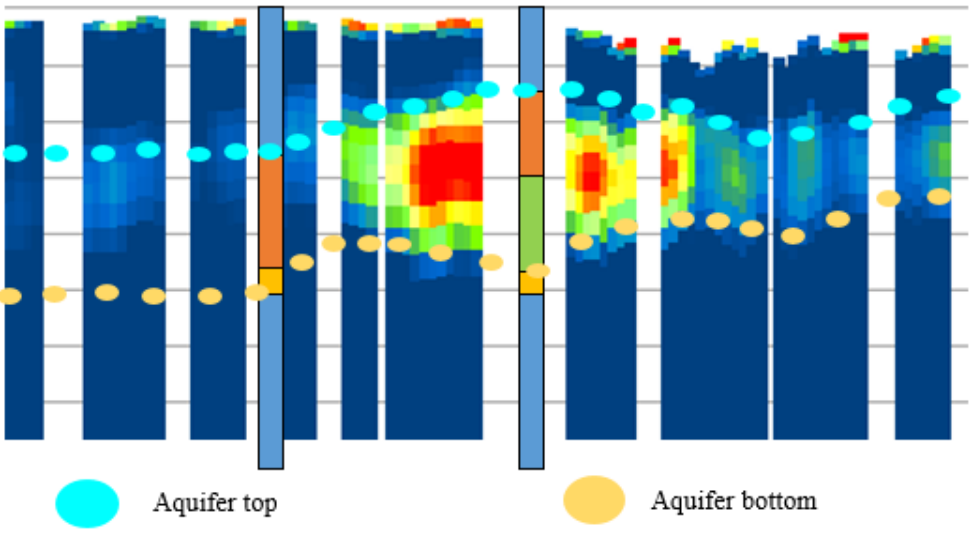

Figure 2 Simplified figure illustrating the cognitive approach with interpretation points along the top and bottom of the aquifer using the boreholes and AEM data as a guide. These points are then interpolated into a surface, creating an aquifer layer.

Cognitive modeling has been employed in numerous studies. Researchers used a numerical and cognitive approach incorporating geologic knowledge to achieve a geologically realistic interpretation of the Chalk in the London Basin, an area of variable data density (Royse, 2010). A cognitive geological model was created in Denmark by using lithological information and knowledge of the stratigraphy (Scharling et al., 2009). The cognitive approach has also been applied to non-AEM geophysical data. Researchers used seismic and ground-penetrating radar along with sedimentological data to improve understanding of the subsurface in southern Ontario (Sharpe et al., 2003).

The cognitive modeling approach incorporates geologic experience and understanding to describe hydrogeology of complex areas. It is a subjective method because different modelers may interpret the same data differently. Therefore, it may be difficult to determine if any given model is credible. The method is also time-consuming and difficult to reproduce (Høyer et al., 2015; Jørgensen et al., 2015; Sapia et al., 2015). Nevertheless, the cognitive method can be combined with other modeling methods to confirm results or to complete missing portions of a model. It appears that the best application of cognitive modeling is to widely-spaced AEM flightlines crossing simple, layered aquifers (Jørgensen et al., 2015, 2013).

2.2.2 VOXEL-BASED GEOSTATISTICAL MODELING:

A voxel model is a 3D grid consisting of regular arrangement of volumetric pixels or voxels (Kaufman, et al., 1993). Voxels are 3D cubes that contain certain resistivity ranges and are divided into different classes. Figure 3 shows the same flightline as Figure 2 using a voxel modeling approach and illustrates how we can model the geology showing more irregular patterns. Each voxel can contain a number of different attributes of the study area, such as a resistivity value or an integer representing a lithology. Vast amounts of attributes can be accounted for in voxel grids. Several commercially available software programs can be used to generate voxel models and transform resistivity to lithology, including GeoScene3D, Geosoft Oasis Montaj, and Aarhus Workbench (Jørgensen et al., 2013). The resistivity of the AEM data is put in as an attribute. Geostatistical interpolation techniques (e.g. inverse-distance weighted, kriging) or other methods (e.g. multi-point statistics) can be used to directly translate AEM resistivity data into a voxel model. Voxel models offer tremendous flexibility in how the resistivity-lithology relationship is incorporated into the model. These models can accommodate a variety of probabilistic approaches, but they do not exclude deterministic methods.

Voxel models are useful in areas that are geologically heterogeneous (Jørgensen et al., 2015, 2013). They are also helpful in areas exhibiting complicated geology that cannot be modeled as horizontal layers (Sapia et al., 2015). Though voxel models provide an objective approach and can be created quickly, the resulting models may be inaccurate in areas with sparse or low-quality data (Jørgensen et al., 2013). Furthermore, voxel models do not create smooth layers and may not be able to resolve small details (Høyer et al., 2015;

Jørgensen et al., 2015, 2013; Sapia et al., 2015). Significant errors and uncertainties may exist due to the automated approach and the lack of a modeler's intuition and geological knowledge.

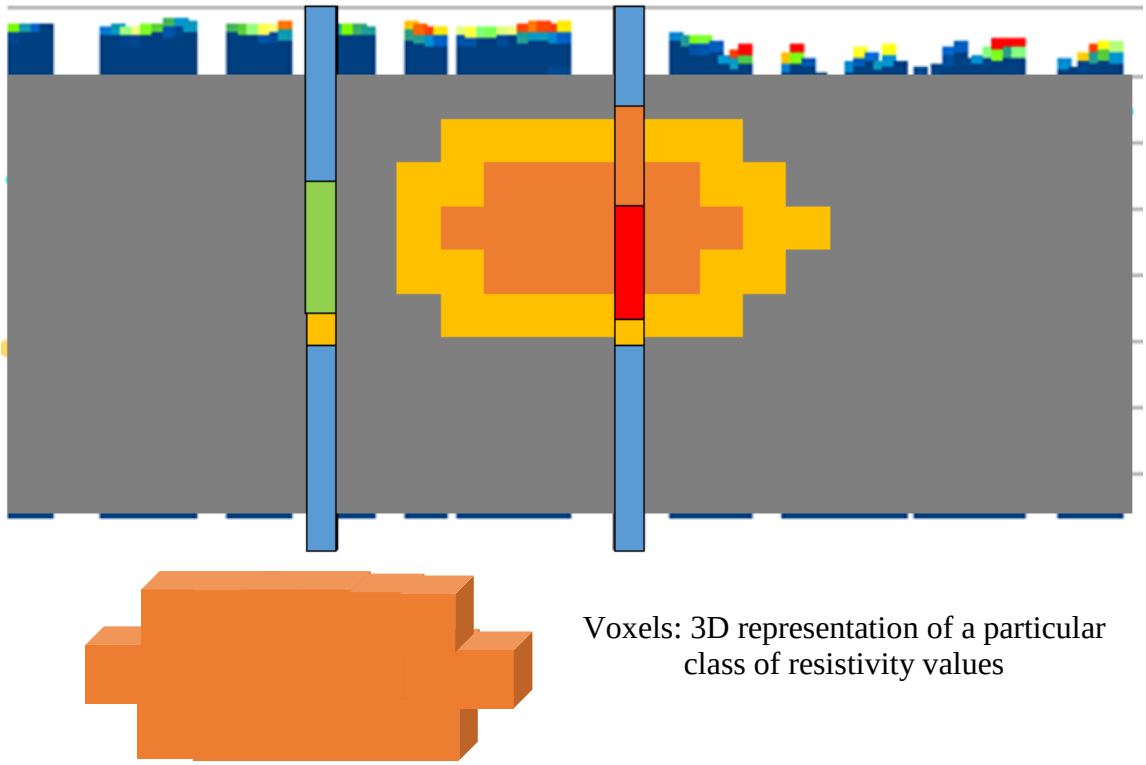

Figure 3 Simplified figure illustrating the statistical approach with voxels in a region of the flightline and a 3D view. The orange represents the best aquifer material, the yellow is good aquifer material, and the gray color represents poor aquifer material.

2.2.3 OTHER MODELING TECHNIQUES:

Although sophisticated modeling techniques are not the focus of this study, these methods are briefly summarized here as a means for comparison to the simple methods described above. The errors associated with this kind of modeling are a topic of concern. Jorgensen et al. (2015) explored new techniques in modeling in southern Denmark with the borehole data and the AEM resistivity surveys. They began using modeling techniques

of clay fraction (CF) method, multiple point statistics (MPS), and a cognitive approach where applicable. Next, the authors created a voxel model using all of the available information (Jørgensen et al., 2015). Other researchers developed alternative groundwater models using the traditional aquifer testing methods and the differences in the models were then analyzed (Christensen et al., 2016). This attempt at improving accuracy resonates with the methodology of an AEM study in the Spiritwood Valley Aquifer System in Canada. Seismic reflection, geophysical logs of boreholes, and other geologic knowledge were also incorporated into the cognitive and voxel modeling process (Sapia et al., 2015). The authors incorporated these additional data sources in order to address some of the errors inherent in the AEM modeling method.

The translation of geophysical properties (resistivity) into hydrogeological properties (lithology) is not straightforward and it is usually site-specific. Mathematical concepts involving differential equations, statistics, and geophysical data have been incorporated in order to lower the uncertainty. Knight et al. (2018) explored a bootstrapping approach to refine the resistivity-lithology relationship in the agriculturally critical Central Valley of California. Christensen et al. (2017) used Monte Carlo simulations to combine sparse borehole data and dense geophysical data.

The U.S. Geological Survey (USGS) has applied AEM to groundwater-surface water relationships in both extant alluvial valley aquifers and buried glacial-aquifer systems with the intent of improving aquifer maps, models, and management (Abraham et al., 2019). Aquifer characterization and mapping improves with the application of both

AEM surveys and continuous water-level monitoring; Korus et al. (2017) applied these combined methods at three sites in glaciated eastern Nebraska.

2.3 WELL HYDROGRAPH INTERPRETATION

Measurements of groundwater levels are useful in many ways: natural fluctuations can be used to study recharge (Moon et al., 2004; Obuobie et al., 2012). pumping tests give information about the hydraulic properties of the aquifer (Paul et al., 2011), and long-term drawdown and recovery data from irrigation pumping can be informative of basic aquifer characteristics (Butler et al., 2013).

A pumping test is a controlled experiment involving a single pumping well and one or more observation wells that record the response of the hydraulic heads to pumping over a set period of time, typically hours to a few days. Data on the recovery of hydraulic head after pumping has ceased is also informative. Well hydrographs can be used to calculate the transmissivity (*T*) and storativity (*S*) of the aquifer (Sanders, 1998). The Theis (1935) nonequilibrium well flow equation describes the drawdown in an idealized confined aquifer where there are no contributions from other beds around the aquifer being pumped (nonleaky):

$$\boldsymbol{h - h_0 = \frac{Q}{4\pi T W(u)}}$$

$$\boldsymbol{u = \frac{r^2 S}{4Tt}}$$

A plot of drawdown (*s*) versus time will yield a type curve, the slope of which depends on the properties of the aquifer (Dawson & Istok, 2002). Deviations from the type curve may occur for one or more reasons. Vertical flow (leakage) of groundwater through confining layers will cause the slope to decrease at late times (Figure 4b). An unconfined

aquifer will behave initially like a confined aquifer, but at later times the drawdown will be delayed due to the effect of drainable porosity (Figure 4c); (Neuman, 1975a).

Confined aquifers release water from decreased water pressure and compression of the aquifer material, releasing small amounts of water per unit volume of the aquifer (Alley et al., 1999; Ritter et al., 2011; Theis, 1935). Unconfined aquifers partially desaturate, releasing large amounts of water per unit volume (Alley et al., 1999; Neuman, 1975b; Ritter et al., 2011; Theis, 1935). Thus, with all else being equal, the displacement is larger and more rapid in a confined aquifer than in an unconfined aquifer.

Bounded aquifers show distinct deviations depending on whether the boundary is a no-flow boundary (an impermeable barrier) or a constant-head boundary (recharge from a surface water body). In the case of a recharge boundary, the slope of the drawdown curve begins to decrease when the cone of depression reaches the boundary (Figure 4d, Dawson and Istok, 2002; Driscoll, 1986). In the case of an impermeable boundary, the slope of the drawdown curve increases (Figure 4d, Dawson and Istok, 2002; Driscoll, 1986).

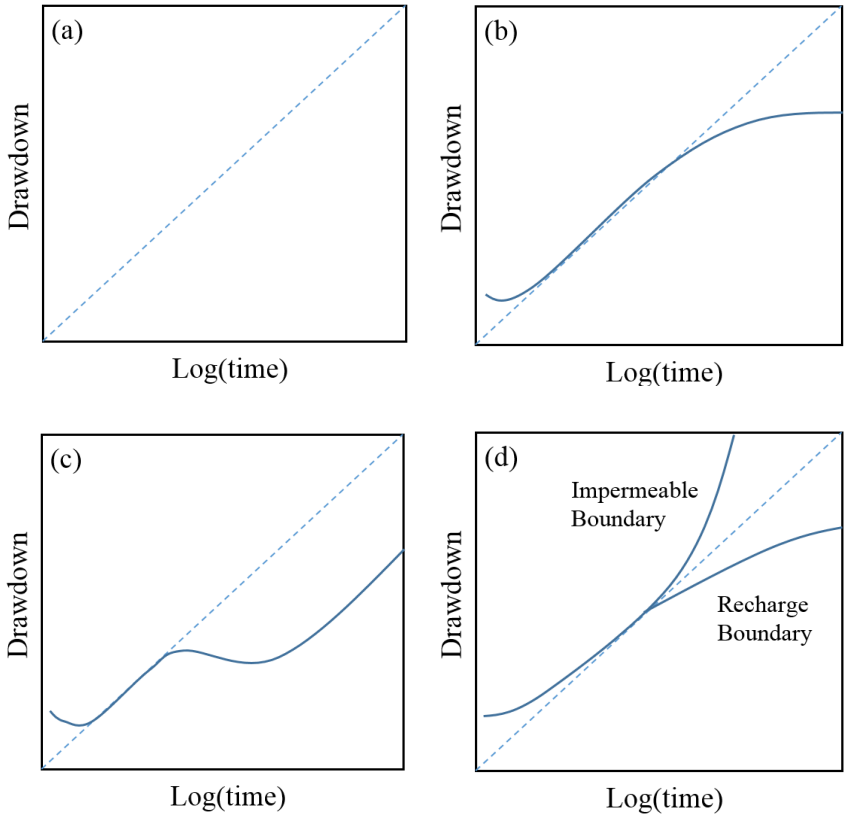

Figure 4 General well hydrograph trends showing early water-level responses over time (on a logarithmic scale) to pumping of different aquifer types: (a) 1:1 Ratio (b) leaky confined aquifer (c) unconfined aquifer and (d) bounded aquifer.

Aquifer boundaries can be further explored by image-well theory. An imaginary well is placed on the opposite side of the boundary. Based on the principle of superposition, the resulting cones of depression are summed to give the expected drawdown. For a recharge boundary, the imaginary well is an injection well that diminishes the drawdown of the actual pumping well. In the case of an impermeable boundary, the imaginary well is a pumping well that adds to the drawdown of the actual well (Driscoll, 1986).

Observation wells installed with pressure transducers may show changes in head over multiple years due to nearby irrigation pumping. These well hydrographs can be examined to understand the aquifer behavior and define certain properties of the aquifer

even if they are not part of a traditional pumping test. The fundamentals of pumping test analyses are still useful for certain irrigation pumping periods.

Butler et al. (2013) presented such an application for the High Plains aquifer in Kansas. Two separate sites had borehole logs to describe the confinement of the aquifer at multiple irrigation wells. Researchers recorded water levels hourly, and hydrographs from both locations were put together from 2007 to 2011 and were examined (Figure 5). There was evidence for closed systems at both locations. The Haskell site had an unconfined aquifer located above a confined aquifer, but the bounded aquifer only showed in the unconfined layer. The Thomas site wells were located in an unconfined aquifer, which explained the modest drawdown. This aquifer was a closed system. These boundaries were shown in each of the hydrographs by the drawdown slope leveling out and becoming a straight line (Figure 6).

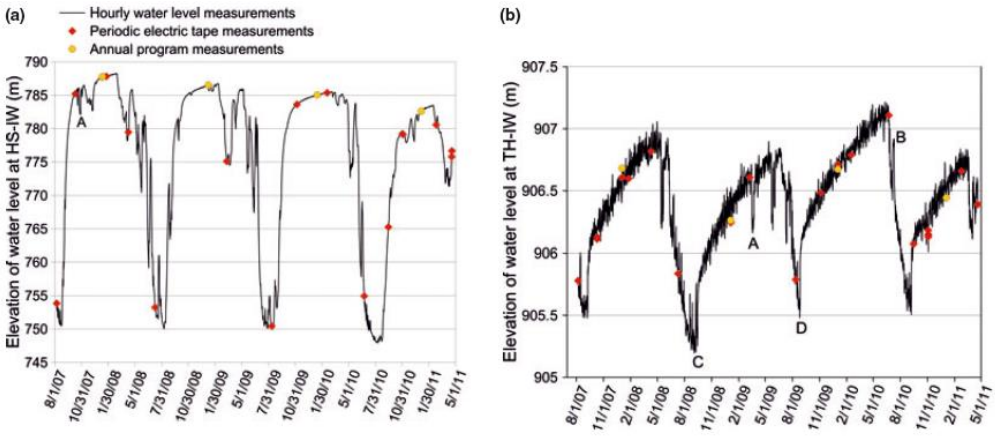

Figure 5 Well hydrographs for Haskell (left) and Thomas (right) sites showing the observed seasonal pumping drawdown curves (Figure 3, Butler et al. 2013).

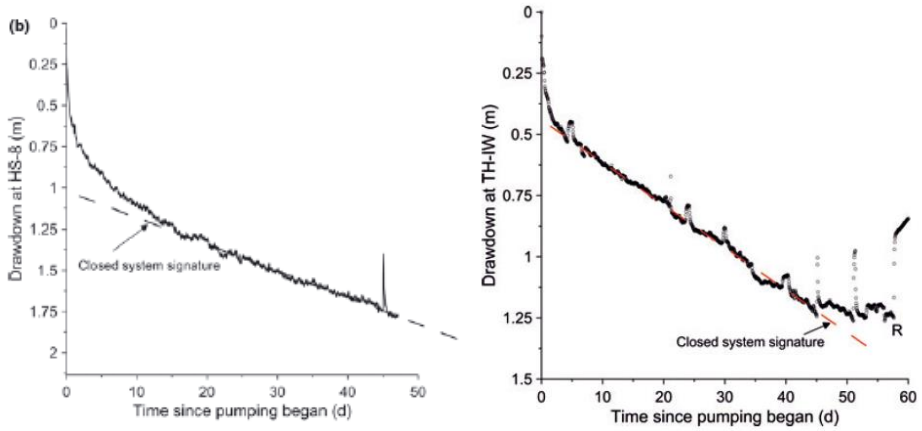

Figure 6 Analysis of pumping curves at Haskell Site (left) and Thomas Site (right) showing evidence of bounded aquifer through tracing the straight line after many days of continuous pumping (Figure 4 and Figure 8 from Butler et al., 2013)

These characteristics are relevant to water management decisions in the High Plains aquifer, and this approach can be used at any site. This study shows that continuously monitored wells are more informative about the aquifer behavior than simply using periodic measurements (Butler et al., 2013). Hydrographs for water levels in wells that are continuously monitored can give evidence for the type of aquifer that is being pumped based on the pumping and recovery responses.

In another example, Korus (2018) compared hydrological data from a continuously monitored well in a glacial aquifer of eastern Nebraska. On a full hydrograph of one well, a straight dashed line traces the pumping response curve and the rapid recovery both show evidence of a boundary (Figure 7). Resistivity-depth profiles from AEM surveys in the area showed evidence of the impermeable boundary, suggesting that the combined use of hydrographs and AEM can result in more robust interpretations of hydrostratigraphy.

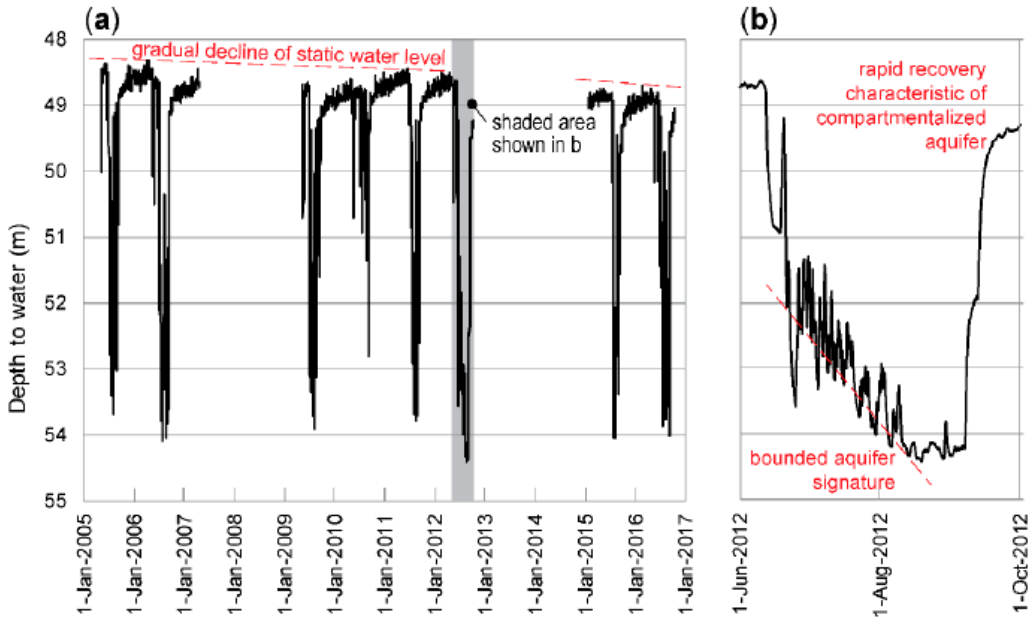

Figure 7 Well hydrograph showing a bounded aquifer. Both the straight line along the pumping curve and the rapid recovery indicate a closed system (Figure 4, Korus, 2018)

CHAPTER 3. SITE DESCRIPTION

3.1 GEOLOGIC SETTING

Cretaceous sedimentary rocks underlie much of eastern Nebraska (Figure 8). These strata are the oldest bedrock units relevant to this study. The Dakota Group, which comprises interbedded sandstone, conglomerate, siltstone, mudstone, shale, and lignite, is the oldest unit in the Cretaceous succession in Nebraska. That succession continues with, in ascending stratigraphic order: Graneros Shale, Greenhorn Limestone, Carlile Shale, Niobrara Formation (shaly chalk and limestone), and Pierre Shale. Cenozoic strata lie unconformably atop the Cretaceous units. In eastern Nebraska, only the Ogallala Group (sand, sandstone, siltstone, and gravel which make up the Ogallala Aquifer) and the Broadwater Formation (and correlative sand and gravel units) are preserved.

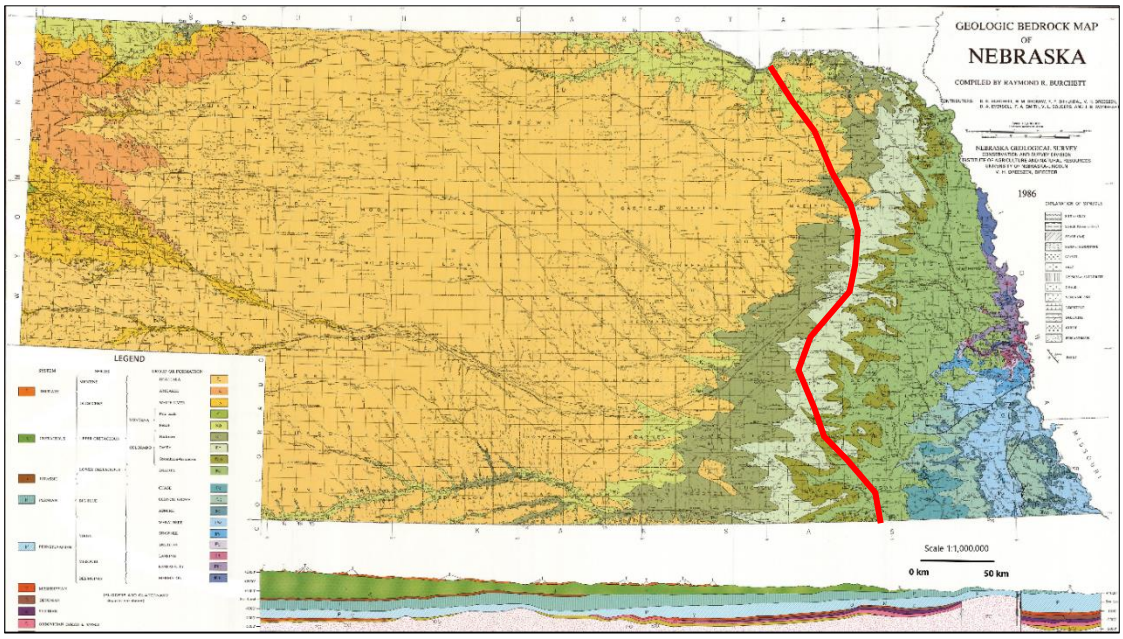

Figure 8 Map of the exposed geology of Nebraska. The red line represents where the glacial sediment-lain region begins on the east (Burchett, 1986)

The eastern part of Nebraska contains sediments that fall into three different categories: coarse-grained stratified sediment, till, and loess (Soller, 1997). Coarse-grained stratified sediment was deposited by rivers during the late Pliocene and early Pleistocene (Soller, 1997). These sediments filled valleys that were presumably formed by the previous drainage system of the Rocky Mountains and then later buried by younger sediments (Dreeszen & Burchett, 1971). The buried valleys extend from eastern Nebraska into western Iowa and northwest Missouri (Bettis, 1990; Heim & Howe, 1963). Glaciated sediments are primarily Quaternary in age (deposited between 2.6 and 0.6 million years ago) and were left behind by continental glaciers which covered much of north-central North America beginning in the late Pliocene and early Pleistocene (Roy et al., 2004). Glacial sediments form complex surficial geology in this area (Soller, 1997). The lithology and mineralogy of different till groups in Iowa, Missouri, Kansas, and Nebraska suggests that there were at least six glacial advances into the area prior to 600,000 years ago (Roy et al., 2004). Till is a very poorly sorted ice-laid sediment containing sediment that varies in size from clay to boulders (Ritter et al., 2011). Sorted sediments within tills are uncommon and occur erratically. Tills in the north-central U.S. tills are fine-grained, matrix-dominated, and for the most part homogeneous in both vertical and lateral directions (Roy et al., 2004). Most of the glacial sediments are covered by a thinner succession of wind-blown loess deposited during the Middle to Late Pleistocene (Roy et al., 2004; Soller, 1997).

Eastern Nebraska is hydrogeologically complicated because it lies within a transition zone between different aquifer systems. At this transition zone, three different

aquifers overlap (Hanson et al., 2012). The deepest is the Maha (or Dakota) aquifer, characterized by which contains poor quality water in the west and good water quality in the east. The High Plains aquifer, in contrast, is the most reliable source of good quality groundwater and it is used throughout much of the interior of Nebraska. Glacial sediments overlie and interfinger with, or completely truncate, the geologic units of the High Plains aquifer in eastern Nebraska. Aquifers in the glacial sediments are extremely heterogeneous and discontinuous, and therefore groundwater availability is more variable east of the glacial limit.

The stratigraphically lowest aquifer under most of eastern Nebraska is the Maha (Dakota) aquifer, which consists of permeable sandstones of the Dakota Group. The natural water quality in the Dakota is generally poor, containing high concentrations of dissolved ions from NaCl brines derived from underlying rocks (Gosselin, et al. 2001). Locally, however, the sandstones are saturated with water derived from meteoric recharge, and in these areas, the aquifer is used extensively as a source of water for domestic wells, although it is also used for irrigation, municipal supply, and livestock (Divine & Sibray, 2017).

The High Plains aquifer (HPA) is the shallowest aquifer, and it underlies eight US states on the Great Plains, and attains its maximum thickness west-central Nebraska. The following map (Figure 9) shows that the water depletion primarily in Nebraska, Kansas, and Texas. Despite more depletion existing in other states, groundwater resources in Nebraska still require preservation. The HPA is used in Nebraska for major domestic, municipal, and irrigation; it also has minor domestic use (Korus et al., 2013). This aquifer extends over most of the state of Nebraska (Figure 10).

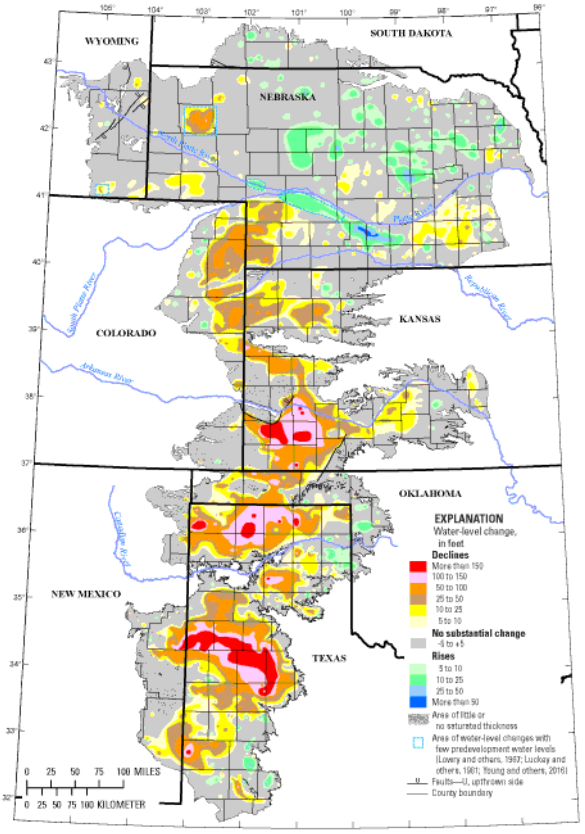

Figure 9 High Plains Aquifer depletion map, where the warmer colors show higher amounts of depletion (McGuire, 2019)

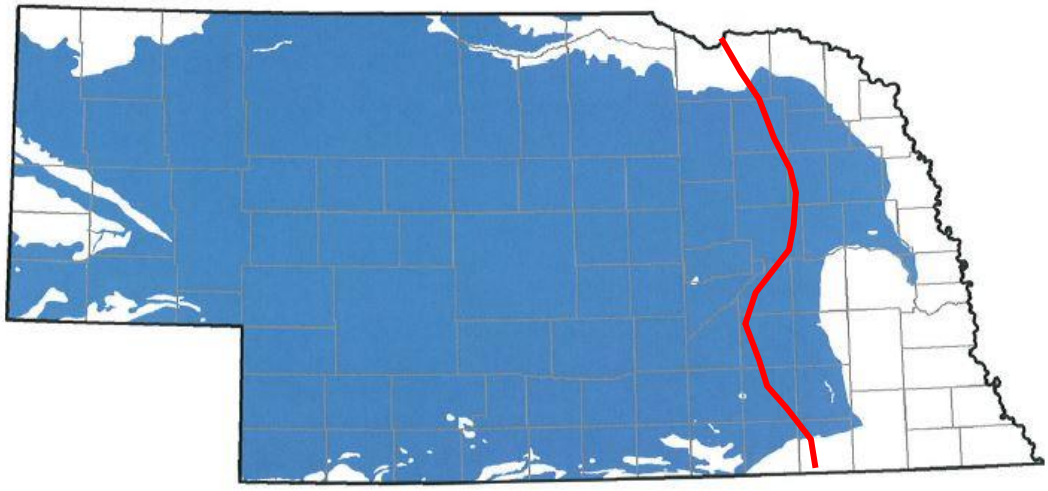

Figure 10 High Plains Aquifer in Nebraska shown in blue. The red line indicates where the glacial sediment-laid region in the east begins (Figure 20, Korus et al., 2013)

Glacial deposits overlie the High Plains Aquifer in eastern Nebraska and contain localized aquifers that have not been mapped in detail (Figure 11). It is difficult to predict how these three overlapping aquifer systems affect one another in the absence of accurate maps.

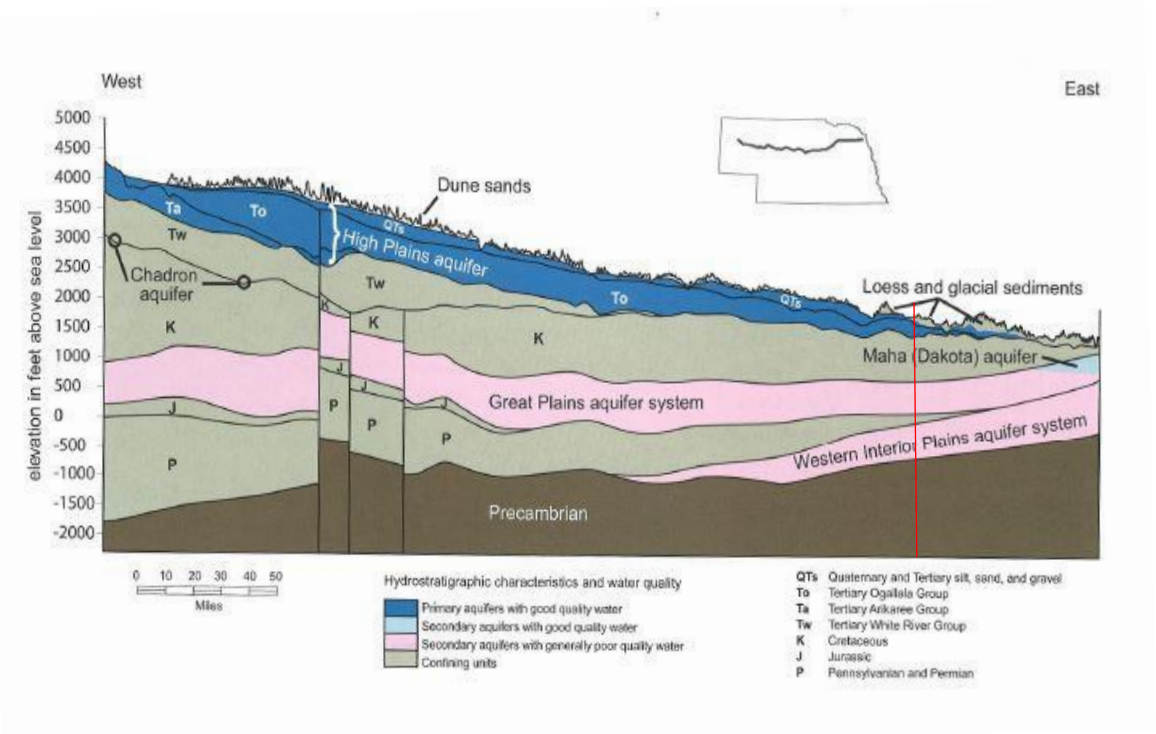

Figure 11 Cross section of Nebraska showing general hydrogeologic map with multiple aquifers, and where the HPA gets more complex in the east. The red line shows (approximately) where the glacial sediment-laid region begins in the east (Figure 14, Korus et al., 2013)

3.2 DESCRIPTION OF STUDY AREA

The study site lies in Lower Platte North Natural Resource District (LPNNRD). The LPNNRD has designated a Special Quantity Subarea 2 (SQS2) to develop management strategies that ensure water is available to farmers. SQS2 is approximately 204 square miles in area where a couple of AEM surveys have been taken (Figures 12 and

13; Aqua Geo Frameworks, 2017). The groundwater levels can be very unpredictable and affected by drought and irrigation pumping in this area (LPNNRD, n.d.). Moreover, a recent report completed on this area mentions that groundwater can become depleted due to extensive pumping for irrigation and typically recharges to the original level, but depletion is worse during drought in areas where aquifer is small and disconnected (Aqua Geo Frameworks, 2017).

The topography in SQS2 is variable and includes valleys, dissected plains, and rolling hills (Korus et al., 2013). The Quaternary surficial geology contains clay, silt, till, sand, and gravel deposits, while loess deposits cover regions of glacial till. This glacial till overlies sand and gravel along with the water table, resulting in complex confining conditions. Groundwater flows predominantly from west to east, similar to the courses if major streams. The localized glacial aquifers may be hydrologically connected to the streams in some areas, but the nature of such connections has not been examined in detail. Unconfined aquifers exist locally, but the area is thought to consist of numerous confined zones near or beneath glacial till (Summerside et al., 2005). Such aquifers can exhibit large drawdowns during irrigation pumping. Hydrogeologists working in this area have recommended that aquifer tests be done in the area to better estimate the aquifer characteristics (Aqua Geo Frameworks, 2017).

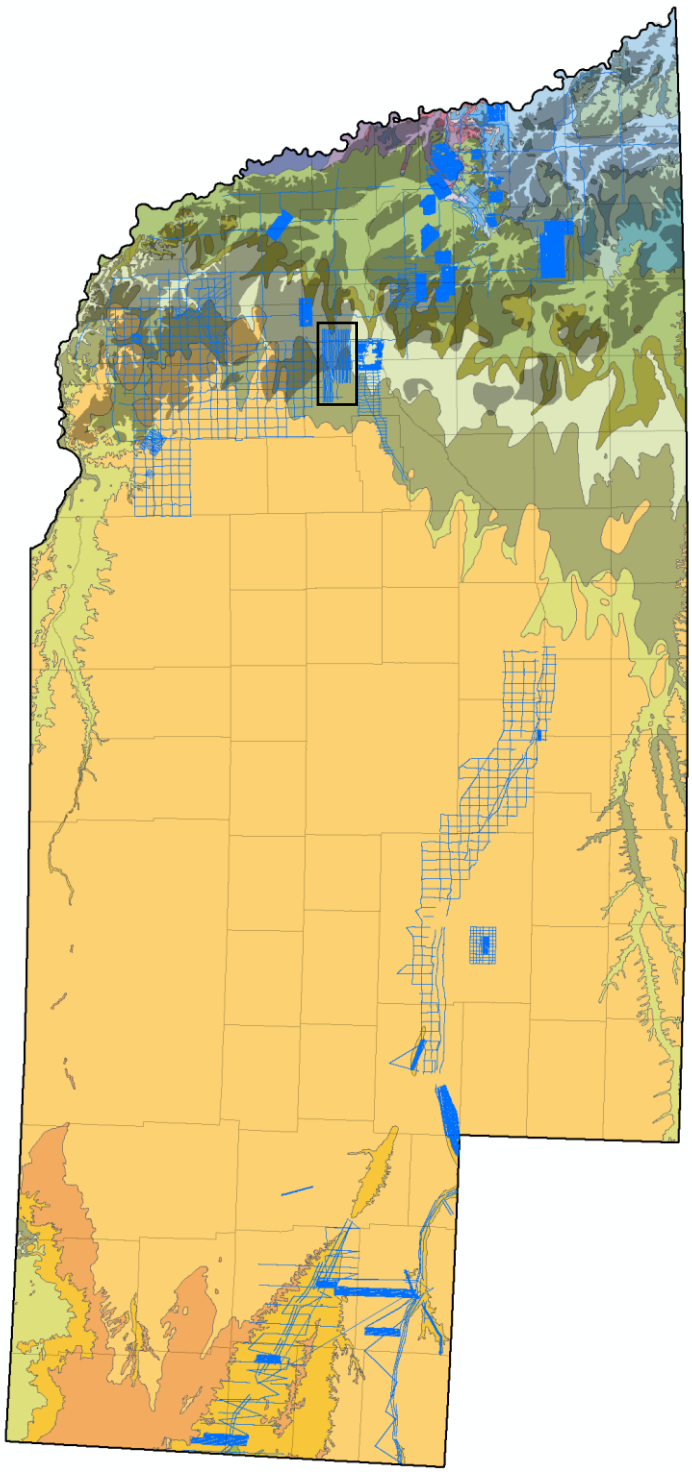

Figure 12 Geologic map of Nebraska showing the AEM flightline surveys. The study area is outlined in black.

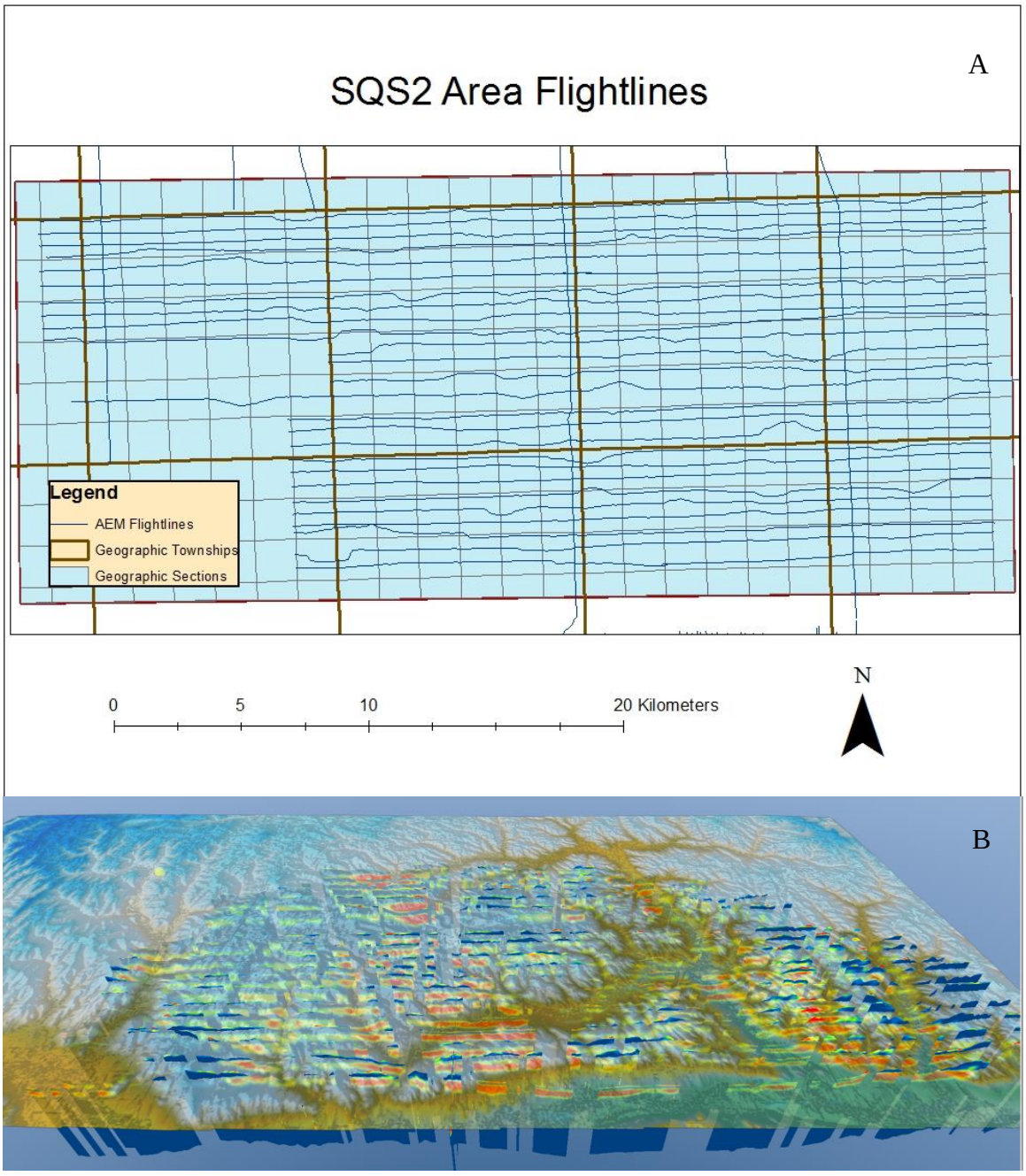

Figure 13 AEM flightlines surveyed in SQS2 including the geographic townships and sections in map view (A) and digital elevation model atop the flightlines in 3D view (B).

CHAPTER 4. METHODS

4.1. INTEGRATION OF EXISTING DATA

Commercial software GeoScene3D (www.geoscene3D.com) was used to combine several different datasets into one 3D virtual environment. The data included AEM resistivity-depth models, borehole logs, and groundwater-level elevations. Also included were geographic data, including public land survey system (sections, townships, and ranges) and a digital elevation model (Figure 13). Data was gathered from consultant reports [Aqua Geo Frameworks (AGF)], the Department of Natural Resources (DNR), and the Lower Platte North Natural Resources District (LPNNRD). All Imperial units were converted to the metric system. The coordinate system was Nebraska State Plane Meters (EPSG 32104).

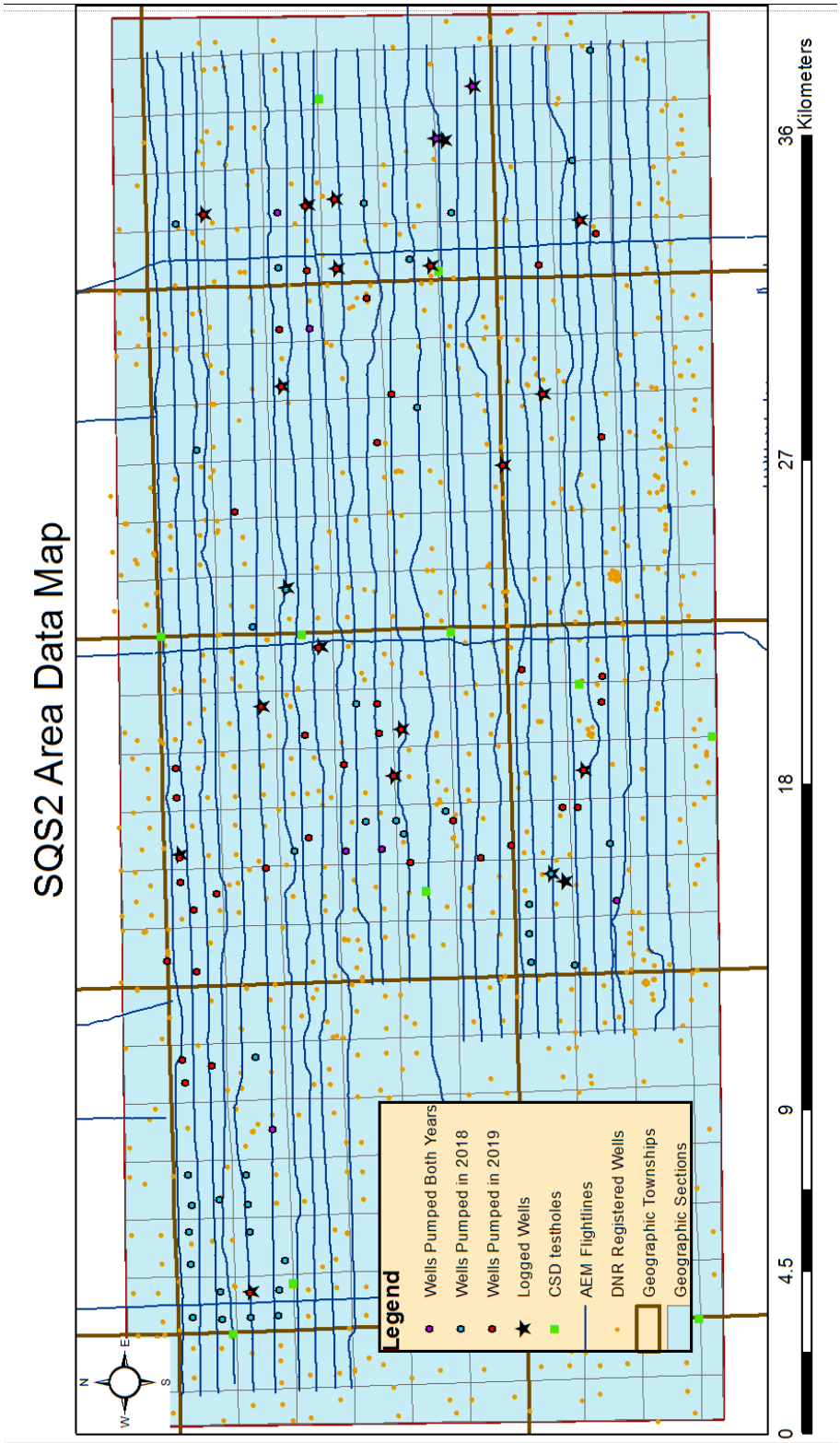

Figure 14 Data Map of SQS2 Area showing DNR registered wells, pumped wells, and logged wells in addition to the AEM flightline data.

4.1.1 AEM SURVEYS

Although several contractors offer AEM survey systems, SkyTEM has been the most widely used system in Nebraska to date. SkyTEM is a helicopter-based survey system utilizing high and low magnetic moments to generate signals capable of resolving near-surface layers while at the same time having a relatively large depth-of-investigation (Sørense & Auken, 2004).

Two SkyTEM surveys have been conducted in the SQS2 area (Figures 13 and 14). The SkyTEM304M system was used in the main survey flown during July 17–20, 2016. This system is optimized for improved resolution of near-surface layers at the cost of reduced depth-of-investigation. Survey planning, coordination, data processing, and inversion was provided by the consulting firm Aqua Geo Frameworks (AGF). Twenty five survey lines were flown in an east-west direction approximately 500 m apart, although actual spacing varied because flight paths were routed around homes, infrastructure, and potential sources of interference (capacitive or galvanic coupling between the transmitter and a man-made source, creating a circuit). One north-south tie line was flown down the approximate center of the study area. The helicopter flew at about 100.5km/hr at about 36.4 meters above the surface.

An additional three flight lines were part of an earlier study in 2014, which was completed using the SkyTEM 508 system. The 508 system has a large depth-of-investigation but near-surface resolution is reduced compared to the 304M. Oversight and inversion was provided by the consulting firm Exploration Resources International

(XRI). One flight was an east-west line through the center of the study area, the other two were north-south lines through the west and east parts of the study area.

The aforementioned consultants provided post-acquisition data processing on all SkyTEM data, which involved removal of electromagnetic coupling effects and noise associated with helicopter flight characteristics. Inversion of the 2016 AEM data was completed using a deterministic spatially constrained inversion (SCI; Viezzoli et al., 2008) in Aarhus Workbench software, version 5.2.0.0. (Aqua Geo Frameworks, 2017). The resulting resistivity-depth model has 30 layers, starting at a thickness of 3 meters and increasing by a factor of 1.08 for each subsequent layer. The thickness of the 29th layer is 25.9 m (the 30^{th} layer has an infinite bottom). The depth to the top of the 30^{th} layer is 311.8. Resistivity is given in ohm-meters.

Inversion of the 2014 AEM data was also completed using SCI in Aarhus Workbench version 4.2.7.2. The resulting model also has 30 layers, but the thickness of the first layer is 5 m with the thickness of each subsequent layer increasing by a factor of 1.1. The 29^{th} layer is 40.7 m thick and the top of the 30^{th} layer is at a depth of 500 m.

4.1.2. BOREHOLE DATA

The borehole data used in this project included data from wells registered at the Department of Natural Resources (DNR) and from test holes drilled by the Conservation and Survey Division (Nebraska Geological Survey; CSD). These registered DNR wells and CSD test holes can be viewed in a map view and within the cross-sections of the AEM flightlines (Figures 14 and 15). These DNR registered wells contain descriptions of geologic materials from cuttings collected during the drilling of water wells. Most of

these descriptions were made by water-well contractors without formal geological credentials, although many have had some cursory training in the description of cuttings. Therefore, these descriptions vary in quality and reliability. The CSD test holes were all drilled as part of a formal geological investigation program and were planned, described, and archived by qualified geologists. Many of these test holes were also logged with wireline geophysical instruments. Although there far fewer of these test holes, the quality and reliability of their accompanying data are much greater than those of other boreholes.

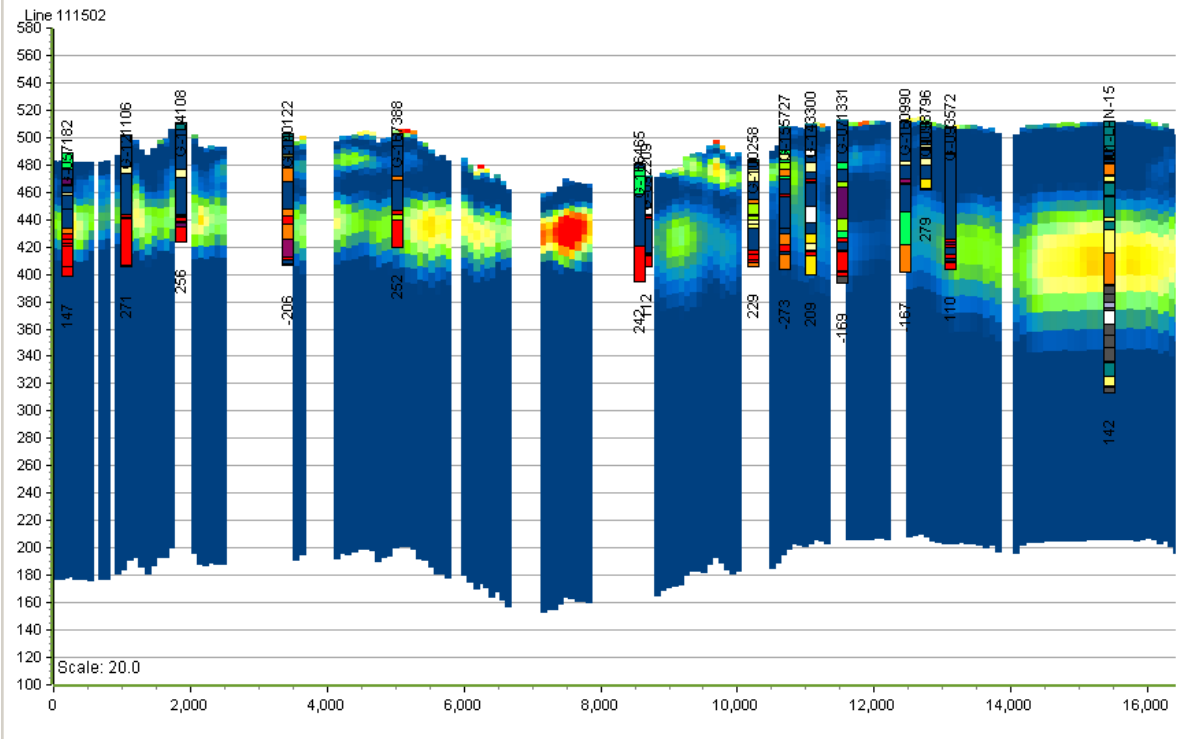

Figure 15 Processed AEM flightline resistivities provided by Aqua Geo Frameworks and borehole data in profile view.

4.1.3. STATIC WATER LEVELS

Static water-level elevations for spring 2017 were provided by the LPNNRD for 116 observation wells in the SQS2 area. A water table/potentiometric surface (2D grid) with 400 m x 400 m node spacing was generated from these data using the kriging method (Matheron, 1963). The surface was refined over several iterations whereby outliers were located from the 2D grid output and then they were removed from the dataset. Two wells were removed before the grid was finalized.

4.1.4. IRRIGATION PUMPING DATA

Irrigation wells in the SQS2 are required by the LPNNRD to have flowmeters. These flowmeters are read and recorded annually. LPNNRD provided a list of irrigation wells that were pumped during the 2018 and 2019 irrigation seasons (Figure 14). It should be noted that not all 2019 pumping data had been reported to the LPNNRD at the time this report was completed. Therefore, this data is incomplete.

4.2. HYDROSTRATIGRAPHIC MODELING

Hydrostratigraphic models were developed prior to the analysis of groundwater-level hydrographs so that the former interpretations would be unbiased by the latter. The models were created in GeoScene3D, which contains tools for both cognitive-layer modeling and geostatistical voxel modeling. The software provides simultaneous visualization of maps, profiles, and 3D views. It also allows for computation and manipulation of grids and voxel models.

4.2.1 ADDRESSING THE RESISTIVITY-LITHOLOGY RELATIONSHIP

A simple approach was used to develop a generalized resistivity-lithology relationship. CSD test hole data within the SQS2 study area were used for this purpose because the lithology interpretations are more accurate and more standardized than driller's logs. The nearest AEM sounding to each test hole was extracted from the resistivity-depth dataset for comparison to the test hole data. This approach is similar to the approaches used in previous AEM studies in Nebraska (Aqua Geo Frameworks, 2017; Carney et al., 2015; Divine & Korus, 2012; Korus et al., 2013; Korus et al., 2017) and elsewhere, such as Denmark (Jørgensen et al., 2013) and Canada (Morgan et al., 2019).

Commercial software, LogPlot8, was used to plot the water levels, interpreted aquifer top and bottom, lithology, geophysical/electrical logs, and AEM resistivities by depth for each test hole for a qualitative analysis (Figure 16). The water level measured during the drilling of the test hole logs was used if one existed. For some test holes, no such measurement was made, so for those sites the interpolated water level was extracted from the spring 2017 water table/potentiometric surface map. GeoScene3D was used to measure an interpreted aquifer top and bottom by depth for both approaches. For all of the plots, if the aquifer top or bottom was the same for both approaches, then only one symbol was used. For the sake of simplicity, the colors used to represent lithology were the same colors as those used in the GeoScene3D project. Geophysical-logs (G-logs) and electrical-logs (E-logs) were plotted for those test holes with such data. The AEM

resistivities were gleaned from the ascii files containing the resistivity and depth for each sounding. The sounding located nearest to the test hole was used for this purpose.

The qualitative analysis focused on relating lithology to AEM resistivity using visual analysis. Because AEM is less vertically resolved than the G-logs, E-logs, or lithological descriptions, it was necessary to identify the dominant characteristics within broad zones and relate them to overall AEM resistivity trends. The AEM resistivity commonly remained the same over large lengths but the lithology changed considerably in thin sections. In such cases the dominant lithology was identified from the log. Data on the static water level allowed for the identification of any trends related to water saturation.

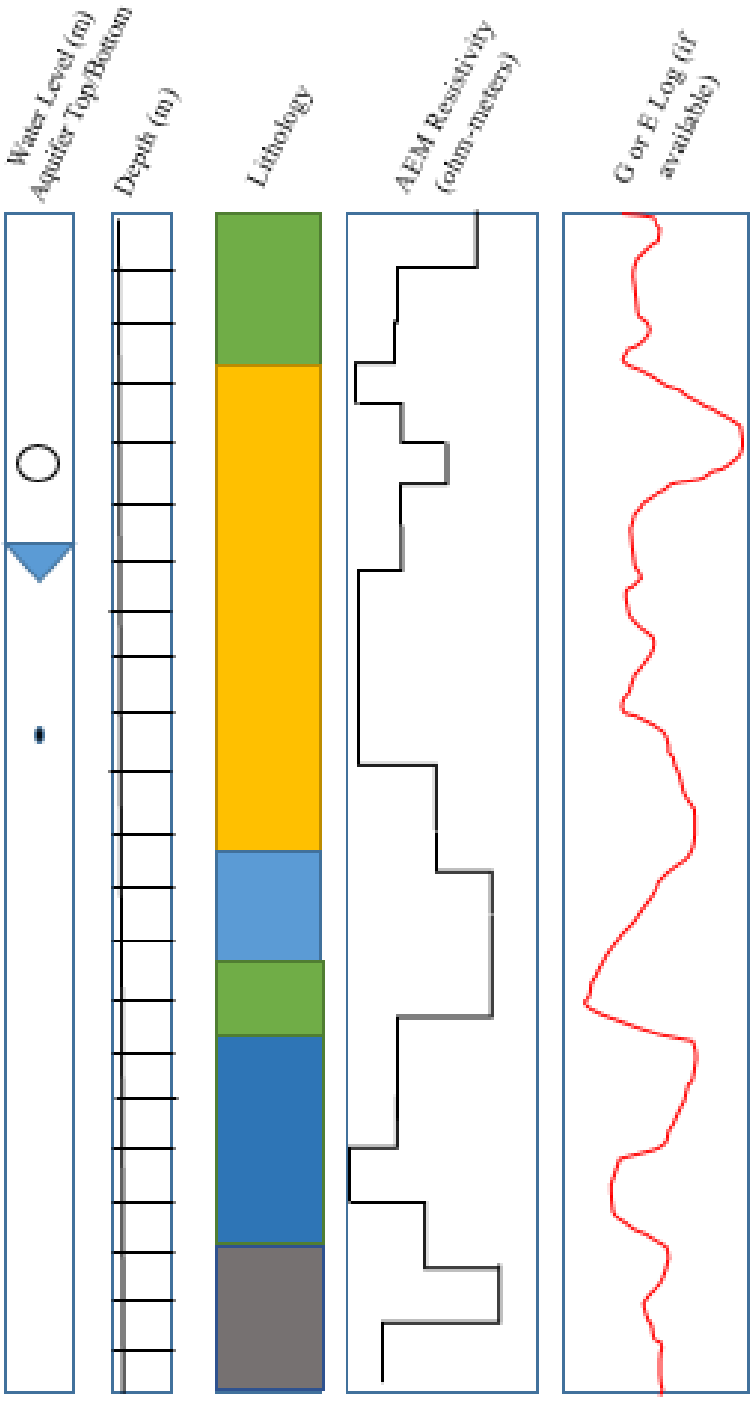

Figure 16 General format of the logplot figures for qualitative analysis. The cognitive aquifer top and bottom symbols are black, while the statistical were violet. The blue inverted triangle represents the water level.

4.2.2. COGNITIVE-LAYER MODELING

The cognitive-layer modeling approach (hereafter called “layer model”) involved viewing borehole lithology logs superimposed on the resistivity-depth profiles in GeoScene3D. The modeler then digitized points along interpreted geologic and hydrostratigraphic contacts in each of the 29 profiles. The x, y, and z coordinates of each point were automatically stored in a background database. Interpretation of Cretaceous stratigraphic units was highly dependent on the stratigraphic information from CSD test holes because the great depths and highly conductive nature of these units limited the ability of AEM to resolve stratigraphic contacts. These units are therefore highly generalized. The bedrock surface was interpreted using all the boreholes (CSD and DNR). Each borehole was examined for bedrock lithology, and the AEM resistivity was used as a guide between boreholes. In many areas, the bedrock surface was defined by a contrast between high resistivity above and low resistivity below.

The top of the aquifer was interpreted by generally following the lithology shown in the borehole logs and using the AEM resistivity as a guide in sparse borehole areas. Multiple profile windows were open at once in order to better visualize the 3D structure during interpretation. Aquifer materials (indicated by warmer colors) were traced along the profiles by digitizing points at regularly spaced intervals. This process was subjective, but it allowed the modeler to use geologic knowledge to generate geologically realistic structures. In general it was understood that the borehole logs and water levels were hard data (therefore more accurate) and the AEM resistivities were soft data—a guide to interpretation between boreholes. In locations where the aquifer material appeared to be

located very near or at the land surface, the points representing the top of the aquifer were digitized above the land surface. Although this is geologically impossible, it allows the resulting grid to be adjusted downward later in the modeling process to exactly match the land surface (described below).

After all of the points were digitized they were then interpolated into a 200 m x 200 m 2D grid using the kriging method. This grid could then be projected onto each profile as a line in the profile window. The grid was edited and refined during several iterations. The spring 2017 water table or potentiometric surface was also projected onto the profiles (Figure 17).

Because the aquifer top sometimes extended above the terrain and the water level, it had to be adjusted by selective filtering in the GeoScene3D toolbox (high pass/low pass). This filtering process adjusted the aquifer top grid downward so that it never exceeds the elevation of the water-level surface. Within each profile, the adjusted aquifer top and the water-level surfaces were plotted for comparison to identify confined and unconfined areas. Wherever the top of an aquifer is lower than the actual water level, that aquifer is confined (Figure 17). This space between the water level and the top of the aquifer is a confining unit composed of clay-rich material. In other areas, the water-level and the aquifer top two surfaces intersect, indicating an unconfined aquifer.

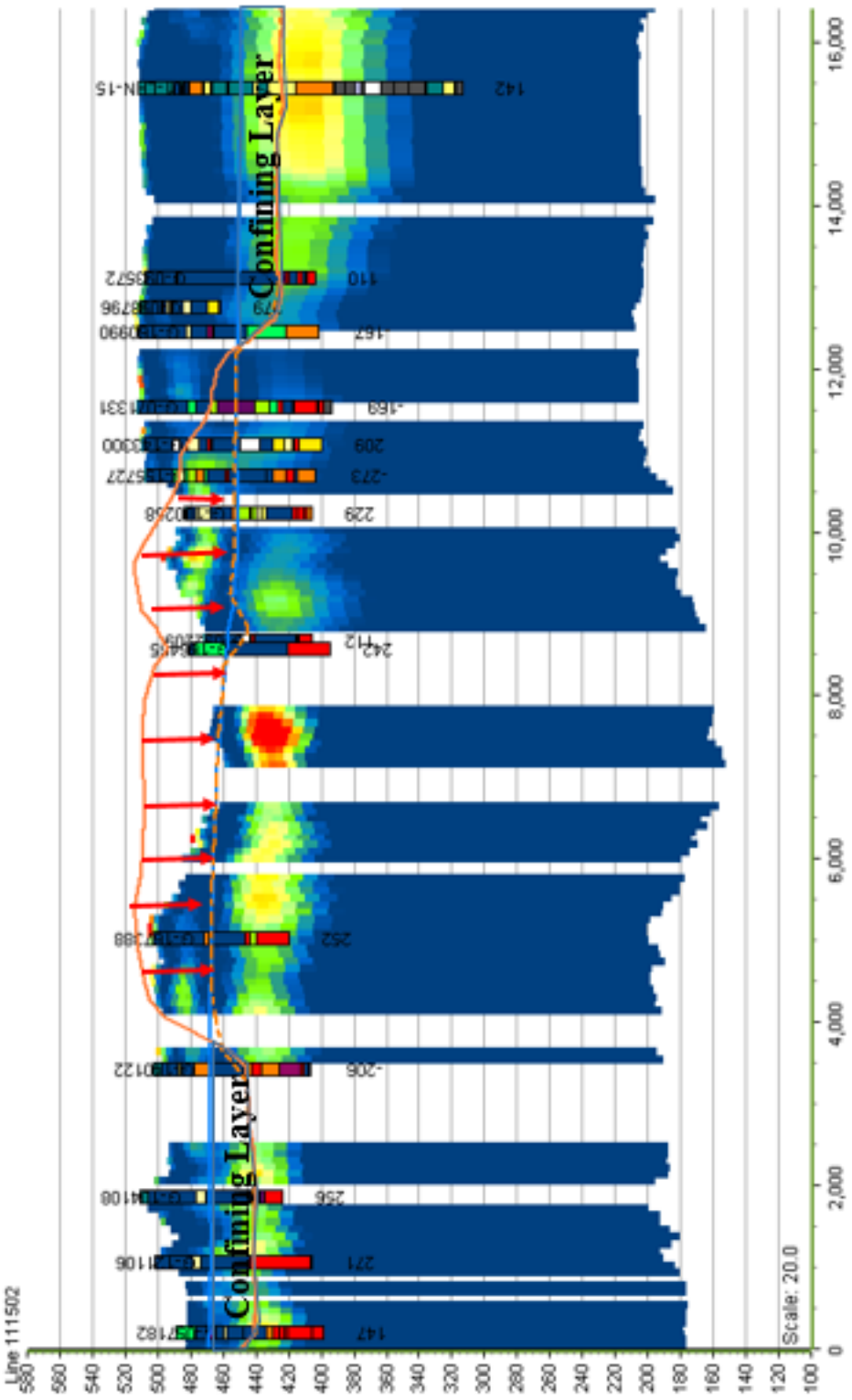

Figure 17 Layer model showing how the aquifer top (orange) was adjusted down to the water level (blue). Where the aquifer top was located below the water level, there's evidence for a confined aquifer.

These two types of aquifer regions were displayed in 3D view and in map view in GeoScene3D. This was done by using both the spring 2017 water level grid and the aquifer top adjusted grid in the toolbox. Grid math was used to create a difference grid whereby the aquifer top was subtracted from the water level, yielding the thickness of the confining unit. The water-level grid was resampled prior to the operation so that its node spacing matched the node spacing of the aquifer-top grid (200 m x 200 m). The color scale was then modified so that areas of zero thickness (unconfined aquifers) were distinguished from areas of nonzero thickness (confined aquifers).

4.2.3. VOXEL-BASED GEOSTATISTICAL MODELING

Voxel-based geostatistical modeling (hereafter called “voxel model”) was completed for the subsurface volume between the bedrock surface and the terrain. The resistivity-depth models were interpolated to a 3D grid using the kriging method. The resulting voxel model contained interpolated resistivity values. This model was then made into a simplified voxel model representing three different classes of lithology based on the earlier comparison of resistivity and lithology. Each cell was classified as either (1) silt, clay, or till, (2) v. fine-medium sand, or (3) Coarse sand-gravel. Each class represents a distinct range of hydraulic conductivities pertinent to hydrostratigraphy. The same flightline shown in Figure 17 is shown in Figure 18, which shows how the voxel model appeared in profile view. It is clear that the voxel model matches well with the AEM resistivities near it because it is solely based on AEM resistivities. It also shows an advantage to the voxel modeling method: it fills in the gaps based on the 3D grid

interpolation of the AEM data as opposed to where the layer model estimates what is between.

The voxel model was truncated at the interpolated water table/potentiometric, surface using voxel tools in GeoScene3D in order to map aquifers. Areas in which silt, clay, or till was intersected by the water-level surface were mapped as confined aquifers. The regions in which the water level surface intersected very fine to medium sand, or coarse sand-gravel, were mapped as unconfined aquifers.

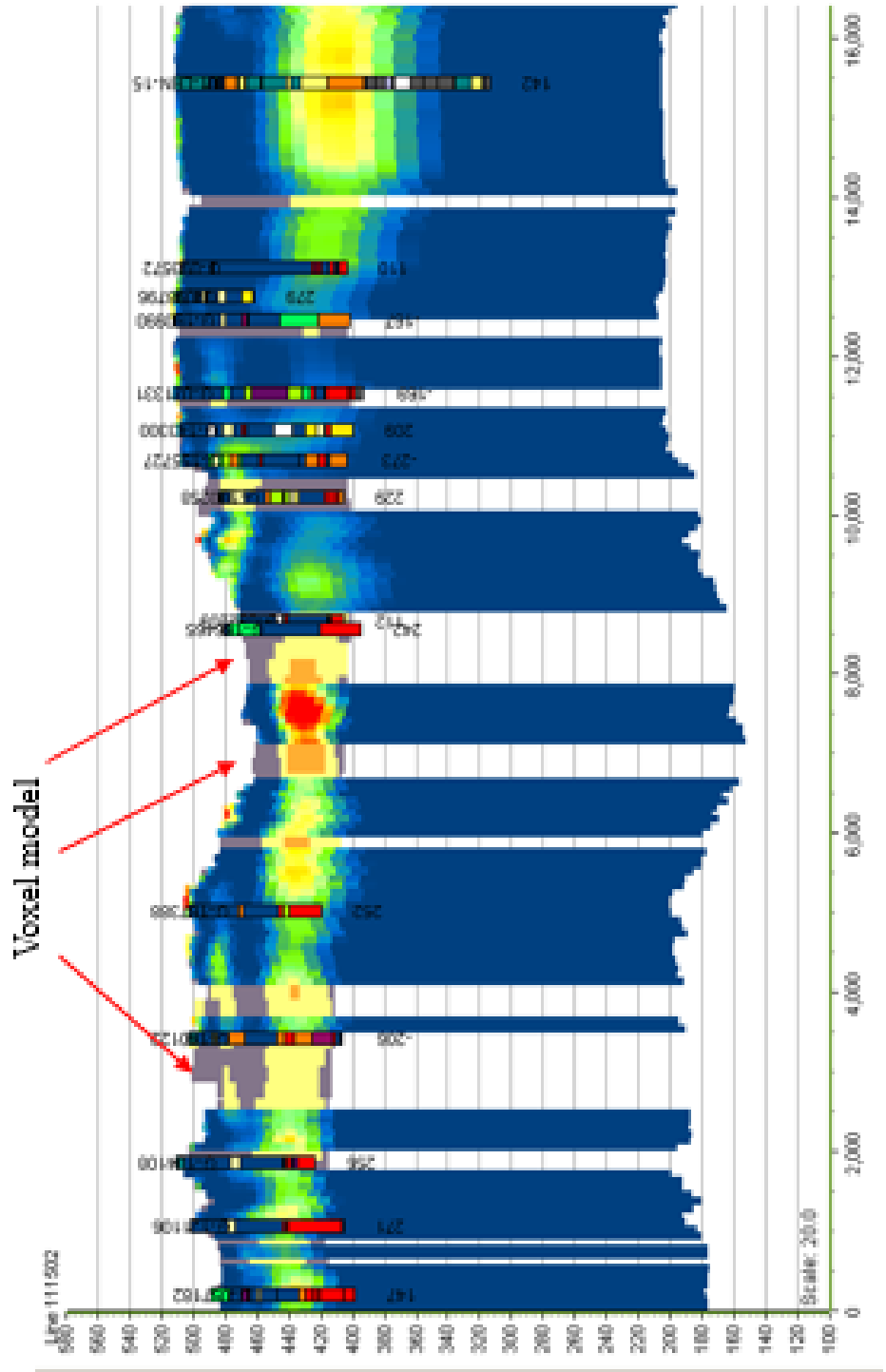

Figure 18 Voxel model shown on profile view which is noticeably based on the AEM data and helps fill in gaps due to the 3D nature of the method

Although kriging is a probabilistic geostatistical model, the way in which the kriging results were converted into lithology was deterministic: we used a binned resistivities approach whereby certain ranges of resistivity were grouped together and converted into different lithologies. The ranges were predetermined on the basis of a deterministic resistivity-lithology transformation. In this way, the voxel model is somewhat of a hybrid approach incorporating both probabilistic and deterministic models.

4.3. WATER-LEVEL DATA COLLECTION AND ANALYSIS

Additional ground-truth data were collected by installing pressure transducers (loggers) in PVC drop pipes installed in the gravel packs of irrigation wells. The drop pipes are required by the NRD as a condition of new well permits. The loggers were set to record hourly measurements of the depth to water. The focus was on the irrigation season, although measurements were made year-round. The hourly logging interval ensured that any sudden changes due to pumping were shown clearly.

4.3.1. WELL SELECTION AND INSTALLATION OF EQUIPMENT

A search using the Nebraska DNR website well data was conducted for irrigation wells that lie within a buffer of 30 meters from a flight line to get a representation of the aquifers located nearest to the AEM. We then went out into the field to consider if these wells could be used as observation wells. The LPNNRD provided a list of recommended wells, including some that are known to go dry as the result of irrigation pumping and others were known to be abandoned and located adjacent to another irrigation well, thereby making an ideal location to observe drawdown. After these wells were all

selected, the LPNNRD assisted in obtaining permission from the landowners to use the wells for obtaining data. Others were already equipped with loggers, so these wells have a relatively long period of record.

The depth of the pump for each well was determined from the DNR registration information. This depth was used to design the necessary cable lengths such that the water level did not fall below the depth of the loggers. Photographs were taken at a couple well sites while manually measuring water levels and downloading water level data from the loggers (Figures 19 and 20). Two types of shelters were used to contain the PVC drop pipe and protect the attached cable for the logger. There were 6 well sites equipped with loggers during the 2018 irrigation season that showed some responses to pumping. By November, 2018, there were 21 well sites equipped with loggers and recording water levels at one hour intervals. These wells recorded data for the following irrigation season in 2019. We did not receive data for wells G-167111 and G-152943 during this season. Therefore, the recorded well water levels in the 2019 irrigation season was a total of 19.

Figure 19 Shelter containing drop pipe with transducer cable showing the connection to the center pivot (A); same well with the water level being taken (B)

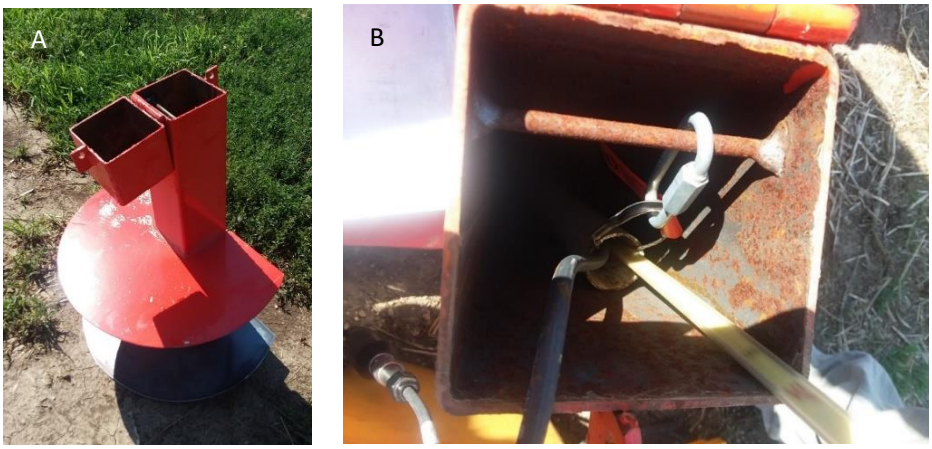

Figure 20 An alternate shelter for pressure transducer within a drop pipe (A) and water level being taken from similar installed shelter showing the PVC drop pipe (B)

4.3.2. HYDROGRAPH FORMULATION AND ANALYSIS

Hydrographs from these continuous water level measurements were plotted using a customized code in Matlab (www.mathworks.com). A generalized, qualitative analysis of the drawdown patterns over time were completed following the methods of Butler et al. (2013). The hydrographs were subdivided into three categories. (1) Hydrographs from

wells that were located adjacent to one another (within a few hundred meters) were plotted together by syncing the test start and end dates and lining up the graphs vertically. (2) Hydrographs showing data from both the 2018 and 2019 irrigation seasons were plotted in full. Then the irrigation periods were plotted separately to zoom in on the drawdown curves. (3) Hydrographs showing only 2019 irrigation season data, and that were located several km away from another logged well, were shown individually. The hydrographs were then interpreted for general characteristics in the aquifer at those points. This interpretation included the continuity of the aquifer between wells (compartmentalized vs. open) and whether the aquifer was confined or unconfined at each site.

CHAPTER 5. RESULTS

5.1. COMPARISON OF BOREHOLE LITHOLOGY AND AEM RESISTIVITY

The geologic materials encountered in CSD test holes were divided into 37 lithological categories (Figure 21). The resistivity-lithology relationship was explored by plotting the lithology, water level, and borehole geophysics next to the nearest AEM resistivity-depth model. The patterns that were exhibited in these figures give a general overview of how the AEM data fits or does not fit the observed geology at each test hole site.

The deep CSD test holes drilled in 2015 and 2018 (Figures 22 – 24) exhibited good correlation between AEM resistivity and lithology. In general, the AEM resistivity is highest—deflecting to the right—where there are thick (> 20 m) layers of aquifer material such as coarse sand and gravel (shown in green boxes). Many thin (< 10 m) layers of sand interbedded with silt and clay do not have a corresponding AEM resistivity deflection, even though the borehole resistivity log does have a rightward deflection (e.g. from 30 – 40 m in 1-LPN-15). Non-aquifer material such as silt, clay, till, and shale appears as relatively low AEM resistivity (deflection to the left). The resistivity generally decreases below the bedrock surface. Overall, the AEM resistivity broadly follows the trend in the borehole resistivity logs, but fine details are not resolved.

The test holes drilled in 1955 show these same general trends (Figures 25 – 28). However, some thin (10 – 15 m) layers of till within sandy units do not appear to be represented in the AEM resistivity.

Using a qualitative review of AEM resistivity and CSD test hole lithology, as well as a comparison between AEM and DNR borehole logs in GeoScene 3D, it was determined that the best-fitting representation of lithology from AEM resistivity was the following; (1) 0 – 17.5 ohm-m representing silt, clay, or till, (2) 17.5 – 25 ohm-m representing very fine to medium sand, and (3) 25 – 100 ohm-m representing coarse sand and gravel. These ranges were used as a general guide to interpreting between boreholes in the layer model. However, the ranges given above were used to directly subdivide the voxel model into lithological categories.

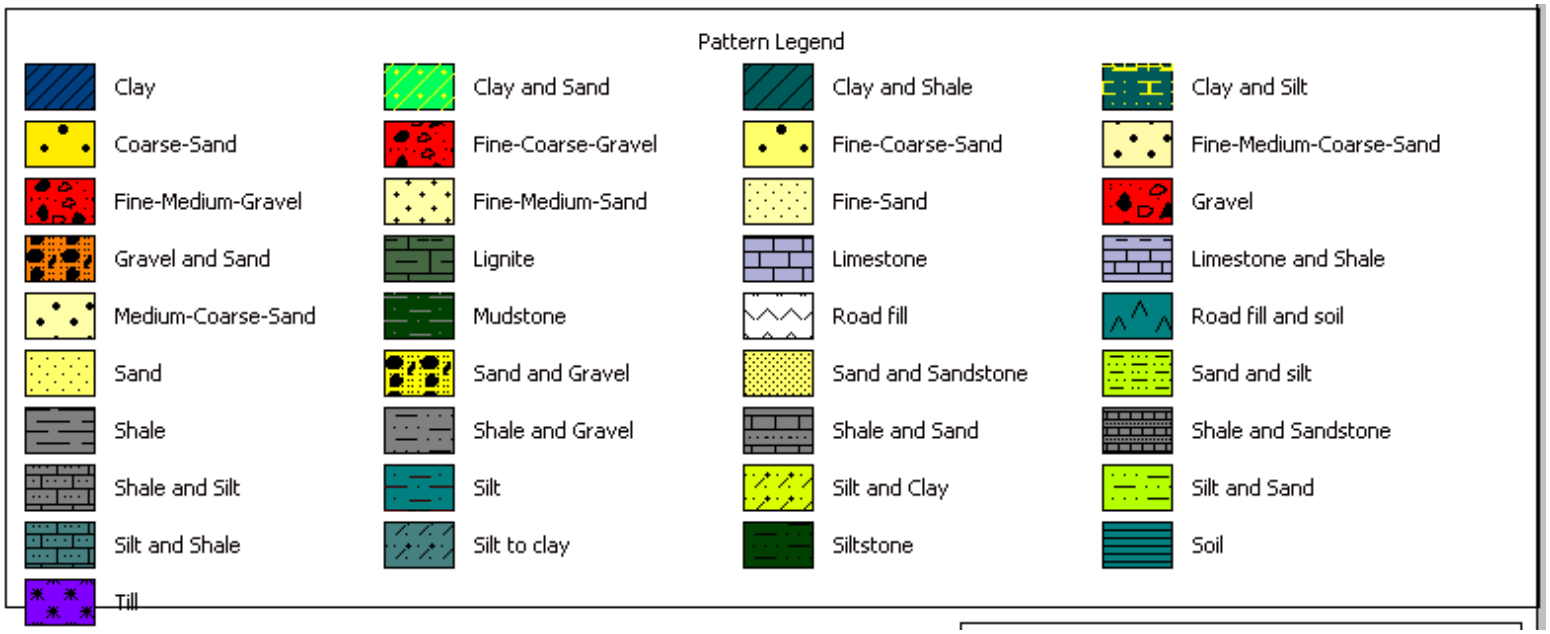

Figure 21 Lithology legend for LogPlot Figures showing CSD Test holes. The colors and terms are the same used in the hydrostratigraphic model borehole descriptions.

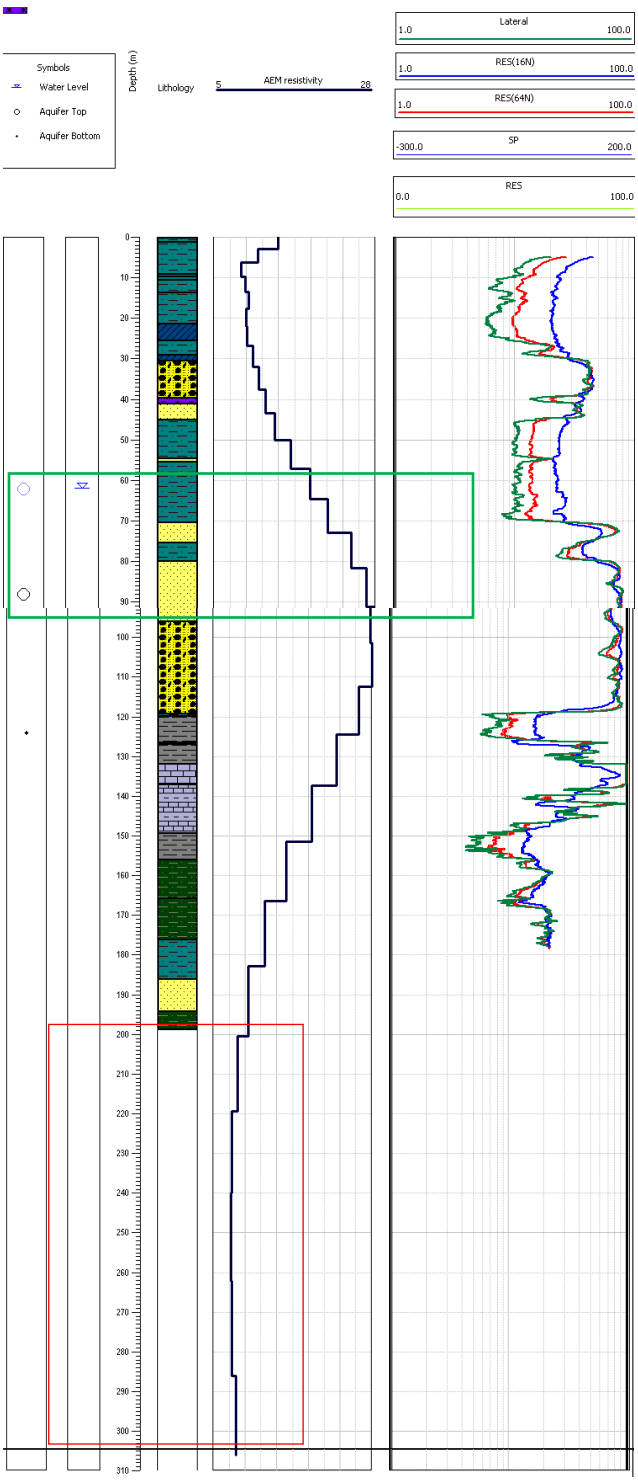

Figure 22 CSD Test hole 1-LPN-15. Boxes show where the AEM resistivity increases when it hits the aquifer material (green) and decreases when it hits the finer grained/bedrock material (red).

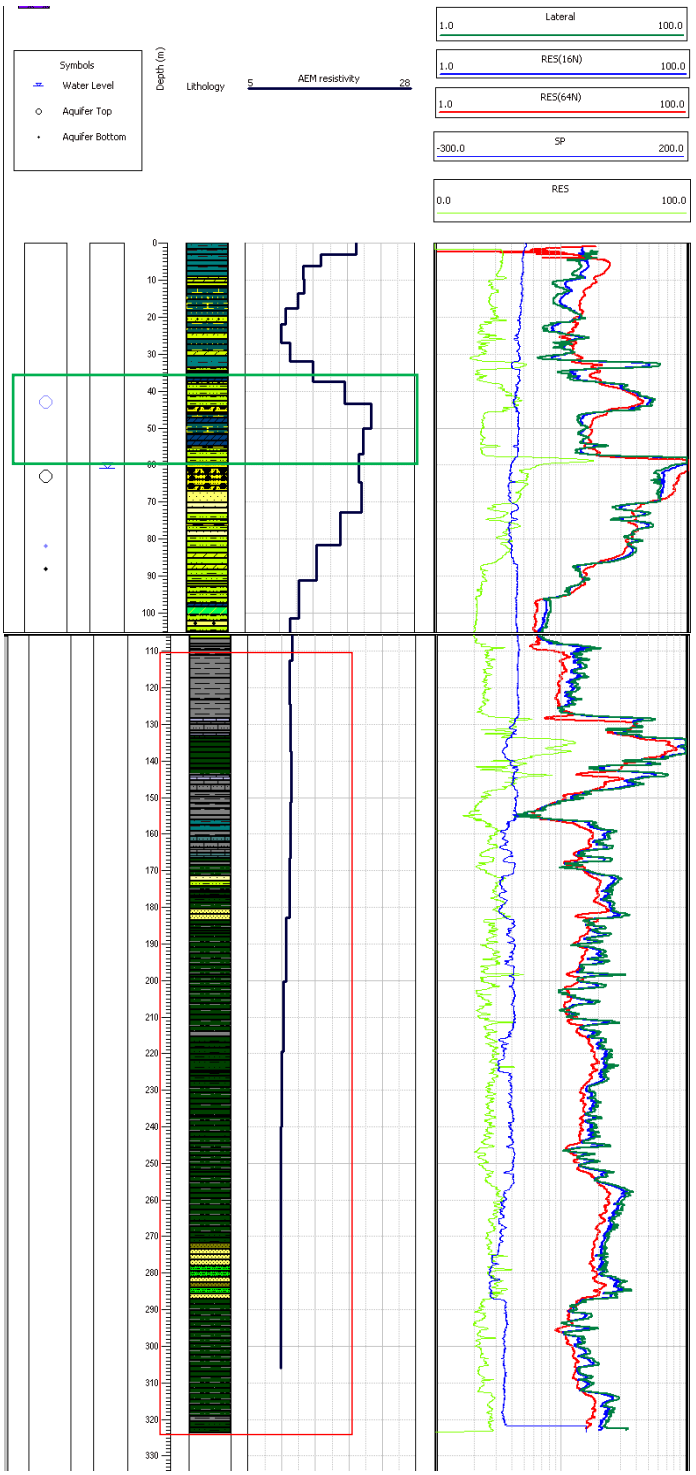

Figure 23 CSD Test hole 2-LPN-18 Boxes show where the AEM resistivity increases when it hits the aquifer material (green) and decreases when it hits the finer grained/bedrock material (red).

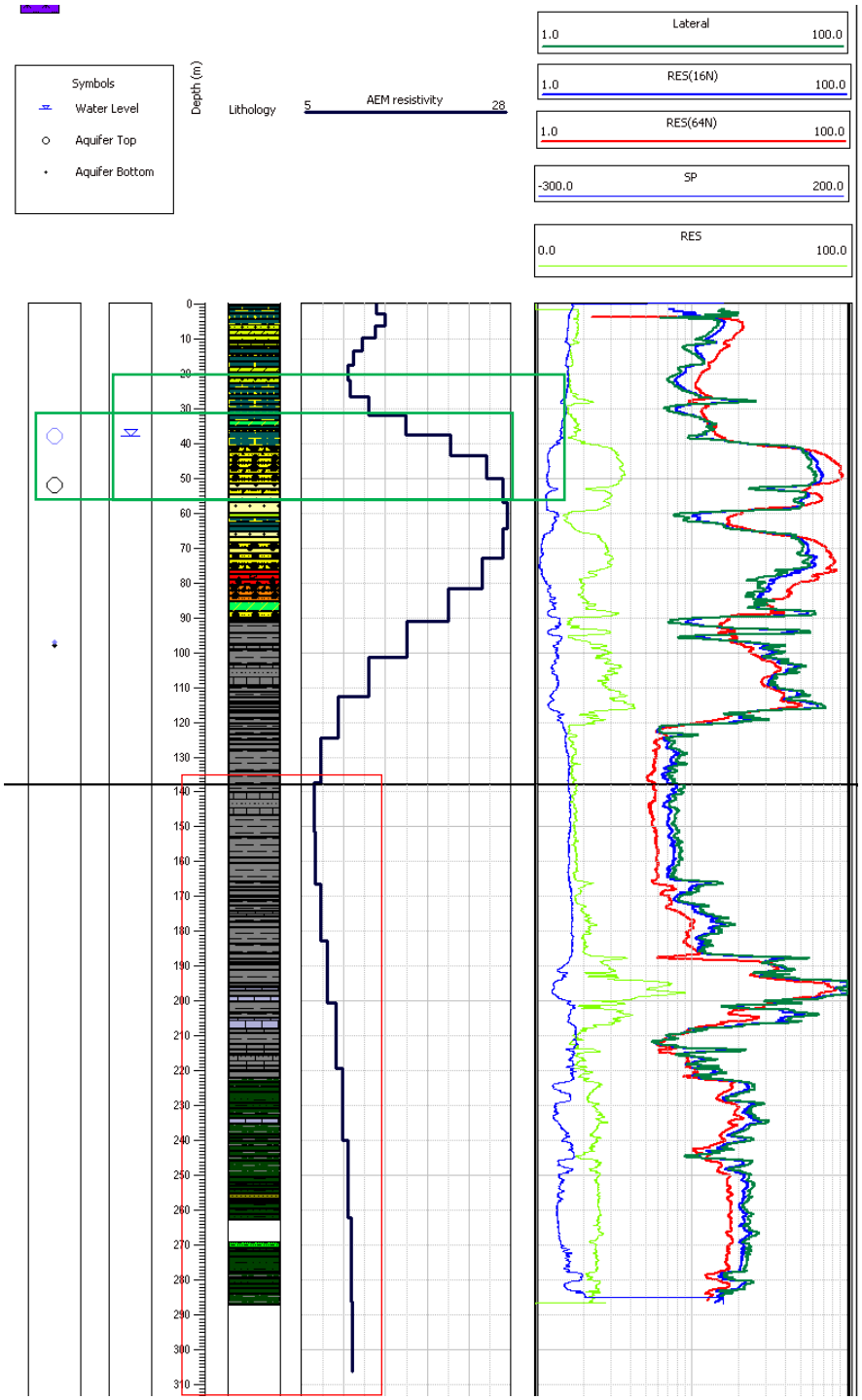

Figure 24 CSD Test hole 3-LPN-18. Boxes show where the AEM resistivity increases when it hits the aquifer material (green) and decreases when it hits the finer grained/bedrock material (red).

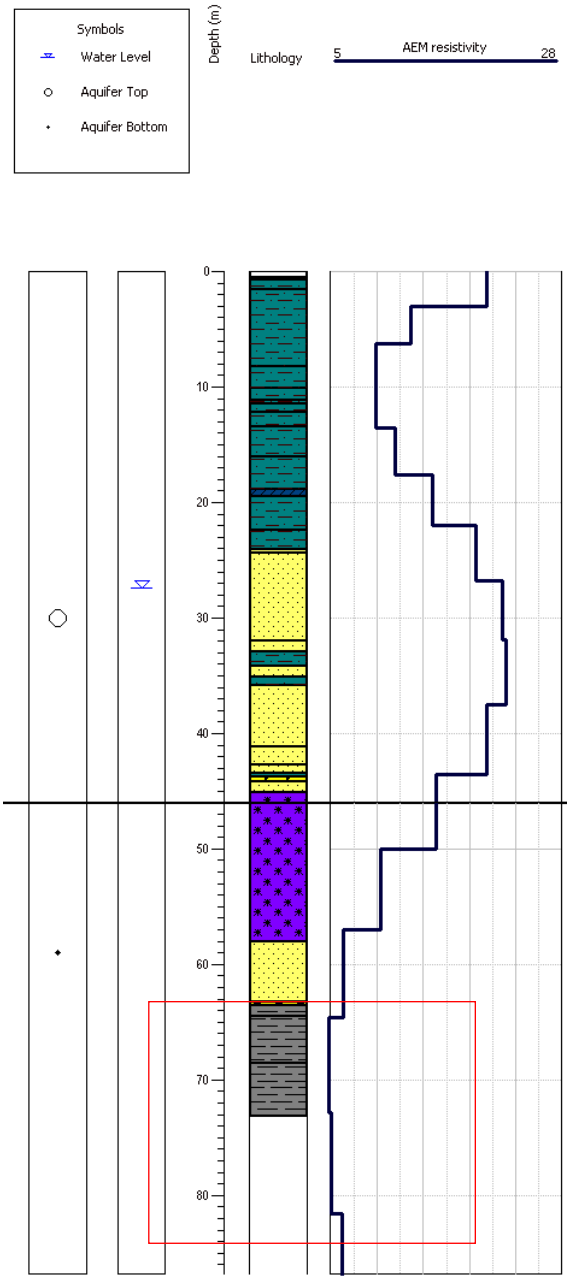

Figure 25 CSD Test hole 1-A-55. Boxes show where the AEM resistivity increases when it hits the aquifer material (green) and decreases when it hits the finer grained/bedrock material (red).

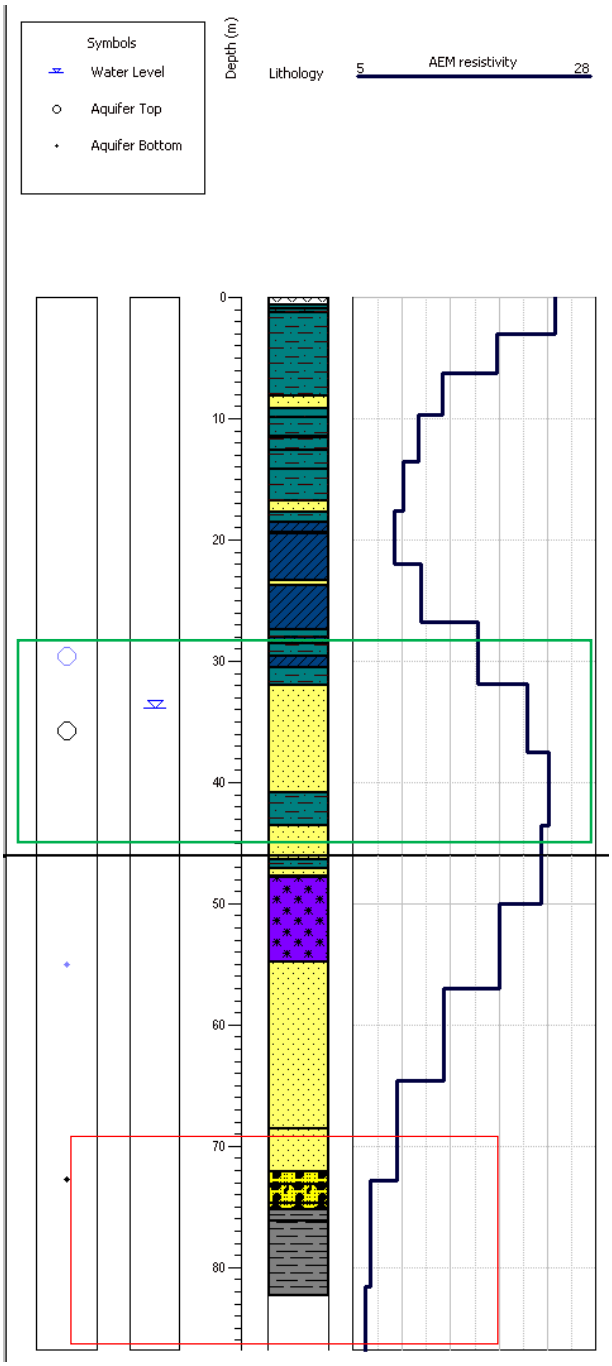

Figure 26 CSD Test hole 2-A-55. Boxes show where the AEM resistivity increases when it hits the aquifer material (green) and decreases when it hits the finer grained/bedrock material (red)

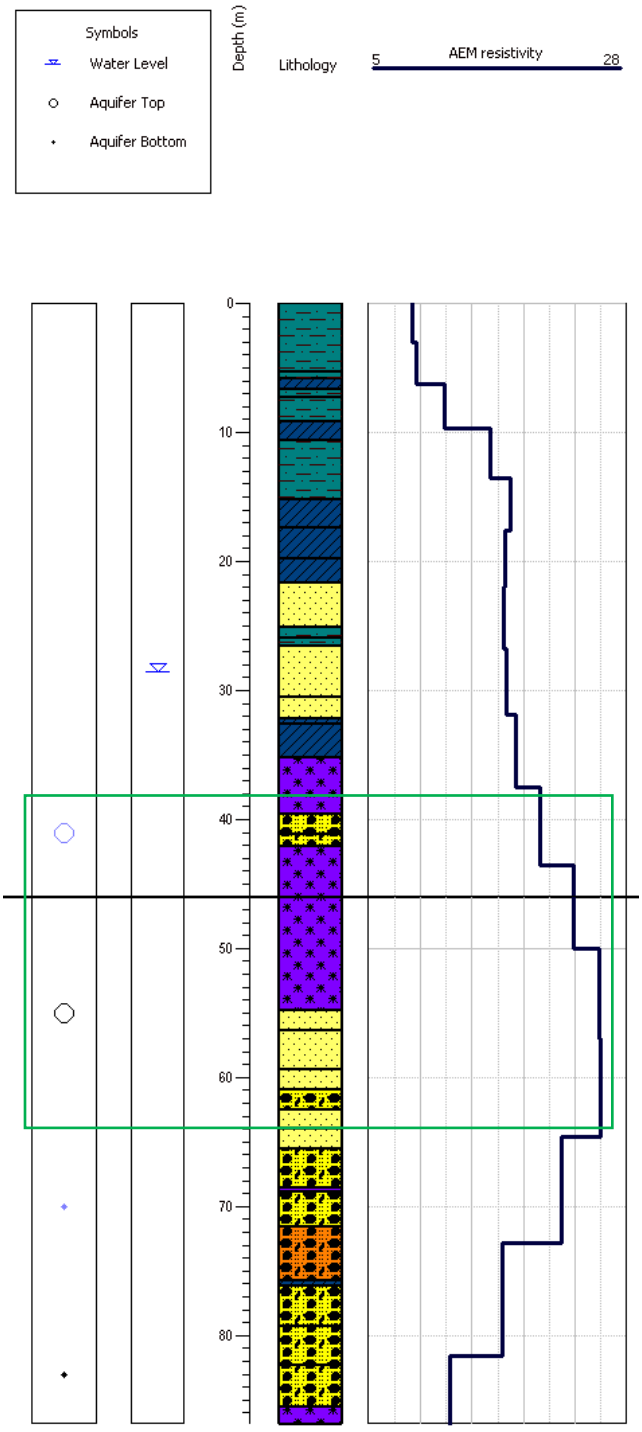

Figure 27 CSD Test hole 3-A-55. Green box shows where the AEM resistivity increases when it hits the aquifer material.

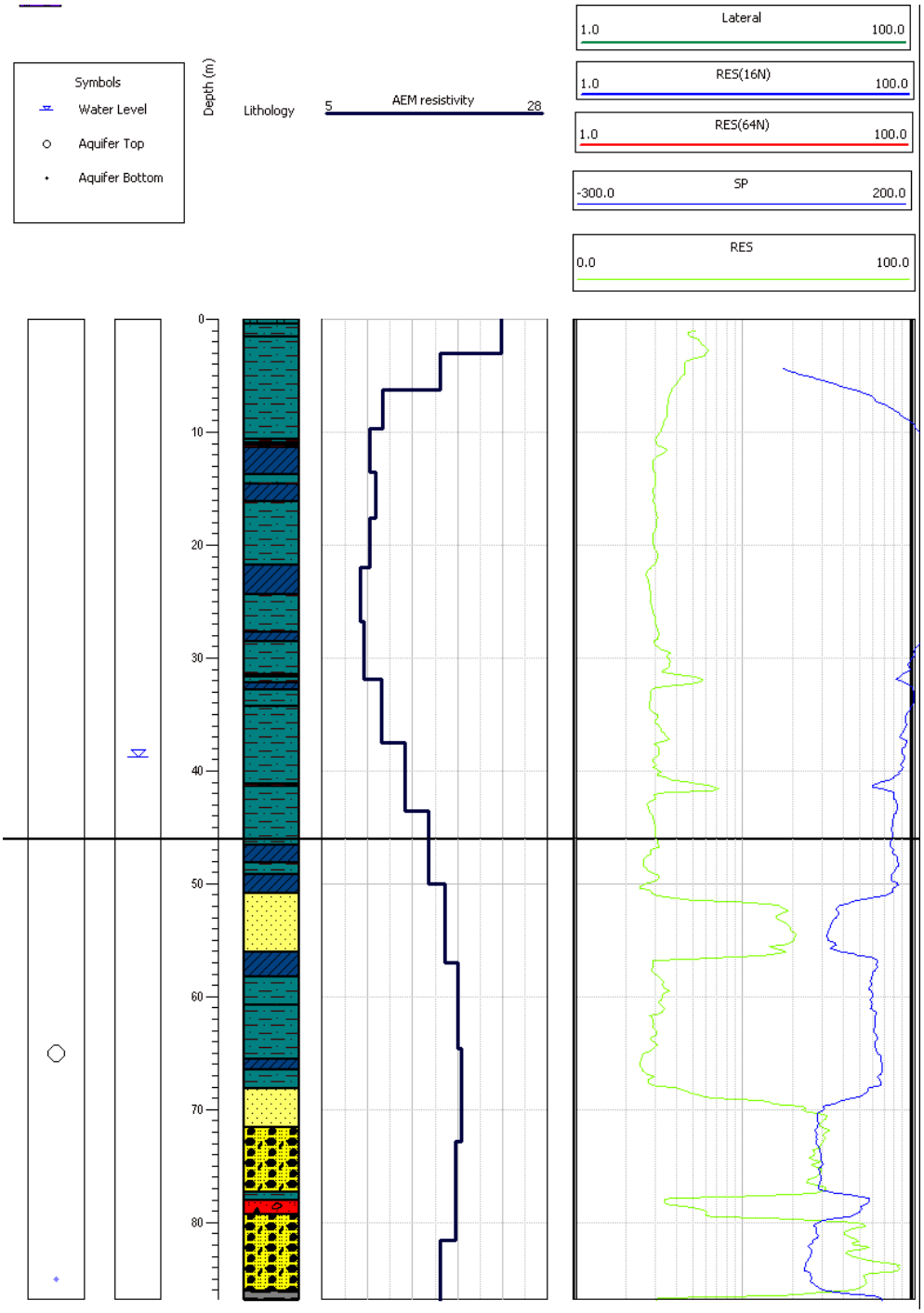

Figure 28 CSD Test hole 22-A-5

5.2. WATER- LEVEL SURFACE

The water-level surface was modeled as a single surface using the static water-level readings from spring 2017. However, this single surface represents one of two possible conditions: it is either the water table surface or it is a potentiometric surface. It is a water table surface in areas where the water level lies below the top of aquifer materials. It is a potentiometric surface where it lies above the top of the aquifer.

The water-level surface ranges from an elevation of 426 m to 492 m above sea level. It slopes generally east-southeast (Figure 29). There is an abrupt “step” in the water level from the south-center to the middle part of the study domain.

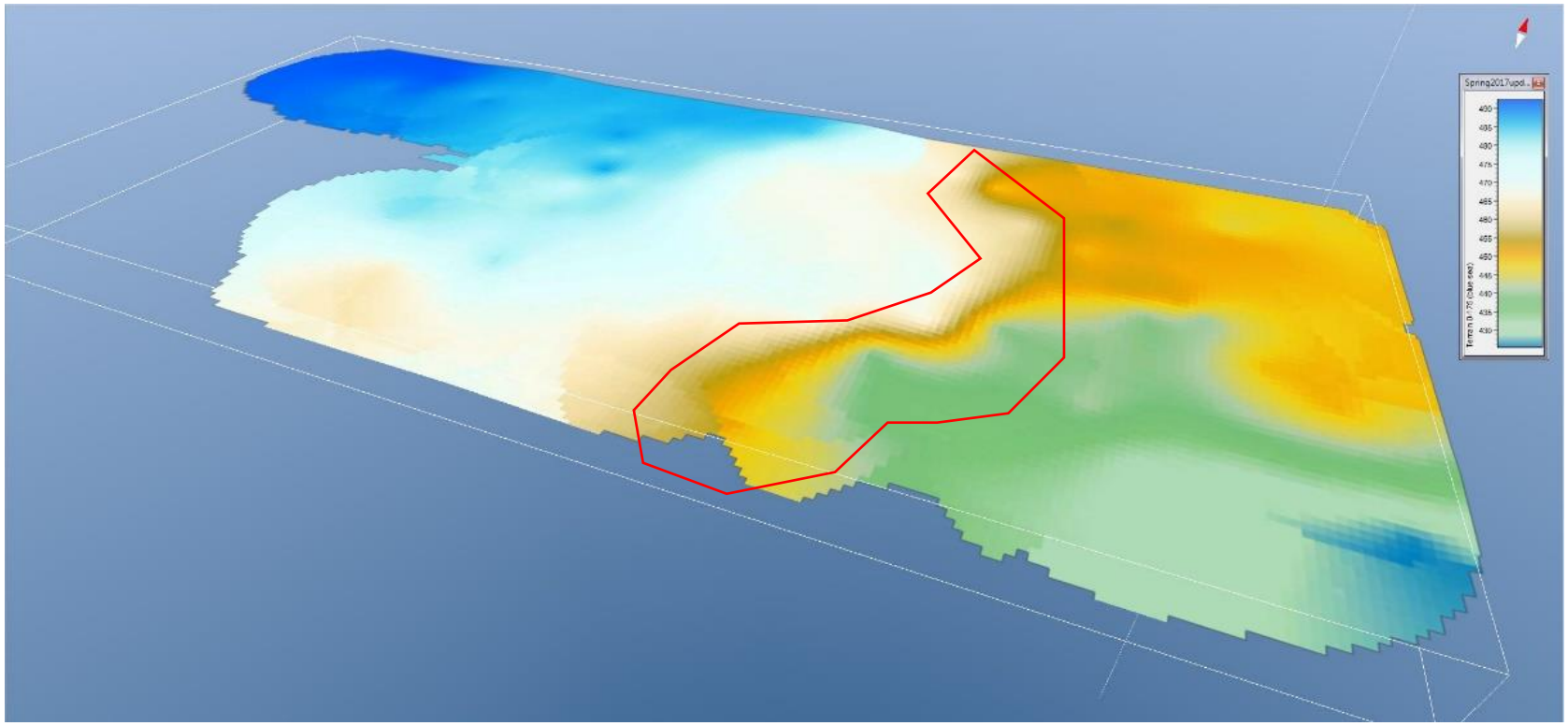

Figure 29 3D view of water-level surface model looking northwest. The abrupt step in water level is outlined in red.

5.3. BEDROCK SURFACE

The bedrock surface represents the base of the principal aquifer (Figure 30). It ranges in elevation from 388 to 442 m above sea level. It slopes generally east, but a narrow, west-east trending, trough-like feature is prominent across the middle of the model domain. Several other irregularities also exist, including a subtle ridge in the southeast part of the model.

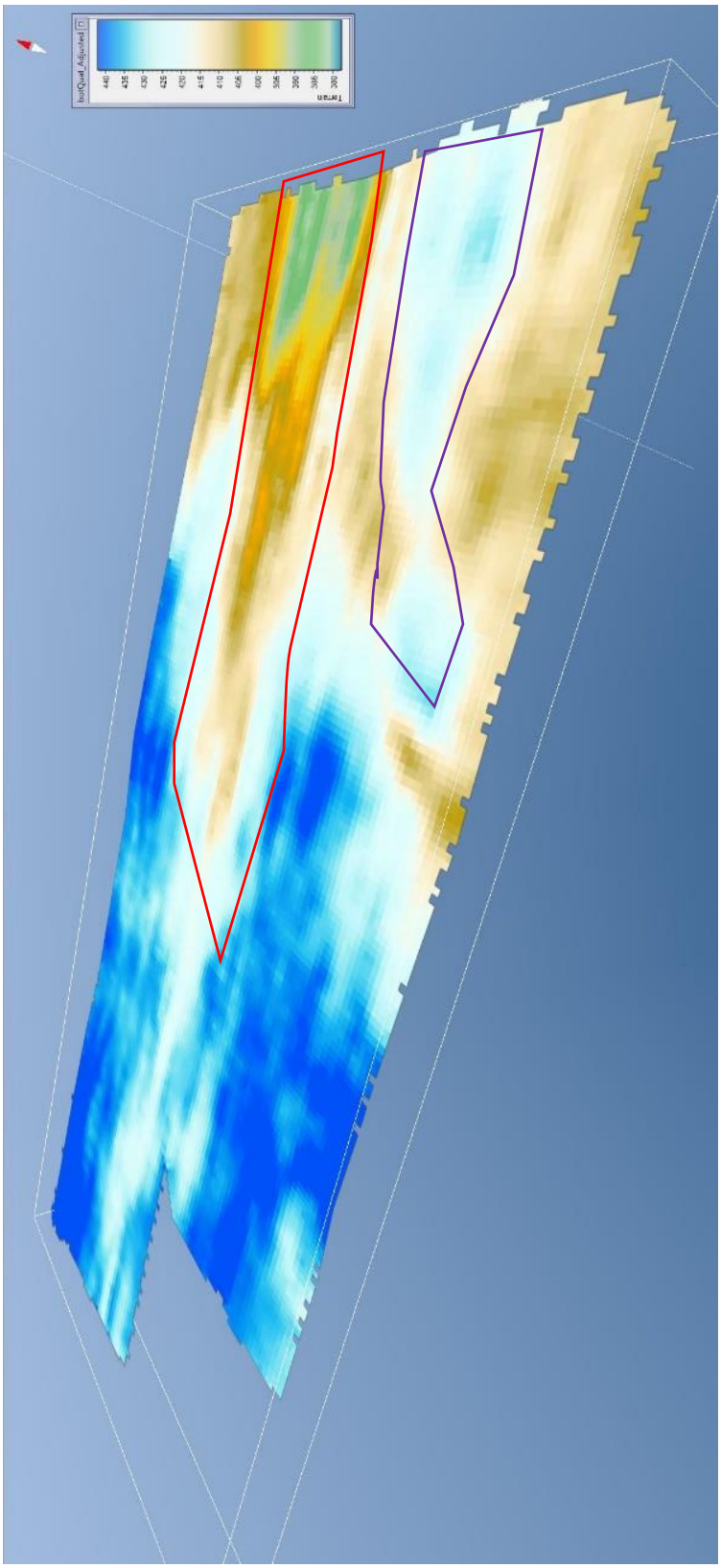

Figure 30 3D view of bedrock surface model looking northwest. Dimensions of bounding box are: x = 37,472 m; y = 15,881 m; z = 200 m. Trough-like feature outlined in red. Ridge outlined in purple.

5.4. HYDROSTRATIGRAPHIC MODELS

5.4.1. LAYER MODEL

The digitized interpretation points were interpolated to two main surfaces: the top of the principal aquifer and the bedrock surface, representing the base of the aquifer (Figure 31). The top of the aquifer represents the contact between generally clay- and silt-dominated material above and materials containing thick (> 10 m) layers of sand and gravel below. In areas where the water-level elevation coincides with aquifer material, the surface was adjusted downward, thereby representing the water table. We chose to define one aquifer layer encompassing all major aquifer zones even though it was clear that in some locations the aquifer is multi-layered. The one-layer model is the most reasonable interpretation given the data. Lithology is highly variable between boreholes, and the AEM resistivity did not prove to be a useful guide to the correlation of fine layers below the uppermost aquifer material. Therefore, one layer was a reasonable first approximation of the dataset. Additional details about the kriging results of the 2D interpolation of the digitized points are given in Appendix A.

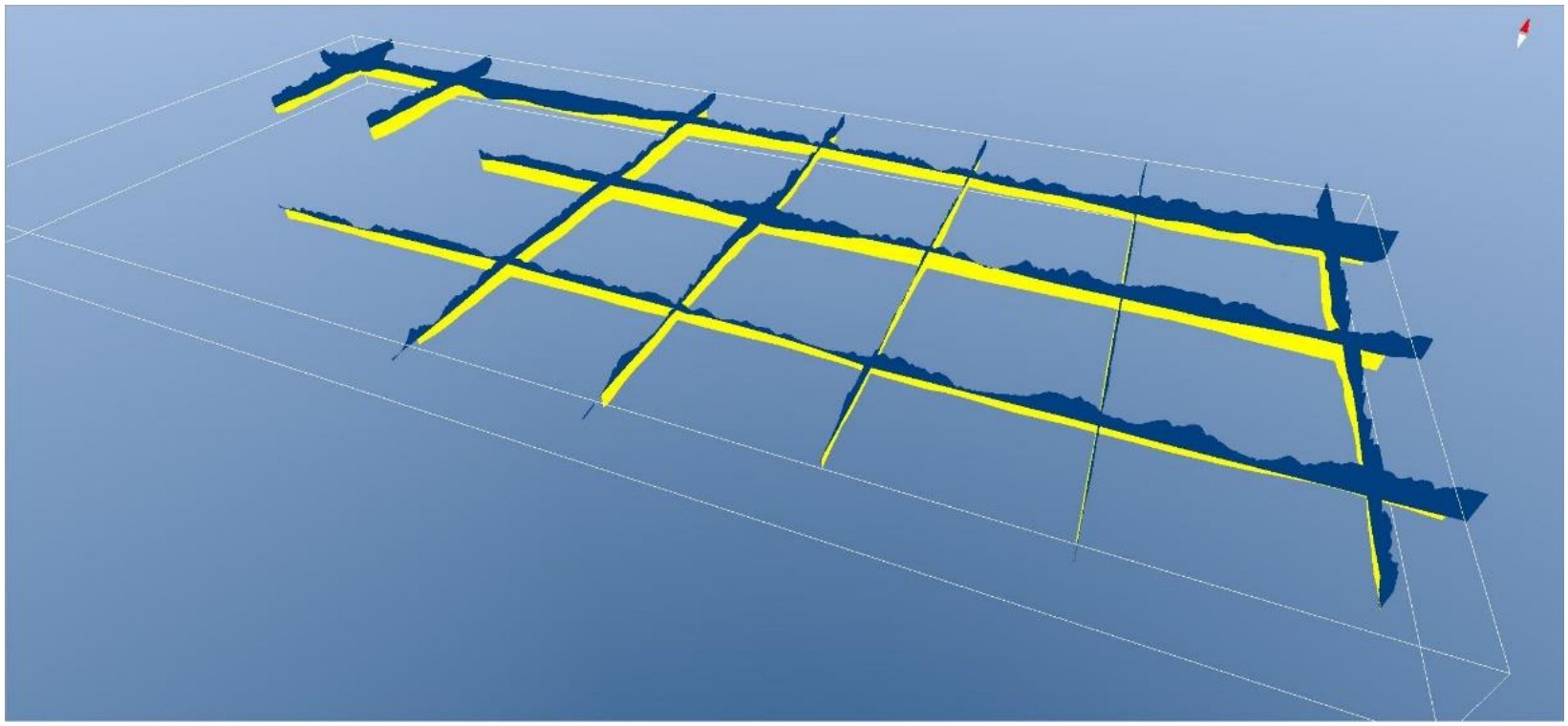

Figure 31 3D view of layer model looking northwest. Aquifer materials (yellow) and geologic materials above the top of the aquifer (blue). Dimensions of bounding box are: x = 37,472 m; y = 15,881 m; z = 200 m

5.4.2. VOXEL-BASED GEOSTATISTICAL MODEL

The voxel model contains 188 columns, 80 layers, and 101 layers. However, only portions of 73 layers between the bedrock surface and terrain were used in this analysis. The cells below the bedrock and above the land surface were blanked using the voxel toolbox in GeoScene3D. Interpolated resistivity ranged between 3.2 and 157.1 Ohm-m. Each cell was classified as either (1) silt, clay, or till, (2) very fine to medium sand, or (3) coarse sand and gravel (according to the resistivity-lithology relationship described above).

Results show that the lithology model contains a semi-continuous, interconnected body of very fine to medium sand or coarse sand and gravel throughout most of the model domain (Figure 32). Only a few small areas lack aquifer materials.
Additional details about the kriging results of the 3D interpolation are given in Appendix A.

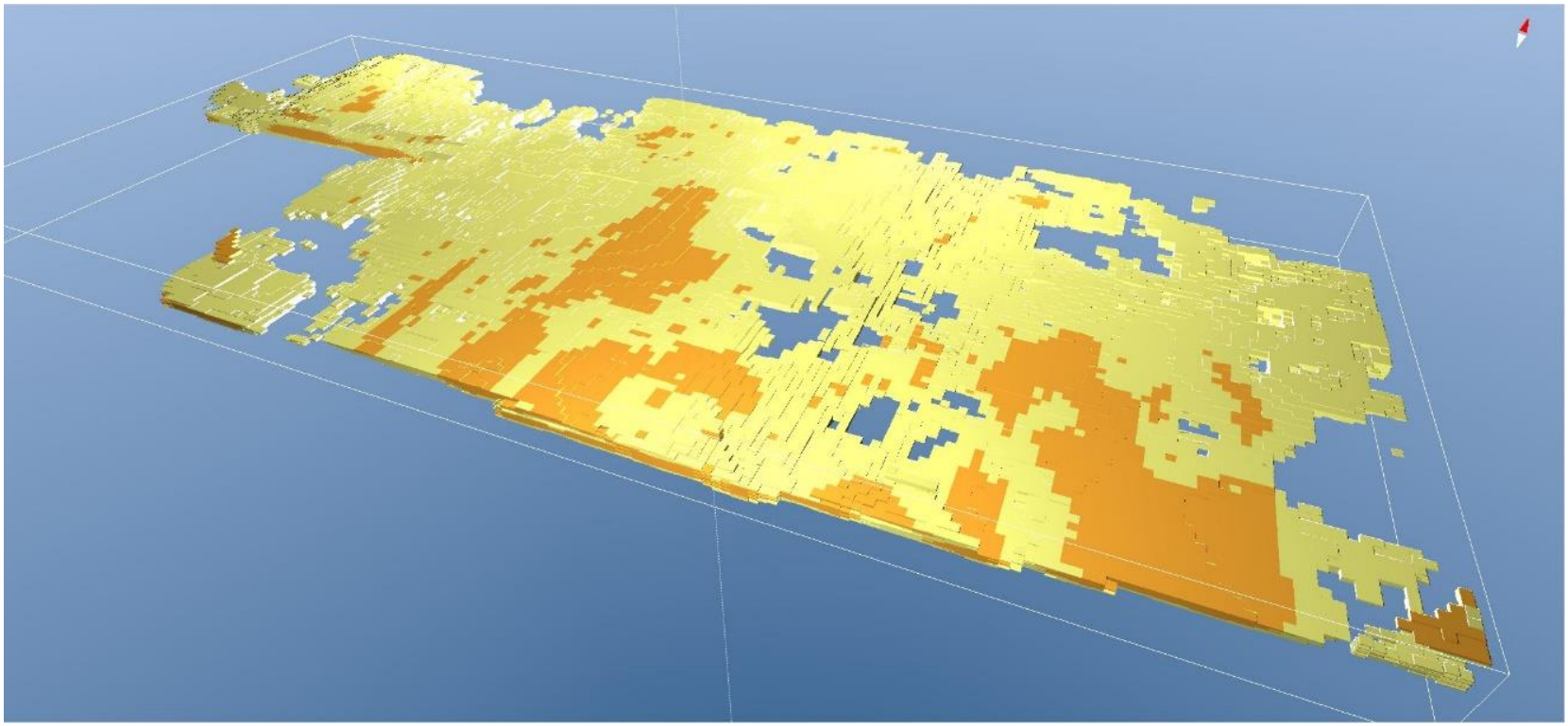

Figure 32 3D view of voxel model looking northwest. Aquifer materials include very fine to medium sand (yellow) and coarse sand and gravel (orange). Only the cells between the bedrock surface and the water-level surface are shown. Dimensions of bounding box are: x = 37,472 m; y = 15,881 m; z = 200 m

5.4.3. MODEL COMPARISON

Comparison of the two modeling approaches in cross sections (i.e. profiles) revealed some important similarities and differences. Because it is impractical to show all of the profiles, the focus here is on three informative profiles that best demonstrated the results of interest (the remaining profiles are provided in Appendix B). A map is provided showing the flightlines included in this comparison (Figure 33). In this comparison, the AEM and borehole data is shown on top, followed by the layer model in the middle (with interpreted aquifer top shown with orange dashed lines and the water level shown with blue lines), and then the voxel model at the bottom (Figures 34-36). It is important to note that the entire AEM resistivity profile is shown in the top two cross sections, whereas the voxel model is shown only between the bottom of the aquifer and the terrain surface.

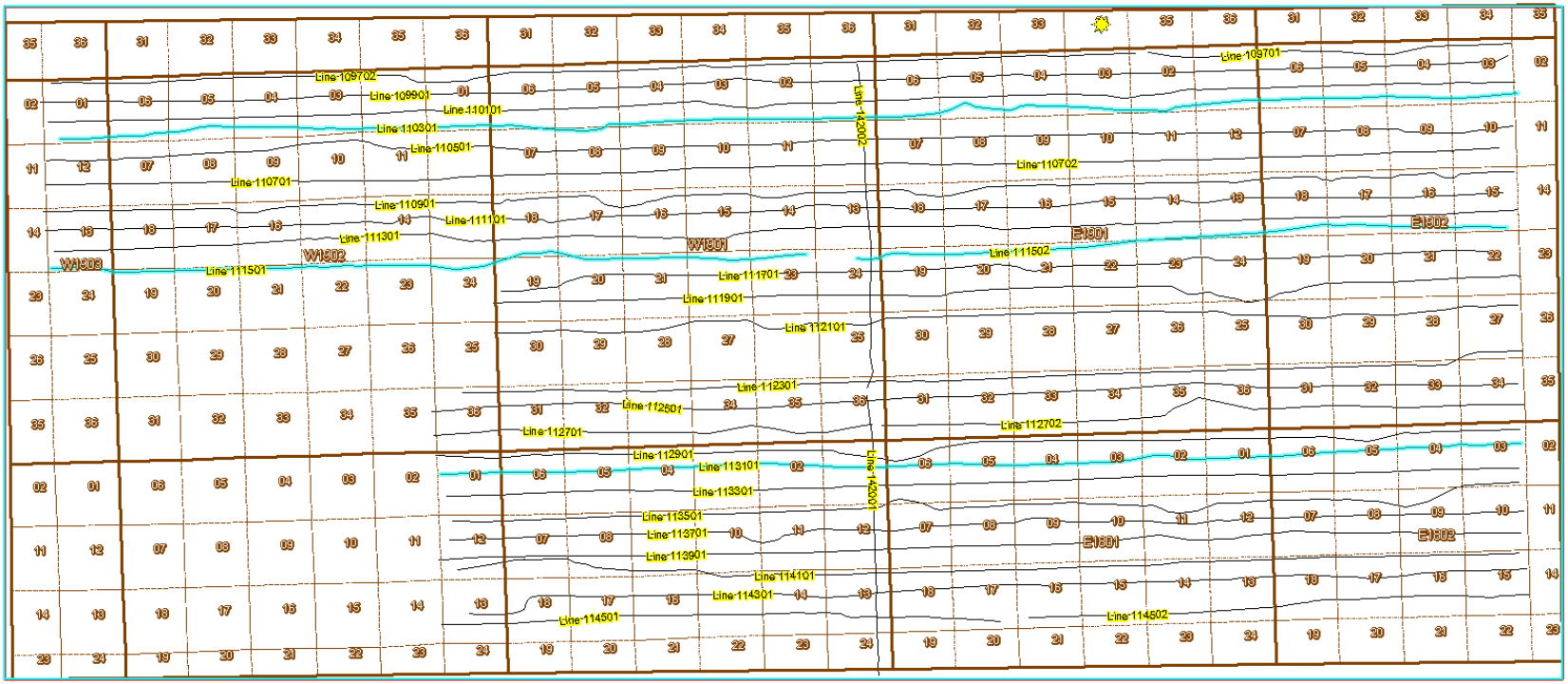

Figure 33 Map of SQS2 area, showing the AEM flightlines. Highlighted lines are shown in profile view in the following figures.

Impermeable units that form continuous boundaries from the top of the aquifer to the bottom (Figure 34). All three cross-sections show evidence of this same boundary. Conversely, the voxel model (Figure 35) shows an impermeable boundary in the center of the profile that is not shown in the layer model. The last flightline (Figure 36) also shows an important difference between the two models. The top of the aquifer in the layer model lies below the water-level surface, indicating confined conditions in the aquifer. However, the voxel model shows unconfined conditions in the same area. The continuity of the aquifer is different in the northern part of the model domain as opposed to the southern part. The voxel model (Figure 34) shows a northern aquifer that is much more disconnected than the more southerly one (Figure 36).

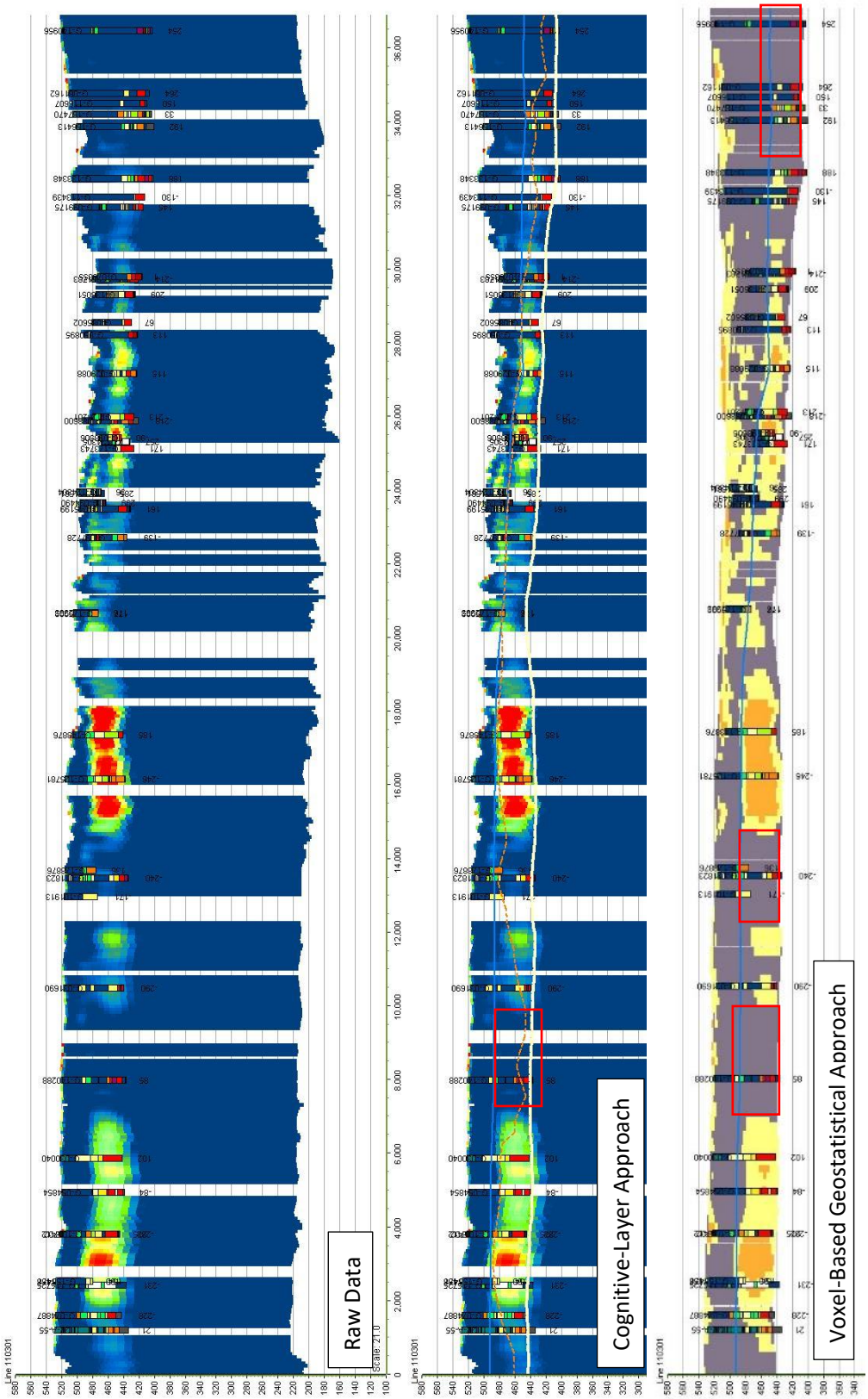

Figure 34 Flight line 110301: Impermeable vertical boundaries outlined in red boxes. Aquifer here is very disconnected. Confinement between the two approaches is similar.

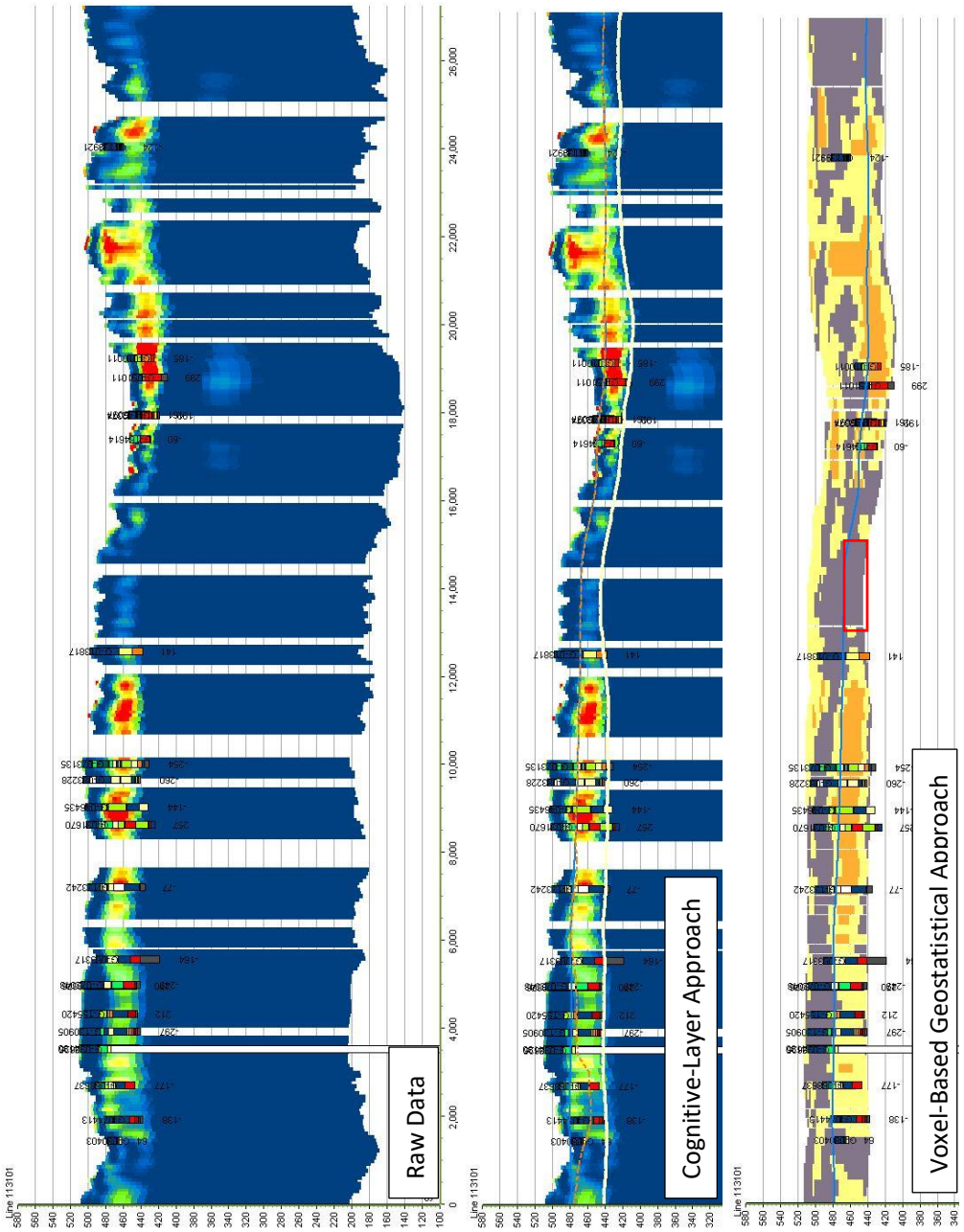

Figure 35 Flight line 113101: An impermeable boundary is shown by the voxel model near the center of the flightline, but the cognitive approach does not show this.

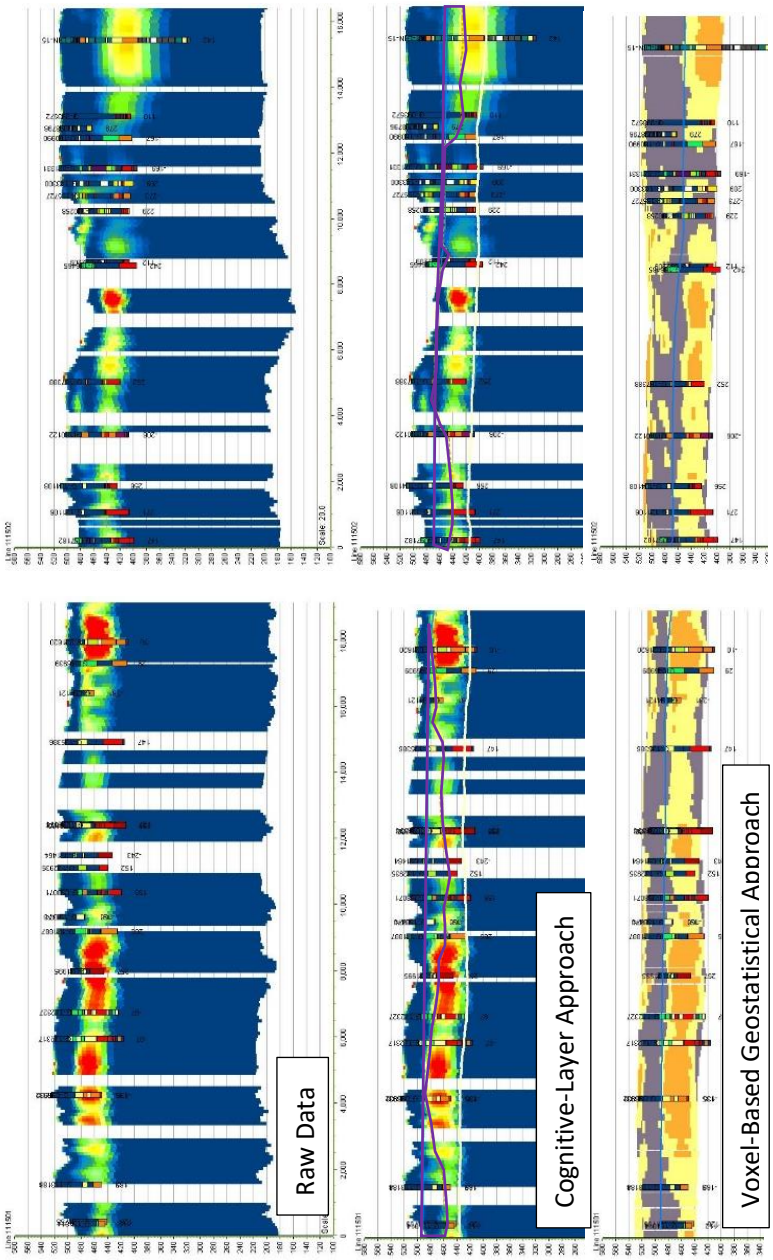

Figure 36 Flight lines 111501 and 111502: The cognitive method shows areas of confinement here that the voxel model does not (outlined in purple). Voxel model shows the aquifer is much more connected here.

Map views were gathered showing the extent of the confining unit based on the layer model (Figures 37 and 38). The confined regions are interpreted based on the difference between the water level and the aquifer-top surfaces. The darker the blue colors represent thicker regions of the confining layer. The voxel model was sliced at the water-level surface and viewed at plan view (Figure 39). The gray regions represent areas where the aquifer is confined (fine grained material above the water-level surface), while the yellow and orange regions show unconfined aquifers (very fine sand to gravel above the water-level surface). The most noticeable difference in these two maps of the confined aquifers are in the east-central part of the study area, shown with a red outline. Here, the layer model indicates that this area is unconfined, while the voxel model shows it as confined.

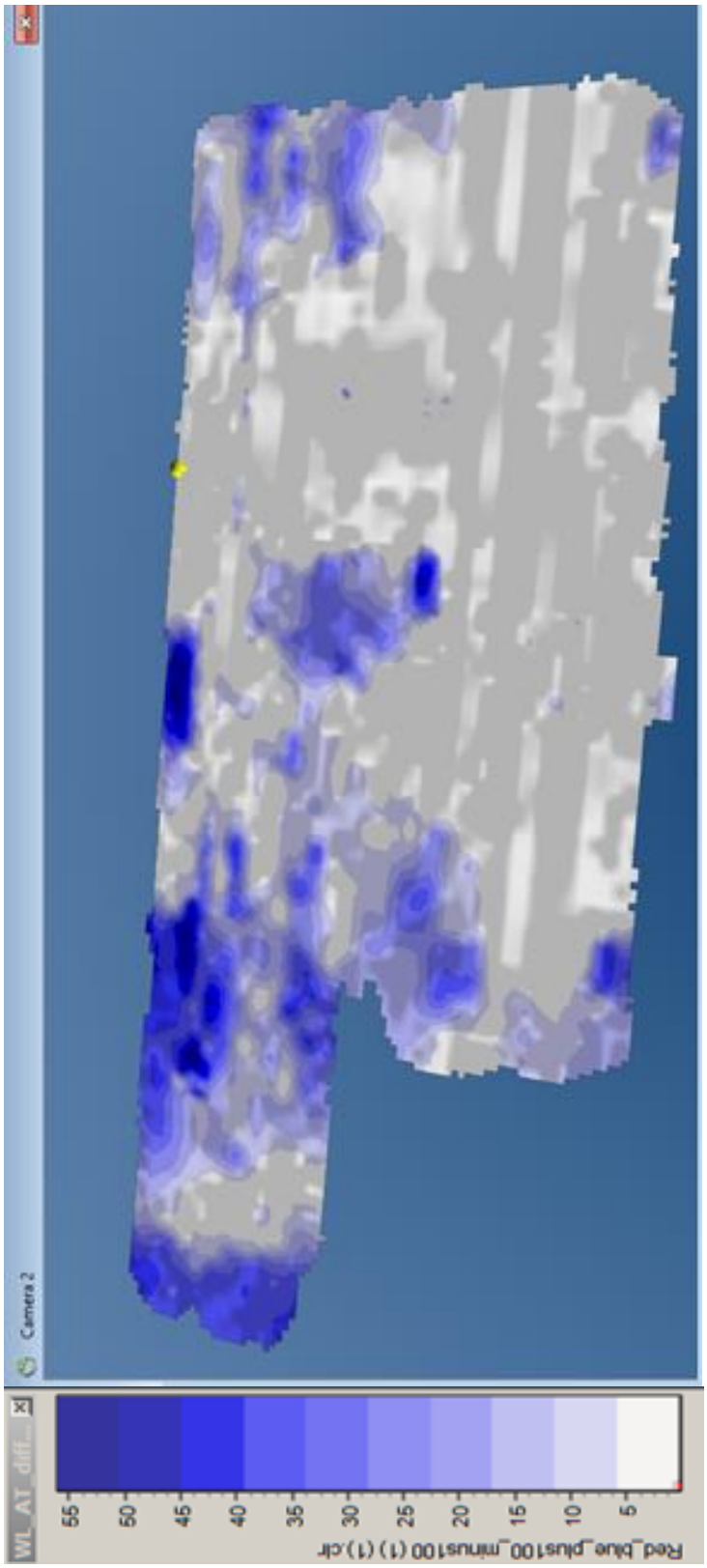

Figure 37 3D view of cognitive approach at water-level surface. The color scale shows the difference between the water-level and aquifer-top surfaces in meters.

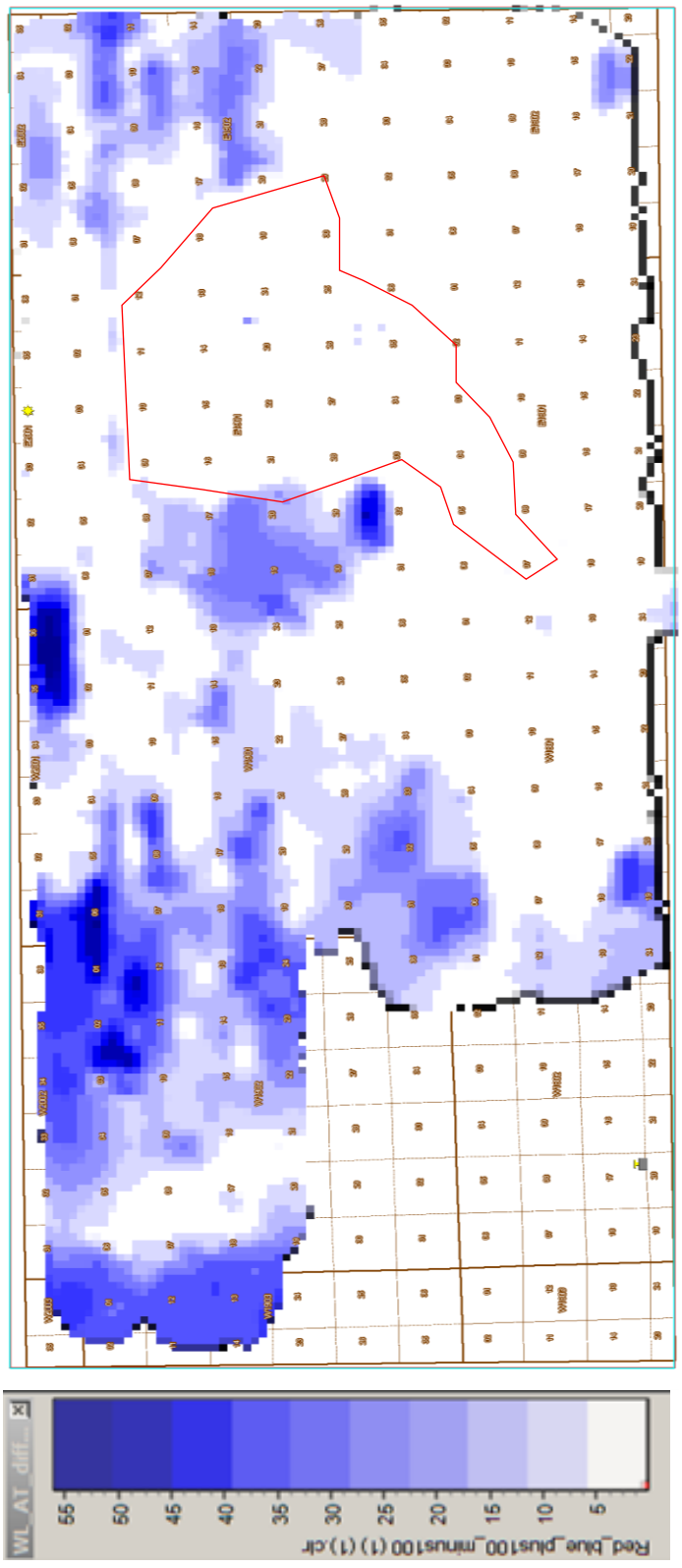

Figure 38 Map view of cognitive approach difference grid at water-level surface. The red shape outlines where this approach shows an unconfined aquifer in contrast to what the voxel model showed.

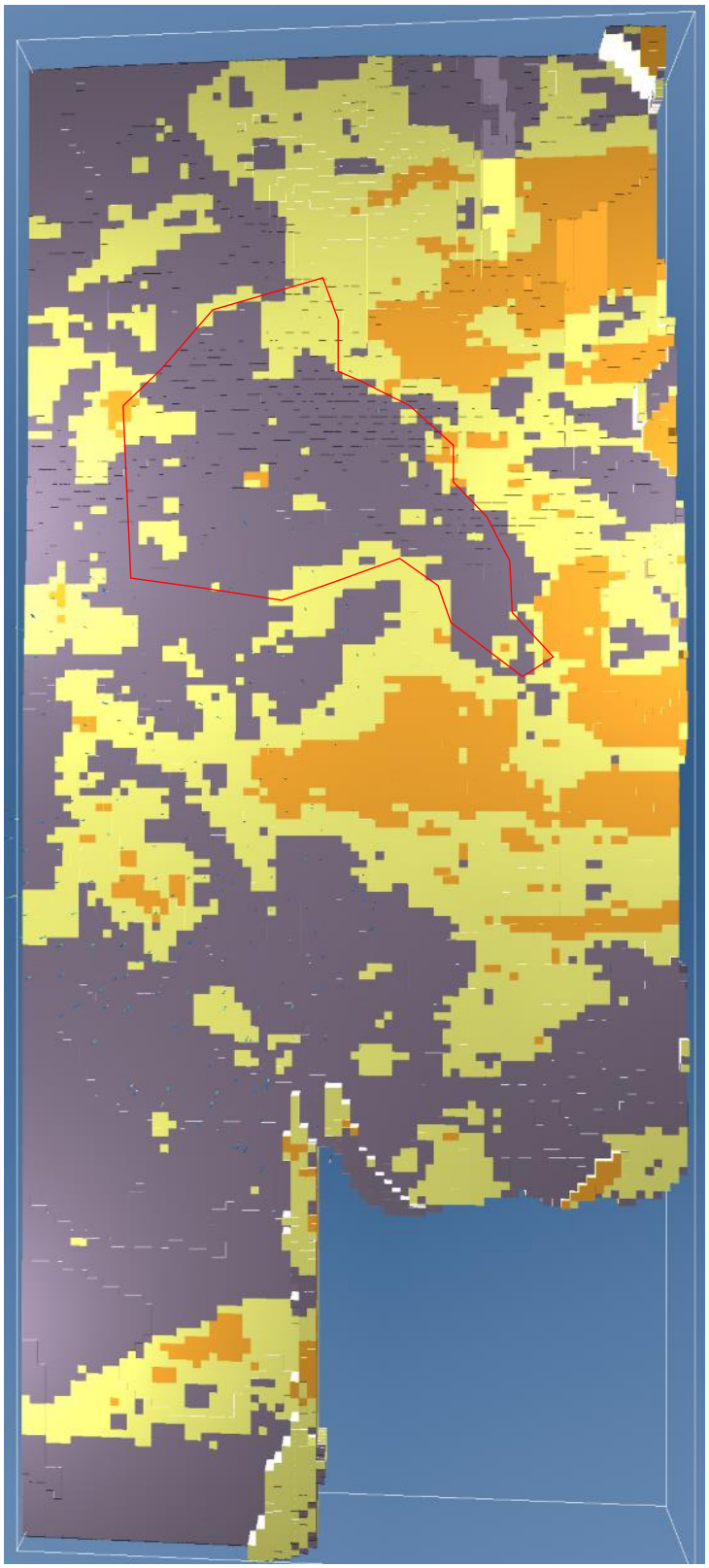

Figure 39 3D View of hydrostratigraphic model at the water level surface, using geostatistical (voxel modeling) methods. Dimensions of bounding box are: x = 37,472 m; y = 15,881 m; z = 200 m

5.5. HYDROGRAPH ANALYSIS

5.5.1. CHARACTERISTICS OF PUMPING-INDUCED WATER-LEVEL CHANGES

Information on irrigation water use for individual wells was obtained from the LPNNRD. This allowed us to examine the proximity of the logged well to other pumped wells. All the wells that were logged using transducers in the 2018 and 2019 pumping season and the pumped wells from 2018 and 2019 are shown in map view for easy reference (Figure 40). It should be noted that the data on 2019 pumped wells is incomplete, as not all water use reports had been delivered to the LPNNRD by the time this thesis was completed.

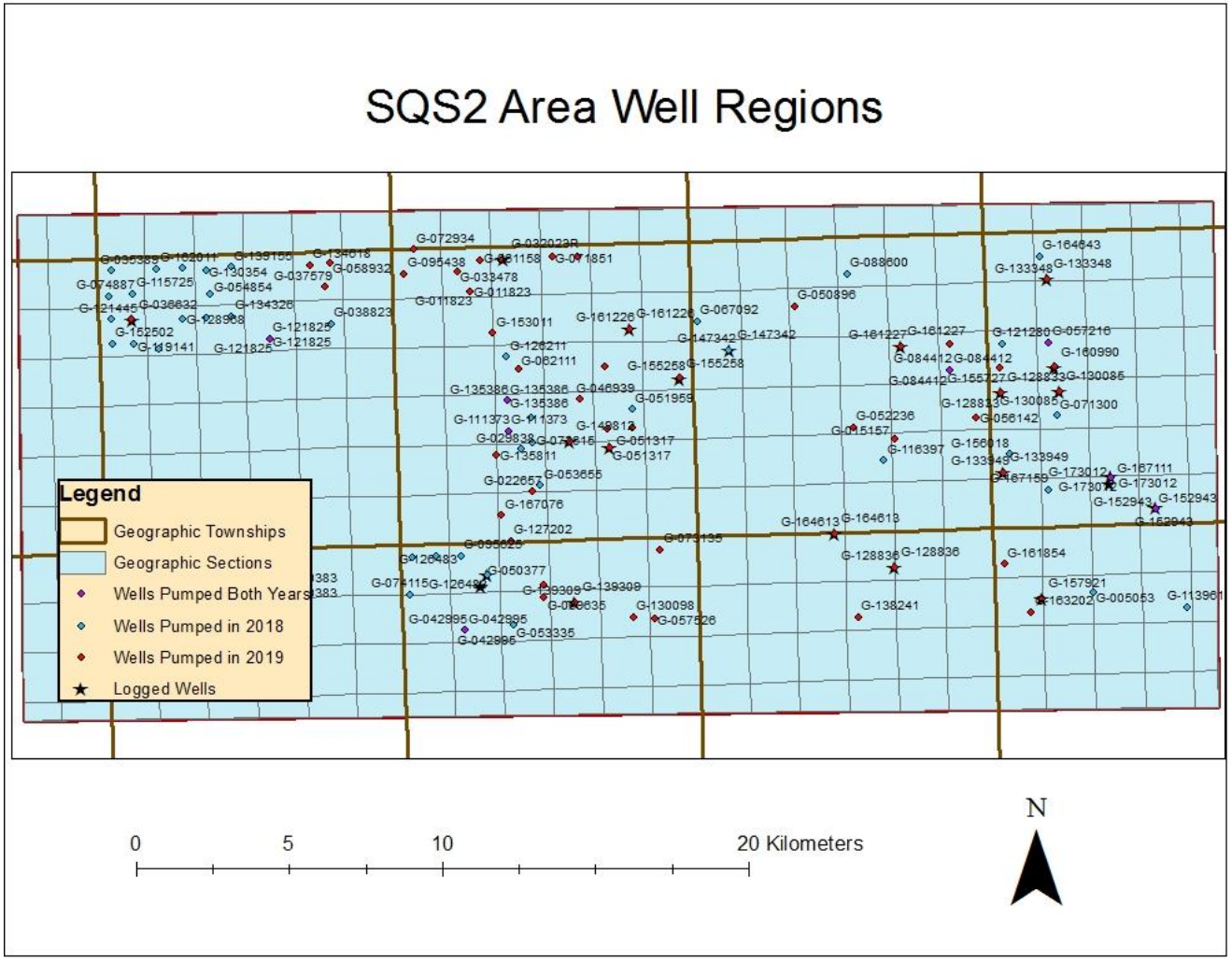

Figure 40 SQS2 Map showing logged wells and pumped wells.

Each hydrograph was examined for several main attributes, summarized in Table 5. Hydrographs shown individually can be found in Appendix C. These attributes describe the background displacement, or those water-level changes from interference with nearby wells (depletion of the "common pool"), water-level changes from pumping of the well containing the transducer (pumping drawdown), total displacement, and the length of the pumping and recovery periods at the well site.

The hydrographs were placed into groups on the basis of proximity and whether or not they were determined to be part of the same "common pool"—a shared groundwater reservoir (Figures 41-47). The x axes of the hydrographs in each group were set to the same scale to allow comparison. The grouping of wells in this manner allowed for the analysis of interconnections between wells or compartmentalization (as in group five).

Background displacement varied from 0 to 16 m. Pumping drawdown is superimposed on the background displacement. In almost every well it was possible to clearly distinguish between these responses because a pumping response stands out as an abrupt (several hours to a few days) fall and rise in the water level. Composite background displacement is a gradual fall and rise over the course of weeks to months, commonly with many small fluctuations from the cycling on and off of nearby wells. Discrete background displacement is short (less than a few days) and abrupt, but the total change is only a fraction of the pumping drawdown. The pumping period was defined as the time between the onset of a rapid, large drop in the water level and the onset of a rapid, large rise. The recovery period is the time between the onset of rapid rise and the

return of the water level to pre-pumping level. In cases where the pumping curve was superimposed on the background displacement, determining cessation of recovery was difficult. Only those pumping curves showing non-noisy pumping and recovery from a single period of pumping were used.

Table 5. Well Hydrograph Interpretations by Group

Group	Well Registration Code	Year	Pumped? Yes/No	Distance to Nearest Pumping Well (m)	Maximum Background Displacement (m)	Type of Background Displacement	Maximum Pumping Drawdown (m)	Total Displacement (m)	Recovery Period (days)	Pumping Period (days)	Pumping to Recovery Ratio	Off-Season Recharge (m)	Interpretation
1	G-050377	2018	No	430	4.2	Discrete	--	4.2	--	--	--	<1	
1	G-126483	2018	Yes	1050	3.5	Discrete	15.7	17.2	20	5.1	3.9	< 1	Confined, open
1	G-126483	2019	Yes		1	Discrete	20.8	26.1	?	?	?	< 1	Confined, open
1	G-139309	2019	Yes	1033	13	Discrete	25.8	29.1	5	1.3	3.8	?	Confined, open
2	G-032023	2019	Yes	751	5.5	Composite	11.5	16.4	6.6	2.8	2.4	2	Confined, open
2	G-051317	2019	Yes	614	5	Composite	5	9.4	1	3.4	0.3	?	Unconfined, bounded
2	G-149812	2019	Yes	1280	~ 5	Composite	< 3.7	7.7	> 30	29	> 1	?	Unconfined
2	G-161226	2019	Yes	1460	7.4	Composite	2.9	10	1.2	1.1	1.1	> 1.2	Unconfined, open?
3	G-147342	2019	No	1894	15.9	Composite	--	15.9	--	--	--	> 0.4	
3	G-155258	2019	Yes	2318	12.3	Composite	3.1	15.5	0.1	0.4	0.25	> 0.5	Unconfined, bounded
4	G-128833	2019	Yes	800	9.4	Composite	16.6	23.5	0.4	3.1	0.13	~ 7.5	Confined, bounded
4	G-130085	2019	Yes	800	8.4	Composite	8.6	16.8	?	?	?	6.4	Unconfined, bounded
4	G-133348	2018	No	792	?	Composite	--	--	--	--	--	--	
4	G-133348	2019	Yes	2850	7.4	Composite	2.2	8.6	0.1	1	0.1	3.4	Unconfined, bounded
4	G-160990	2019	Yes	804	9.5	Composite + Discrete	6.7	13.4	1.9	4.6	0.41	~ 7	Unconfined, bounded
4	G-161227	2019	Yes	1596	8.3	Composite	3	10.8	1.1	2.9	0.4	> 0.7	Unconfined, bounded

Table 5, continued

Group	Well Registration Code	Year	Pumped? Yes/No	Distance to Nearest Pumping Well (m)	Maximum Background Displacement (m)	Type of Background Displacement	Maximum Pumping Drawdown (m)	Total Displacement (m)	Recovery Period (days)	Pumping Period (days)	Pumping to Recovery Ratio	Off-Season Recharge (m)	Interpretation
5	G-128836	2019	Yes	2013	0	None	1.6	1.6	0.4	1.1	0.4	0.7	Unconfined, bounded
5	G-133949	2019	No	1966?	0	None	0	0	--	--	--	0	bounded
5	G-152943	2018	Yes	1790?	0	None	6.5	6.5	4.9	2.1	2.3		Unconfined
5	G-157921	2018	No	1663	0	None	10.1	10.1	0.92	3.8	0.2	0.7	Confined, bounded
5	G-157921	2019	Yes	577	0	None	8.8	8.8	0.3	0.7	0.4	0.7	Confined, bounded
5	G-164613	2018	No	2861	1.8	Composite + Discrete	--	1.8	--	--	--	0.7	
5	G-164613	2019	Yes	2259	12.4	Composite + Discrete	15.6	23.5	0.3	0.4	0.8	0.7	Confined, bounded
5	G-173012	2018	Yes	1790	0	None	18.1	18.1	3.1	2	1.55	4	Confined, bounded
5	G-173012	2019	Yes	?	0	None	21.3	21.3	1.6	1	1.6	4	Confined, bounded
6	G-036632	2019	Yes	4550?	8.3	Composite + Discrete	< 5	11	0.4	0.2	2.2	> 1.6	Unconfined, open

Terminology

Background displacement: the gradual and shallower drawdown curve exhibited in some hydrographs

Composite: a smooth curve

Discrete: a rigid, noisy curve

Total displacement: addition of all kinds of drawdown from the original water level

Pumping to Recovery Ratio: comparison of the sizes of the drawdown curve and the recovery curve

Off Season Recharge: addition to the water level that is not classified as recovery from pumping, but instead due to recharge due to precipitation

Bounding terms in interpretations: either a bounded/isolated/compartmentalized aquifer or an open system/connected aquifer/common pool

5.5.2. INTERPRETATION OF AQUIFER CONDITIONS

Group 1 hydrographs (Figure 41) are characterized by the occurrence of discrete, coincident drawdown and recovery curves between all three wells. Except for changes < 2 m, the discrete displacements are observed in all wells. G-050377 is an observation well located ~ 400 m from G-126483, clearly showing the response of the nearby pumping well as well as the changes observed farther away at G-139309. However, there is no background displacement within this group of wells. The lack of common-pool depletion despite the large-magnitude (~ 20 m) pumping drawdown suggests that these wells have large cones of depression, both in magnitude and radius, which would be expected of a confined aquifer. The ratio of recovery to pumping is ~ 4. This large value, along with observed hydraulic communication between wells, suggests that the aquifer is not locally bounded (i.e. it is open).

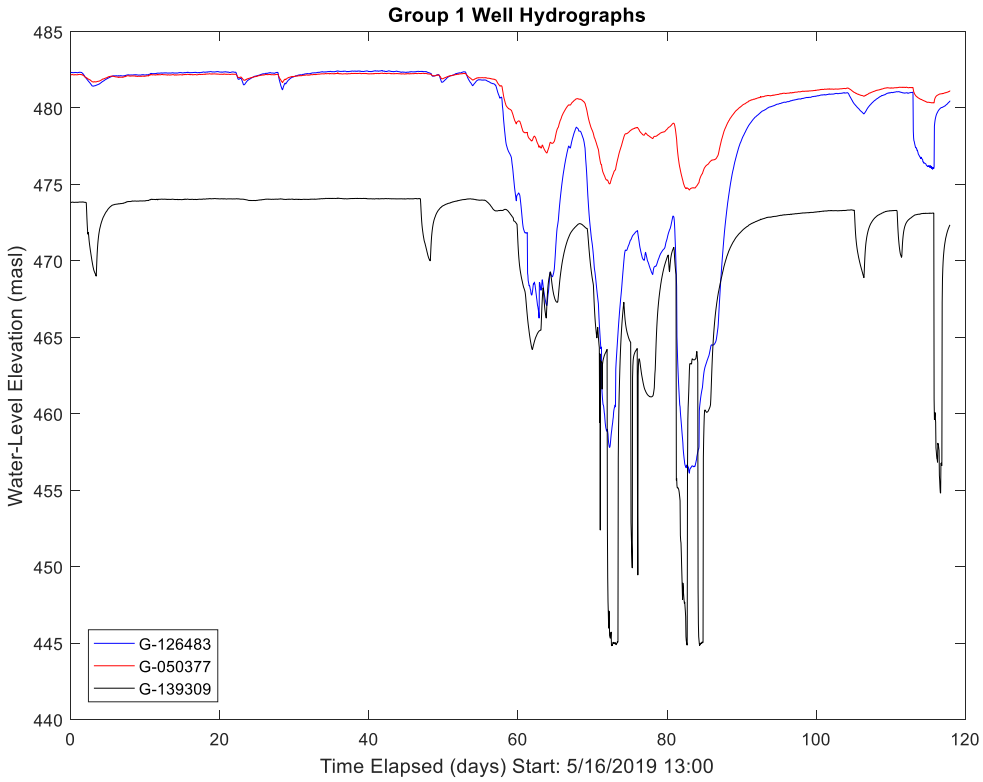

Figure 41 Group 1 wells that show discrete displacement and curves that overlap in time, indicating an open system between them. No background displacement and the high drawdown points towards a confined aquifer.

Group 2 hydrographs (Figure 42) are characterized by a large (5 – 7 m), composite background displacement period of > 60 days that contains many small fluctuations (it is noisy). After the pumping period ceases around day 70, recovery continues to the end of the period of record. Pumping drawdowns are between 3 and 5 m, suggesting unconfined conditions; however, drawdown is 12 m in well G-032023, so the aquifer may be confined in some areas. Pumping curves are sharp and recovery is rapid, showing that aquifer boundaries are affecting the water levels. Despite the evidence of boundaries, the aquifer in this area appears to be connected between the wells because the background displacement clearly shows the effect of many wells removing water from

the same common pool. The gradual recovery of the background displacement suggests a source of recharge to the system.

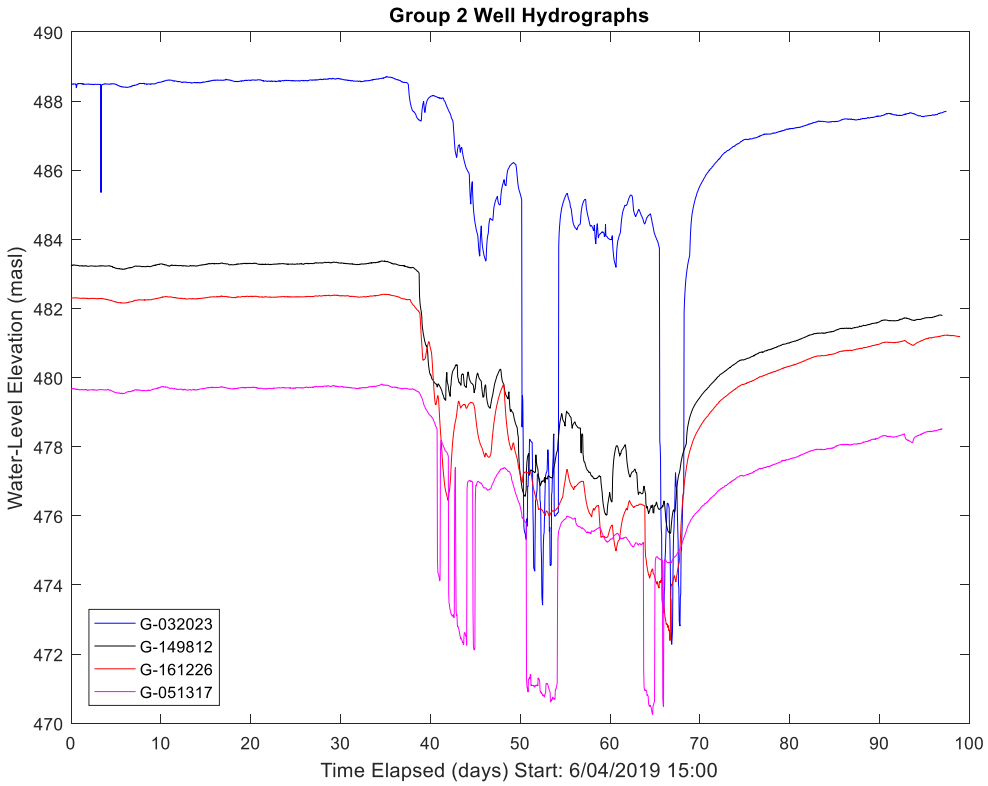

Figure 42 Group 2 hydrographs (G-032023, G-149812, G-161226, and G-051317) that are noisy, showing background displacement indicative of a common pool. Small drawdowns suggest unconfined aquifers.

Group 3 hydrographs are characterized by large (~ 12 – 15 m), sustained (> 60 days) depletion of a common-pool aquifer (Figure 43). Pumping drawdown is small (~ 3 m) and subdued, with gradual falls and rises. This group of wells is located between groups 2 and 4. Despite its proximity to these other groups of wells, the background displacement has a different appearance, suggesting that these wells belong to a separate, bounded aquifer. The small recovery to pumping ratio is further evidence for bounded conditions.

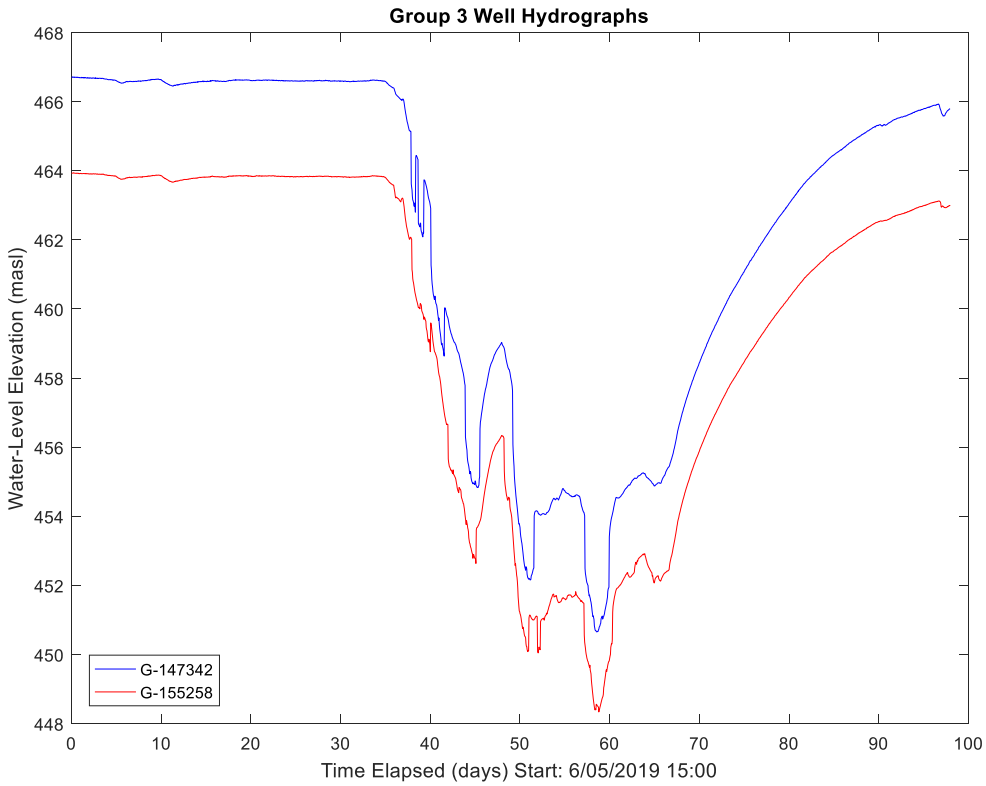

Figure 43 Group 3 hydrographs (G-147342 and G-155258) showing similar displacement and higher pumping responses than recovery responses, indicating an open system between the two and the presence of boundaries.

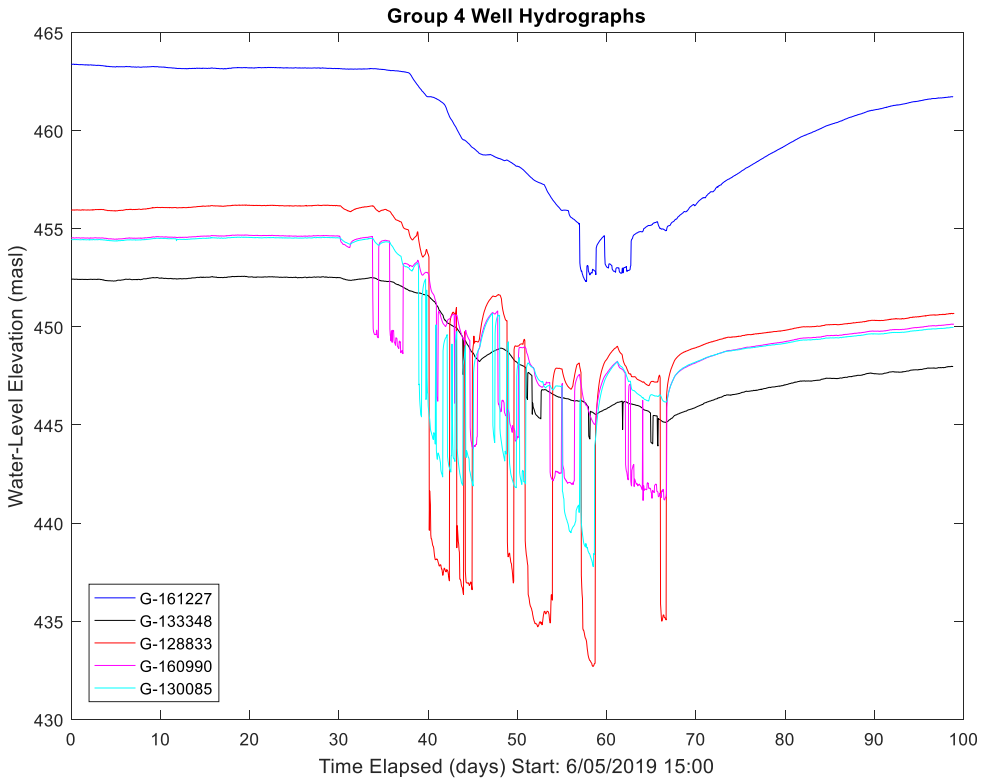

Figure 44 Group 4 hydrographs (G-161227, G-133348, G-128833, G-160990, and G-130085) showing sharp responses to pumping, and a similar gradual background response. This indicates an interconnected aquifer.

Group 4 hydrographs show 8 – 9 m of background displacement with superimposed, sharp pumping responses (Figure 44). Drawdown ranges from small (2 m) to large (17 m), suggesting a range of unconfined and confined aquifer conditions. Pumping recovery is a small fraction of the pumping period, showing that aquifer boundaries have affected the water level responses. The similarities between the background displacements, however, provide evidence that the aquifer is interconnected between the wells in this group.

Group 5 hydrographs (Figure 45) come from six wells located in the southeast part of the study area. The data comes from different periods in 2018 and 2019, so not all hydrographs overlap in time. Nevertheless, all six hydrographs have their own unique characteristics. The pumping drawdown in any given well does not have a corresponding response in surrounding wells. The hydrograph for G-133949 shows no changes during the 2019 irrigation season even though surrounding wells drops by as much as 23.5 m. The only well exhibiting a background displacement is G-164613, but this response is not recorded in any of the other wells. With the exception of G-152943 (which is indeterminate), all of the wells show evidence of boundaries in the short recovery periods. The differences between these hydrographs, despite their close proximity, is evidence that this area contains many small, isolated aquifers bounded by impermeable material.

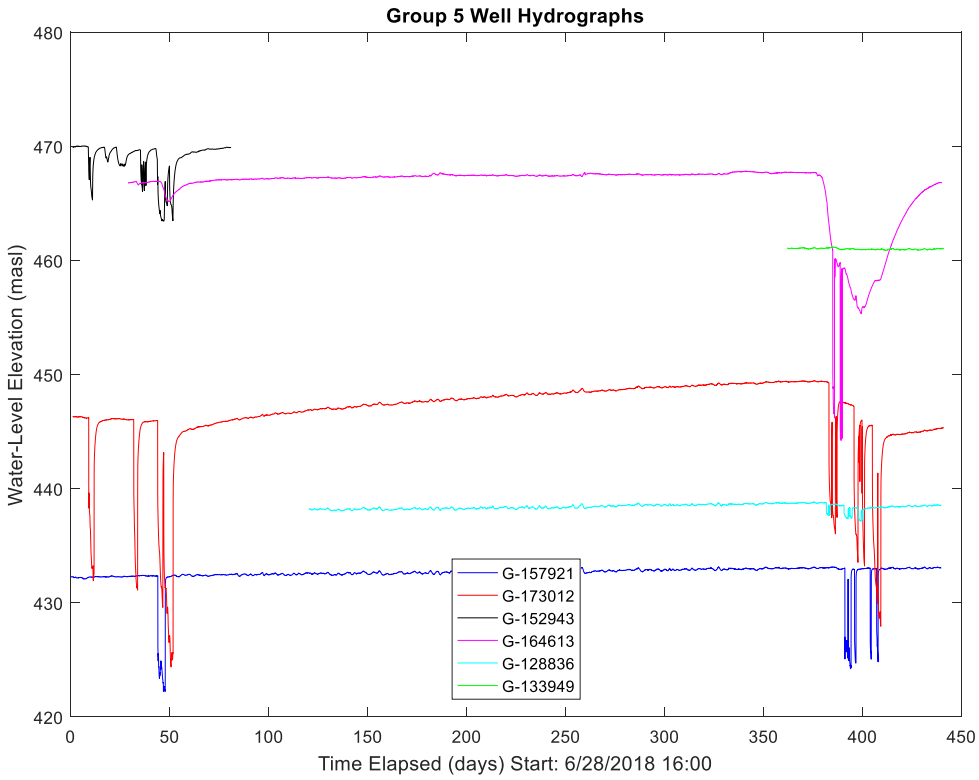

Figure 45 Group 5 hydrographs (G-157921, G-173012, G-152943, G-164613, G-128836, G-133949) each showing unique characteristics. The sharp recoveries point towards small aquifers separated by boundaries.

The hydrograph for well G-173012 was studied in more detail because it shows responses from several sustained periods (2 – 3 days) of continuous pumping without interference from any surrounding wells (Figure 46). This makes some aspects of traditional pumping test analysis applicable to the data. The slope of a line plotted on a semilog graph can reveal information about the aquifer. In both examples shown below, after the first few hours of pumping the slope increases, then it increases dramatically after the first full day of pumping. No other wells nearby have an effect on the water level at this well, so the changes in slope can only be caused by the cone of depression encountering a boundary.

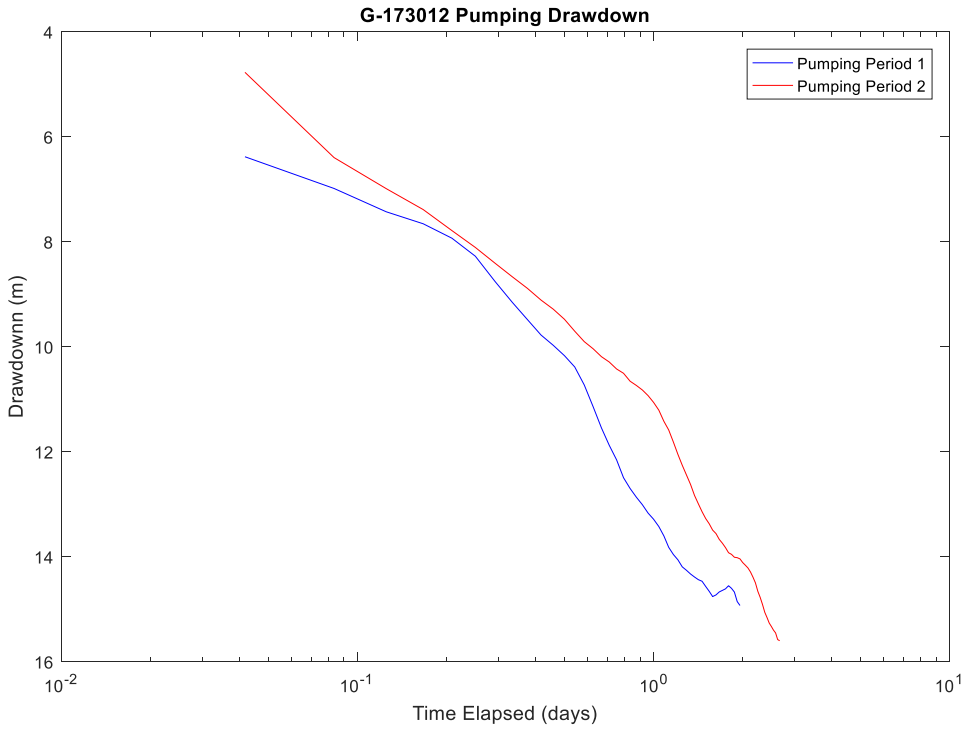

Figure 46 Comparison of two pumping periods for G-173012 on a semi-log plot. Shows sharper slope later in the curve, indicating a boundary nearby.

Well G-036632 is separated from the other wells by many kilometers. It shows a large (~ 8 m) background displacement and smaller, discrete displacements likely from interference with surrounding wells (Figure 47). Even though water use data confirms that this well underwent substantial groundwater pumping, it is not possible to find clear evidence of pumping drawdown in this hydrograph. It is likely that noise from well interference obscures the pumping response. Nevertheless, the largest single drop in water level is < 5 m, so the pumping drawdown did not exceed that amount. The large background displacement, evidence of well interference, and lack of large drawdown suggests an open, unconfined aquifer.

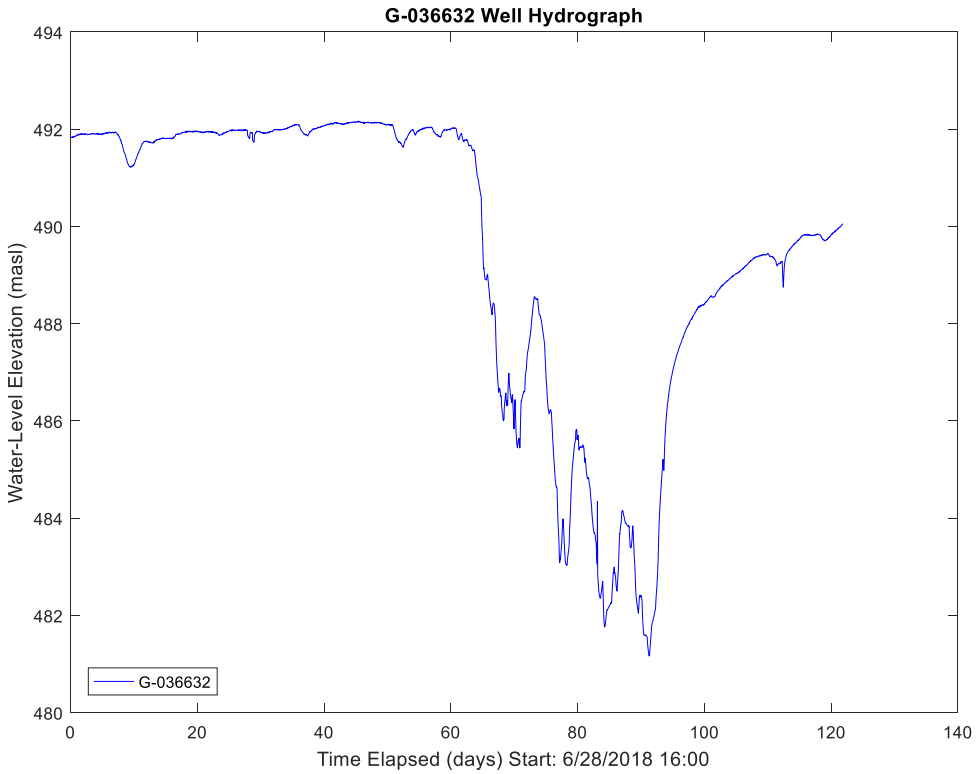

Figure 47 Hydrograph for G-036632 showing no clear pumping response due to the influence of pumping other wells, which means it's likely an open system. Low drawdown points towards unconfined conditions.

5.6. COMPARISON OF HYDROGRAPH RESULTS AND HYDROSTRATIGRAPHIC MODELS

After completing the hydrograph interpretations, the hydrostratigraphic models were examined to determine the expected aquifer characteristics throughout the model domain. Confined and unconfined aquifers were mapped in GeoScene3D by examining the thickness of impermeable material between the water level surface and the aquifer top. Confining units < 2 m thick were considered too thin to be mappable because it is estimated that error could be as much as 2 m. Furthermore, the thickness of a voxel model layer is 2 m, so it is not possible to map layers less than the thickness of an individual layer. The extents of aquifer boundaries were mapped by examining the thickness of the aquifer. Boundaries were drawn where the aquifer became very thin or pinched out. The maps in this section compare the hydrograph interpretations to the hydrostratigraphic interpretations in the layer model and the voxel-based geostatistical model.

5.6.1. LAYER MODEL

In the layer model, confined aquifer areas were mapped mainly in the west and northeast parts of the study area (Figure 48). However, at least six wells exhibiting evidence of unconfined conditions in the hydrographs are located within the regions mapped as confined. Moreover, only two wells inferred to be located in confined aquifers lie at the margins of the mapped confined areas: none of them completely within the confined areas. In general, there does not appear to be any correspondence between the hydrostratigraphic model and the interpreted aquifer conditions at the well sites.

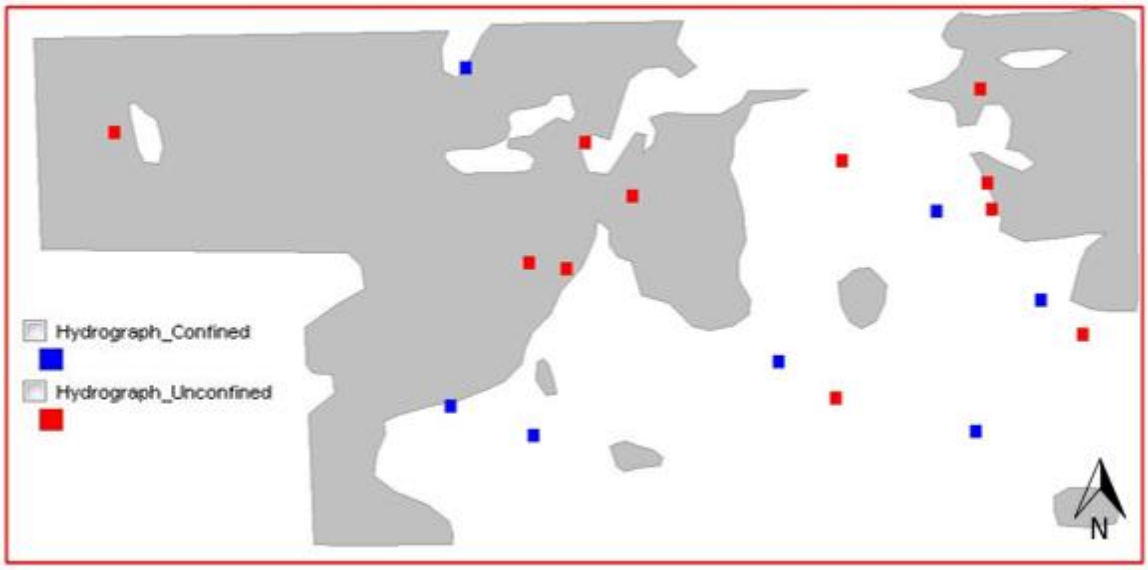

Figure 48 Confined aquifer areas (gray shading) on the basis of the layer model shown in relation to interpreted aquifer conditions at well sites (symbols).

The layer model shows several small areas where the aquifer becomes very thin or pinches out completely (Figure 49). These areas are widely distributed throughout the model, and they do not appear to have any regular arrangement that would suggest they are related to the bounded aquifer conditions interpreted at the well sites.

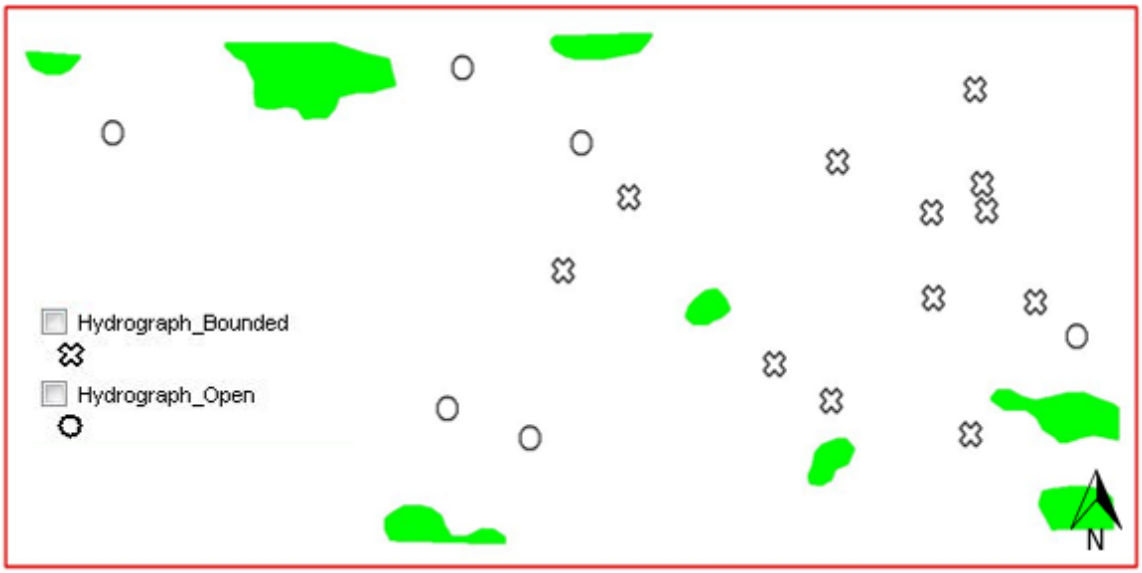

Figure 49 Impermeable boundaries (green shading) based on the layer model shown in relation to the interpreted aquifer conditions at well sites (symbols)

The groups of hydrographs showing common-pool groundwater resources are examined in relationship to the modeled aquifer boundaries (Figure 50). The modeled aquifer boundaries are not extensive enough to compartmentalize the groundwater system in this area. Thus, there does not appear to be a relationship between the mapped extent of these boundaries and the groups of well hydrographs.

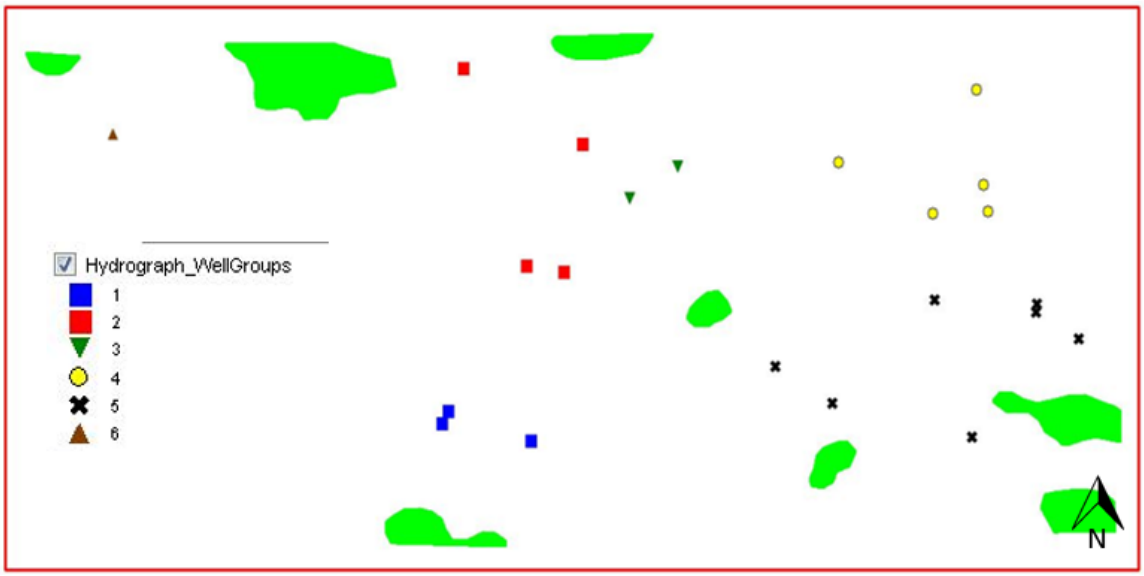

Figure 50 Impermeable boundaries (green shading) based on the layer model shown in relation to the common-pool aquifers based on groups of hydrographs (symbols). They are isolated, compartmentalized aquifers.

5.6.2. VOXEL MODEL

The voxel model shows confined and unconfined aquifer conditions on the basis of the thickness and composition of overlying materials (Figure 51). Like the layer model, there does not appear to be any regular relationship between the well sites and the hydrostratigraphic model. Only two wells inferred to be completed in confined aquifers are mapped within the shaded area. The confined aquifer area contains at least 5 of the 11 wells drilled into unconfined aquifers.

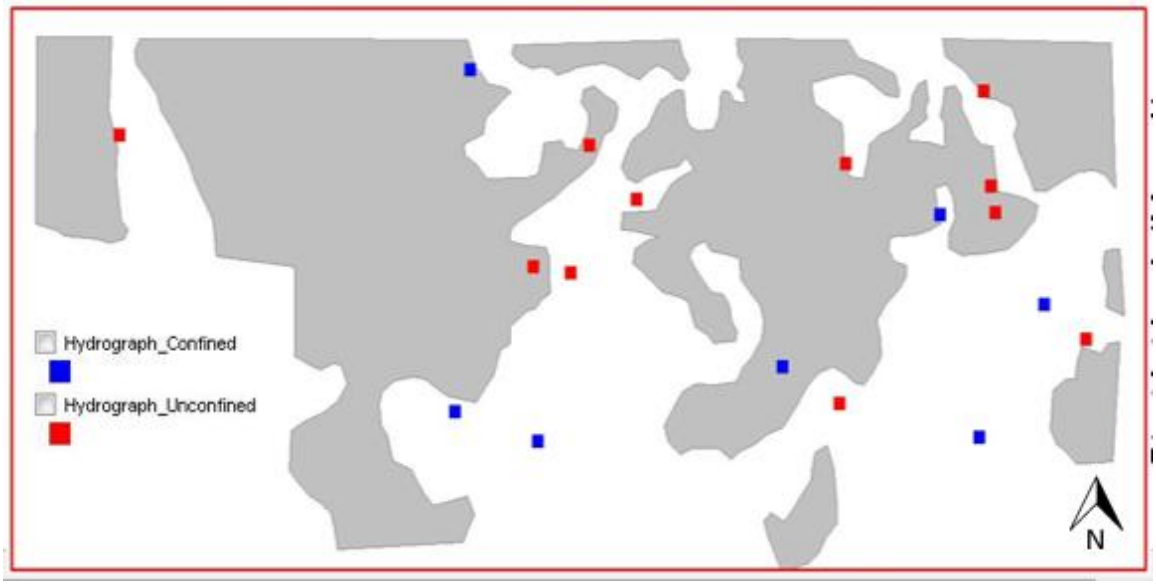

Figure 51 Confined aquifer areas (gray shading) on the basis of the voxel-based geostatistical model shown in relation to interpreted aquifer conditions at well sites (symbols). Red boxes are unconfined. Blue boxes are confined.

The voxel model shows many small areas in which aquifer materials are thin (< 2 m) or absent, representing aquifer boundaries (Figure 52). Many of the bounded aquifers shown in well hydrographs are located in close proximity to these boundaries. Nine of 12 of the bounded aquifers are within ~ 1 km of a modeled boundary. Four of the 6 wells interpreted as being drilled into open aquifers are located in areas relatively free of aquifer boundaries. However, two of these wells are located directly adjacent to modeled

aquifer boundaries. In general, the eastern part of the study area contains many small to large aquifer boundaries, and it contains the majority of the wells in bounded aquifers. The western part of the study area contains just several large boundaries separated by large, open aquifers. It also contains 5 of the 6 wells in open aquifers. In summary, it appears that for the most part, there is some relationship between the modeled and interpreted boundaries.

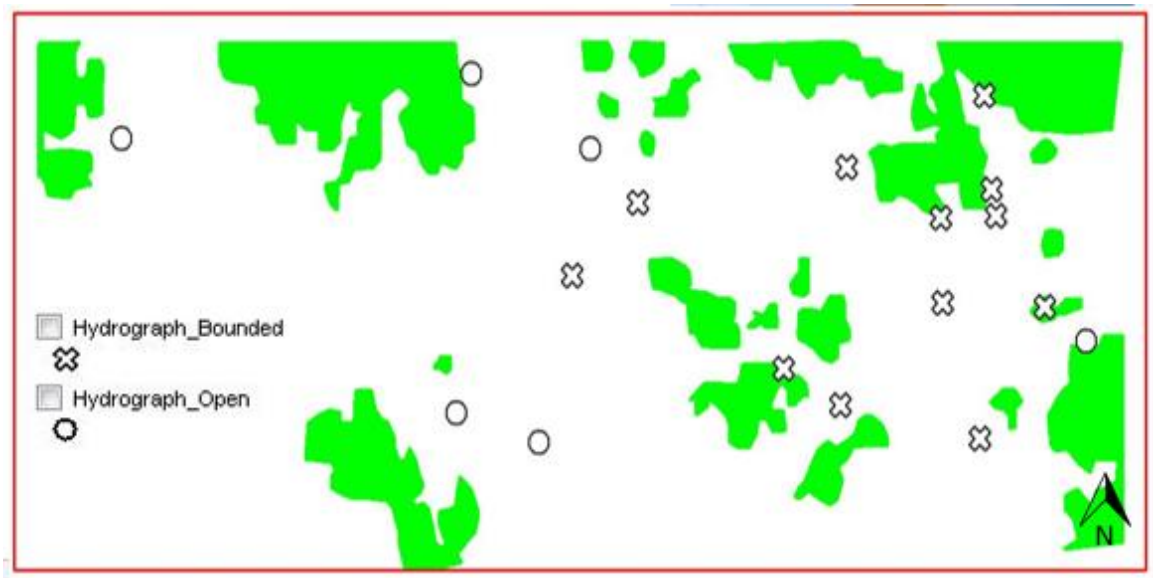

Figure 52 Impermeable boundaries (green shading) based on the voxel-based geostatistical model shown in relation to the interpreted aquifer conditions at well sites (symbols).

The groups of wells showing common-pool groundwater reservoirs are shown in relationship to the aquifer boundaries (Figure 53). Although groups 1 – 3 are located in areas of interconnected aquifer, there are no boundaries separating different well groups. Group 4 wells (yellow circles), which show good evidence of a common-pool, appear to be surrounded by a large impermeable boundary located in the center of the well cluster. In general, the voxel-model boundaries do not explain the groupings shown in the hydrograph evidence.

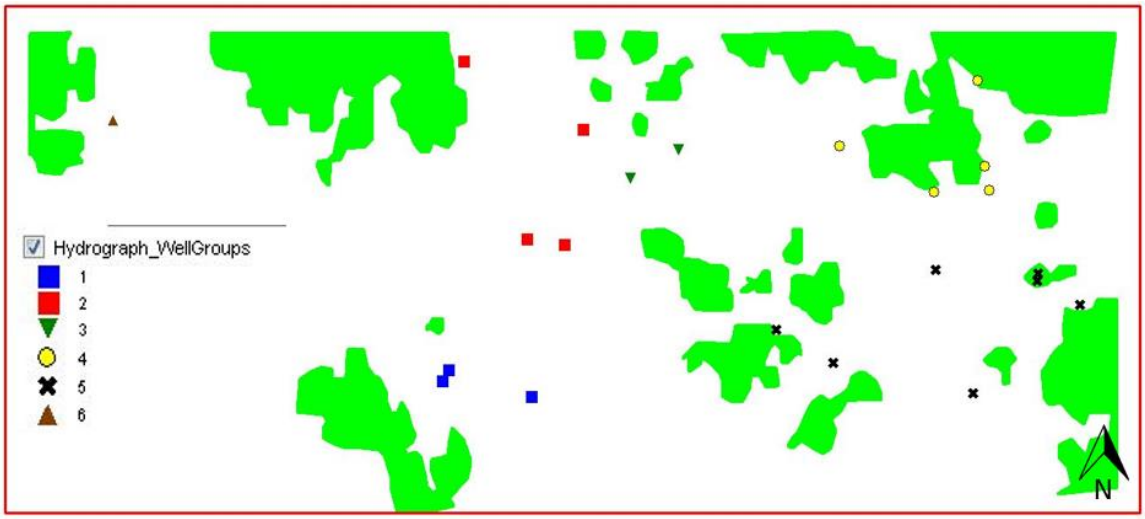

Figure 53 Impermeable boundaries (green shading) based on the voxel-based geostatistical model shown in relation to the common-pool aquifers based on groups of hydrographs (symbols). They are isolated, compartmentalized aquifers.

CHAPTER 6 DISCUSSION

6.1. MAPPING AQUIFER CHARACTERISTICS WITH AEM

Comparison of borehole lithology and AEM resistivity shows that AEM does a reasonably good job of detecting thick zones of sand and gravel surrounded by conductive material such as clay or shale. This general relationship has been demonstrated by many previous studies (Aqua Geo Frameworks, 2017; N.K. Christensen, Minsley, & Christensen, 2017; Høyer et al., 2015; Jørgensen et al., 2013; Knight et al., 2018; J. Korus, 2018; Oldenborger, Pugin, & Pullan, 2013; Vilhelmsen et al., 2019). The ability of AEM to detect resistive sand bodies has been the key to the success of this method for regional aquifer mapping (Auken et al., 2017).

In the study of the SQS2 area, a general correspondence between AEM and lithology allowed the mapping of the bedrock surface (sand and gravel atop shale) and the top of the aquifer materials (clay and silt atop sand). Despite its success in detecting the main zone of aquifer materials, we found a poor relationship between aquifer characteristics interpreted from hydrographs and those interpreted from hydrostratigraphic modeling. The impermeable boundaries mapped from the voxel modeling approach resulted in moderate success: the bounded aquifer signatures observed in hydrographs generally occurred in wells located adjacent to these boundaries.

We attribute the failure of the methods to produce patterns consistent with hydrograph observations as the result of the limitations of AEM and simple hydrostratigraphic modeling approaches we intentionally used in this study. The limitations of the methods are discussed below.

6.1.1. LIMITATIONS OF HYDROGRAPH INTERPRETATION.

Groundwater-level response curves are a direct result of the hydraulic response of an aquifer to pumping. Although this makes the well hydrograph data more informative about the aquifer system than the AEM data, interpretation of these data is not without limitations. The data we collected was not from controlled pumping test experiments, so we do not know the exact pumping rate and period for each well, nor do we have multiple observation wells in combination with the pumping wells. Nevertheless, previous authors have demonstrated successful use of this technique (Butler et al., 2013; Korus, 2018). It is possible that some error could have come from the recording of water levels from the PVC drop pipes instead of the actual irrigation well. There could be impermeable geologic material present on the monitoring pipe but not the irrigation well or vice versa, creating an unreliable hydrograph for the pumping information that was given for that irrigation well.

6.1.2. LIMITATIONS OF AEM RESISTIVITY-DEPTH MODELS

AEM resistivity is not a direct measure of lithology. However, the goal of AEM mapping is to estimate lithology as a means of developing a hydrostratigraphic framework. As long as interference is accounted for in the AEM inversion (removal of power line noise and infrastructure coupling), the AEM response should give an actual estimate of the subsurface resistivity structure. The problem is that there are multiple factors that control resistivity. Chief among them is clay content. If a sand body contains enough interbedded clay, the AEM response will detect a conductive body even though

the sand may have high hydraulic conductivity. If a pure quartz silt is encountered, it will be detected as a resistive body even though it may have low hydraulic conductivity.

One reason that AEM may fail to properly capture the hydraulic response of an aquifer is in the case of a fractured aquifer containing clay. In clay and shale formations, wells may yield substantial groundwater flow if the fracture network is well-connected. The AEM would detect a highly conductive target even though the unit may be an aquifer or it may allow leakage to an adjacent aquifer. In the case of SQS2, fractured, clay-rich tills may yield water to wells or they may serve as conduits for flow between a multi-layered aquifer system. Thus, it is possible that some aquifers modeled as confined may actually behave as unconfined due to fracture porosity in the tills.

Like many modeling approaches, inversion of AEM soundings can either be deterministic or probabilistic. In the present study, a deterministic inversion was used for all subsequent hydrostratigraphic modeling. Any uncertainty or error in the inversion would have been passed down to the hydrostratigraphic models.

6.1.3. LIMITATIONS OF HYDROSTRATIGRAPHIC MODELING

The cognitive approach to hydrostratigraphic modeling is limited because of its subjectivity. In addition, it is best suited for hydrogeologic systems that can be translated easily into a layer model. In folded, faulted, or complexly cross-cutting aquifers, this method is extremely difficult to apply. On the other hand, it is useful because the modeler can choose to make layers that conform with the conceptual understanding of the system or with observations made independently. Unlike the geostatistical approach, the modeler can make adjustments based on geological knowledge. Multiple iterations can result in a

model that explains observations not accounted for by the voxel model. Also, the modeler is not forced to adhere to the resistivity-lithology relationship: he/she can use the borehole data and other data freely.

The voxel-based geostatistical approach used herein is a deterministic method. This method results in a single model of the resistivity volume. Although adjustments can be made to the classification of lithology, there is limited flexibility to make changes for matching the model to observations. However, the geostatistical approach is purely objective and therefore may be useful for hypothesis testing and for discovering geological features that might go otherwise unnoticed. Geologist often see what they are trained to see, and an objective approach can help to overcome these biases. Moreover, voxel modeling is highly useful for areas that are heterogeneous or that can't be described with a simple layer model. Glacial geology is often complex, lacks stratification, and can be tightly folded and faulted. This makes voxel modeling particularly useful in these environments.

6.2. RECOMMENDATIONS FOR FUTURE WORK

It is recommended that several different modeling tools and techniques be used in future 3D hydrostratigraphic models in eastern Nebraska.

Additional AEM inversions should be conducted to determine if the geology of the study area can be further resolved. The hydrogeologists responsible for hydrostratigraphic modeling should collaborate closely with the geophysicist responsible for the AEM inversion. One should not settle for a single AEM inversion model. An iterative approach could improve model outcomes (Høyer et al., 2015).

Probabilistic AEM inversion techniques should be used to capture the uncertainty inherent in the AEM data. An ensemble approach to inversion would yield many models of the same dataset. These models could be combined to yield a most probable outcome, and it would allow the hydrogeologists to know where the inversion is most or least reliable.

More sophisticated hydrostratigraphic modeling methods could be conducted. A variety of other modeling schemes have been proposed in the literature (see Introduction). These methods may help to incorporate model uncertainty into the outputs, and they can help to capture geological realism (Barfod et al., 2018). The drawback to these approaches is that they are often not readily applied, taking additional time and advanced experience and skills to apply.

A potentially useful technique would be to incorporate lessons learned from study of well hydrographs into the modeling workflow. Knowledge of aquifer boundaries and degree of confinement could be used to inform the interpretation of layers, thereby extending the usefulness of cognitive modeling.

Finally, where a 3D AEM resistivity voxel volume is available, the modeler could make use of the voxel model to inform the layer model. This would allow the modeler to create geological structures where they might otherwise be overlooked. For example, in SQS2, use of the voxel model to inform the layer model may have allowed the modeler to draw pinch-outs where they were not obvious. However, this method would only work as well as the voxel model is able to resolve aquifer details correctly.

6.3. IMPLICATIONS FOR GROUNDWATER MANAGEMENT

The hydrograph data showed very large drawdowns, some as much as 26 m. Even some wells that did not pump showed large displacements as much as 16 m. These excessive declines in water level might explain why there are issues in this area with well interference during periods of heavy irrigation. At this time, it appears that the hydrographs provide the most useful information about possible management of the aquifer system. The hydrograph groupings, described in the results, could be used to define management subareas. The depletion characteristics could be used to inform the management plan. It would be beneficial to perform pumping tests within these subareas, as recommended in the AEM report (Aqua Geo Frameworks, 2017), with the information found for each group of hydrographs in mind.

In general, the hydrostratigraphic voxel model provided the most accurate information about the aquifer boundaries. Nevertheless, many questions about the validity of the models remain. Neither model was successful in predicting confined and unconfined conditions. It was also not possible to match the models to the groups of wells which were based on hydrograph characteristics. It is suggested that further hydrostratigraphic modeling be conducted in SQS2 to define the boundaries of aquifer subunits. These modeling efforts should incorporate the five recommendations provided above.

CHAPTER 7. CONCLUSIONS

The accuracy of the AEM modeling approaches was poor compared to the interpretations made from the hydrographs about the local aquifer. Hydrologic evidence of unconfined and confined aquifers did not match either the layer or voxel hydrostratigraphic models. We conclude that both methods have severe limitations, at least in the study area. The voxel model, at least, showed several aquifer boundaries near hydrographs that indicated a nearby boundary.

We intentionally used a single iteration of the layer model and a deterministic geostatistical technique in order to determine if the simplest approaches to modeling hydrostratigraphy are adequate. For this study area, the simplest approach was insufficient to map a heterogeneous aquifer accurately. There was substantial disagreement between the AEM modeling approaches and the interpretations of hydrographs, indicating one or more problems with the methods. In the least, our results show that the resistivity-lithology relationship is non-unique and non-universal. A deterministic model does not account for these uncertainties. To the extent that the hydrographs accurately reveal unconfined and confined responses, the hydrostratigraphic models appear to not have the vertical resolution necessary to detect thin confining units. The impermeable boundaries detected by the interpretation of hydrographs and the layer model did not agree.

Nevertheless, there was some agreement between the locations of impermeable boundaries in the voxel model and the boundaries detected in hydrographs. The resistivity-lithology relationship used in the voxel model was simple and deterministic,

but it seemed to match the hydrograph interpretations reasonably well. This suggests that further refinement of the resistivity-lithology relationship, perhaps using sophisticated techniques, could improve model performance. Because the aquifer in this area was formed by glacial processes, which result in heterogeneity, complex stratigraphy, and structural deformation, it is not surprising that we achieved slightly better results with the geostatistical approach compared to the layer approach. The voxel model captures irregular geological bodies better than a layer model.

The simplified modeling methods would likely work better in aquifers that are more homogeneous in nature, where aquifer boundaries are not as prevalent, and where the geology can be described by simple layers. Furthermore, the information from well hydrographs can be complicated by the overprinting of multiple aquifer characteristics. In areas without multiple boundaries, the interpretations of confined and unconfined conditions may be more straightforward. Without all these boundaries, well interference would be more obvious. The layer modeling approach is likely to be more accurate in this type of aquifer system (Jørgensen et al., 2015, 2013).

Although controlled pumping tests would yield clearer information about the aquifer character in an area, looking at the impact of irrigation pumping on water levels seems to be a good option for a starting point while investigating an aquifer in a particular region that is not well known. It is a cheaper way to begin an investigation into aquifer mapping in a particular area. Permission for monitoring wells and analyzing the regular irrigation pumping is much easier to obtain than to ask to do your own pumping tests in privately owned wells. It also does not require potentially wasteful pumping of

water over many days. As determined from this study, the results from the groupings can give some direction for management in an area in the future as well as problems in the AEM modeling process.

Geophysical methods such as AEM can add more information to describe aquifer properties. The advantage is that they give some information about what is located in between the points of borehole/well data. On the other hand, adding hydrograph interpretations to geophysical modeling would improve the accuracy of the method. This investigation displays the limitations of AEM modeling that other studies have encountered, and the inconsistencies show a potential requirement for more sophisticated methods to be used when modeling the AEM data. The non-unique resistivity to lithology translation, the subjectivity of the cognitive approach, and the rigidity of the statistical approach cause inaccuracy, and they in essence are well-validated with traditional aquifer testing methods which are more reliable. If this method were to be applied to other areas with this sort of geology, it would be recommended that voxel modeling be used and that multiple iterations be made with the layer model. Future hydrostratigraphic modeling work involving AEM should consider the following: (1) use more sophisticated hydrostratigraphic modeling approaches that are capable of modeling and quantifying uncertainty, (2) combine different modeling approaches if necessary to achieve a reasonable fit to hydrologic data, and (3) use hydrograph data and pumping tests to validate hydrostratigraphic model results.

APPENDIX A: AEM MODELING SPECIFICS

AEM Voxel Modeling Details:

1. Interpolation Parameters
   Interpolation Type: 3D Inverse Distance Weighting
   Source Object Name: SkyTEM304M_SQS2
   Source Object Type: ODV Models (1D Geophysics)
   Point Data Info: Resistivity
   Search Radius X: 1500.00
   Search Radius Y: 1500.00
   Search Radius Z: 5.00
   Exponent: 4.00
   Smooth: 70.00
   Max.Count: 0.00
   Quadrant Count: 6.00
2. Grid Info
   Value Type: Single
   Columns (X): 188
   Rows (Y): 80
   Layers (Z): 101
   Cell size X: 200.386
   Cell size Y: 201.022
   Cell size Z: 2.000
   Min value: 3.208
   Max value: 157.098
   MinX - MaxX: 698123.700 - 735595.800
   MinY - MaxY: 190159.200 - 206039.900
   MinZ - MaxZ: 340.000 - 540.000
   Nodes: 1519040
   Memory Usage: 5,933 K

AEM Cognitive Modeling Details:
Kriging method for interpolation parameters
Interpolation Type: 2D Kriging (GSLib)
Source Object Name: Spring 2017 Water Levels
Source Object Type: XYZ Points
Point Data Info: ValueMode=Elevation;ValueName=Elevation
Kriging Type: Ordinary Kriging
Search Radius X: 4000.00
Search Radius Y: 4000.00
Search Radius Z: 50.00
Search Angle 1: 0.00
Search Angle 2: 0.00
Search Angle 3: 0.00

Trim Lower: -1E21
Trim Upper: 1E21
Block X: 1
Block Y: 1
Block Z: 1
Min Data: 1
Max Data: 100
Max per Octant: 0
Variance Grid: No

APPENDIX B: ADDITIONAL AEM FLIGHTLINES

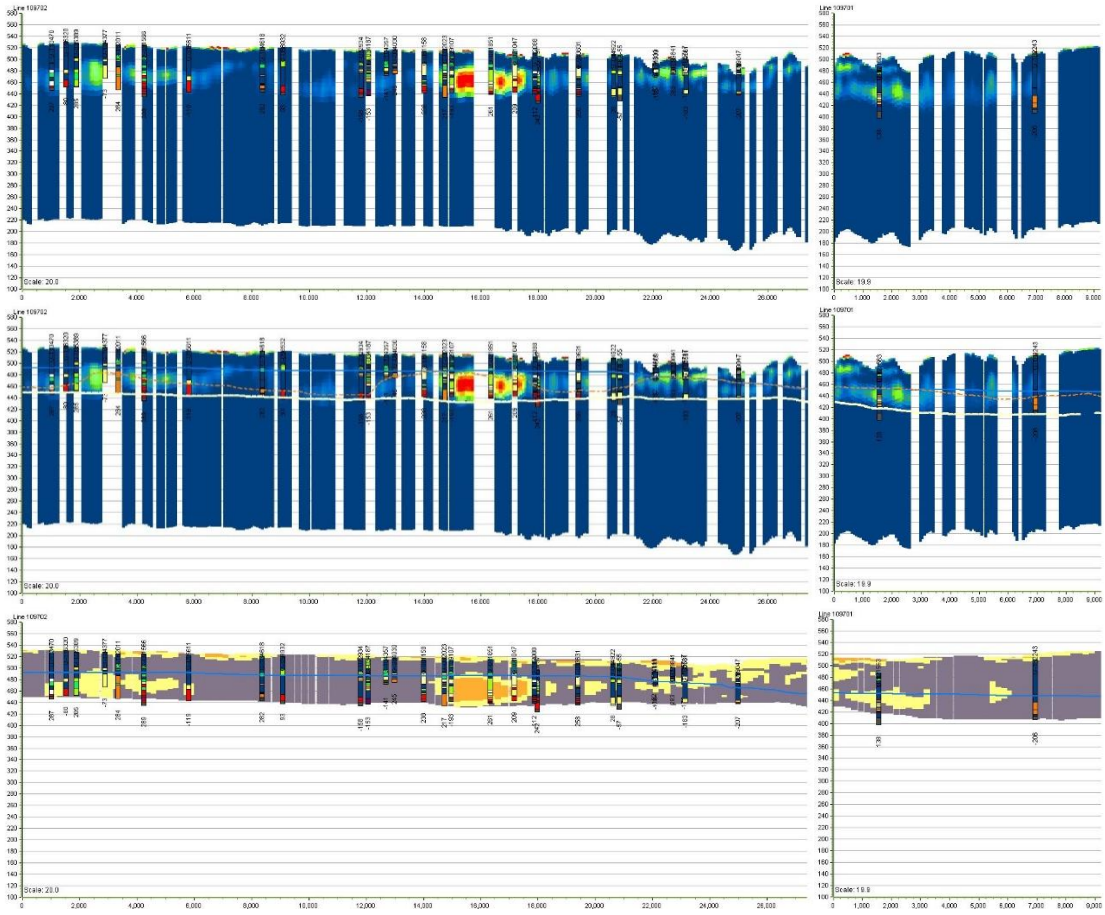

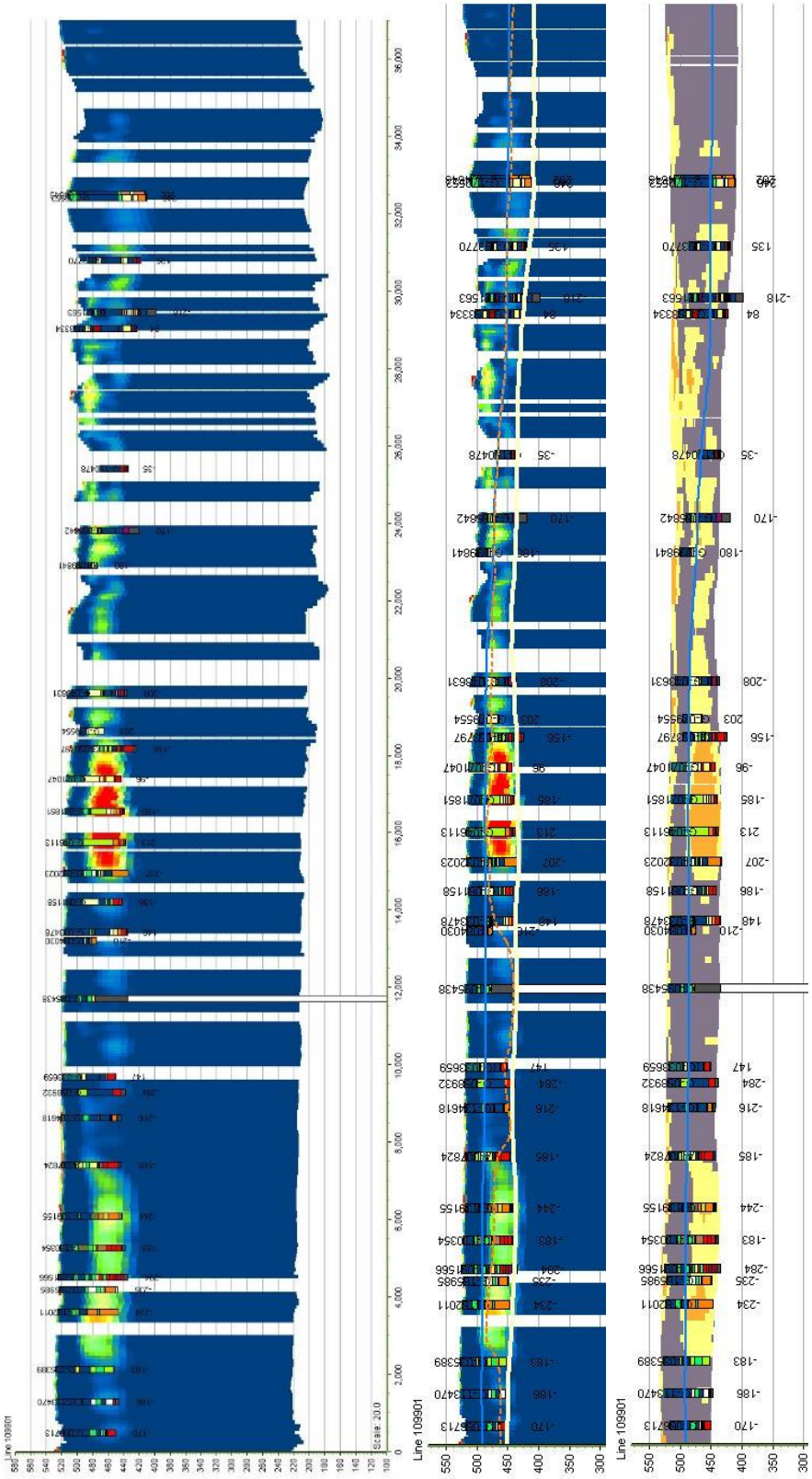

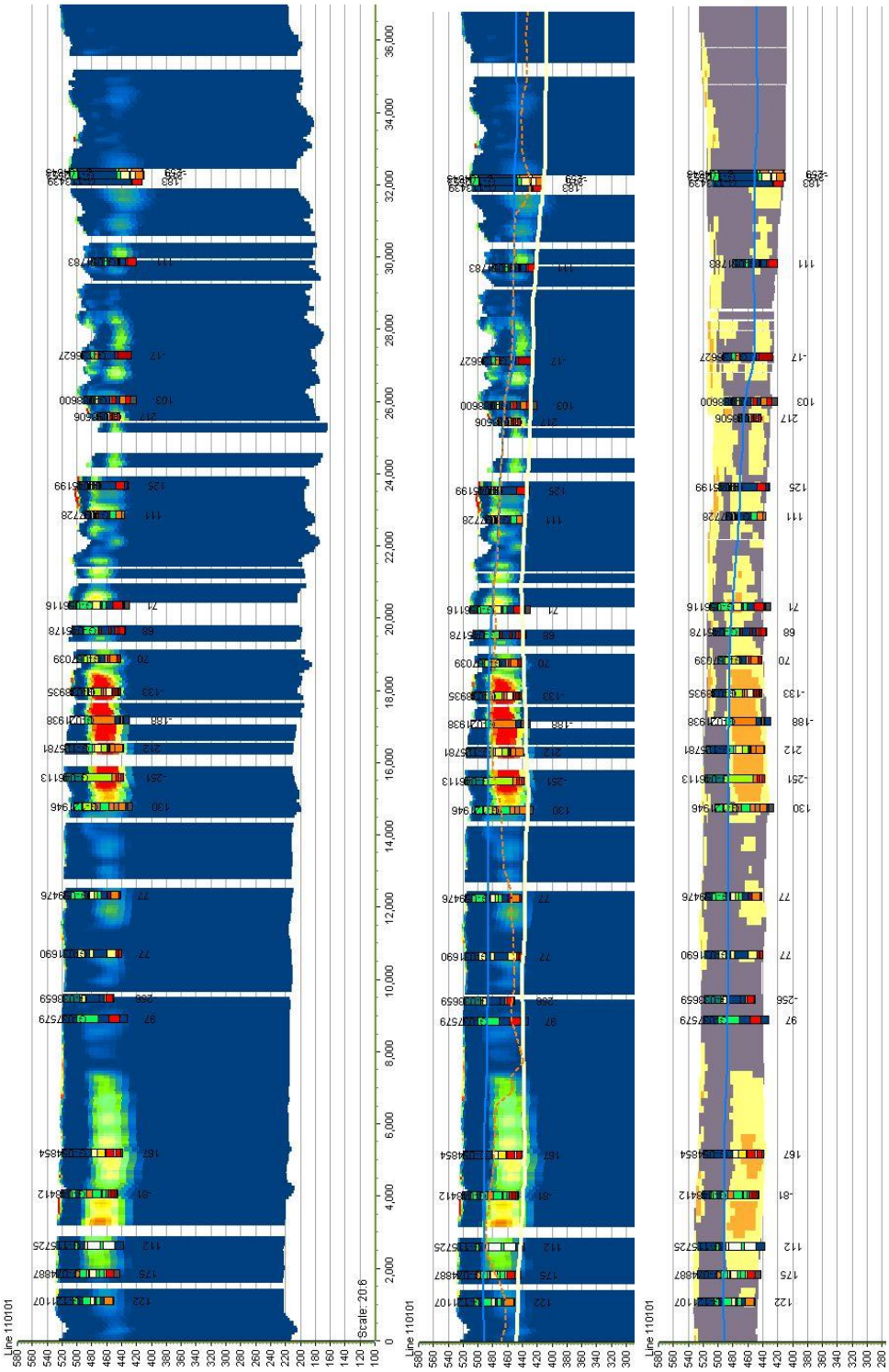
Line 1101101
Scale: 20.6

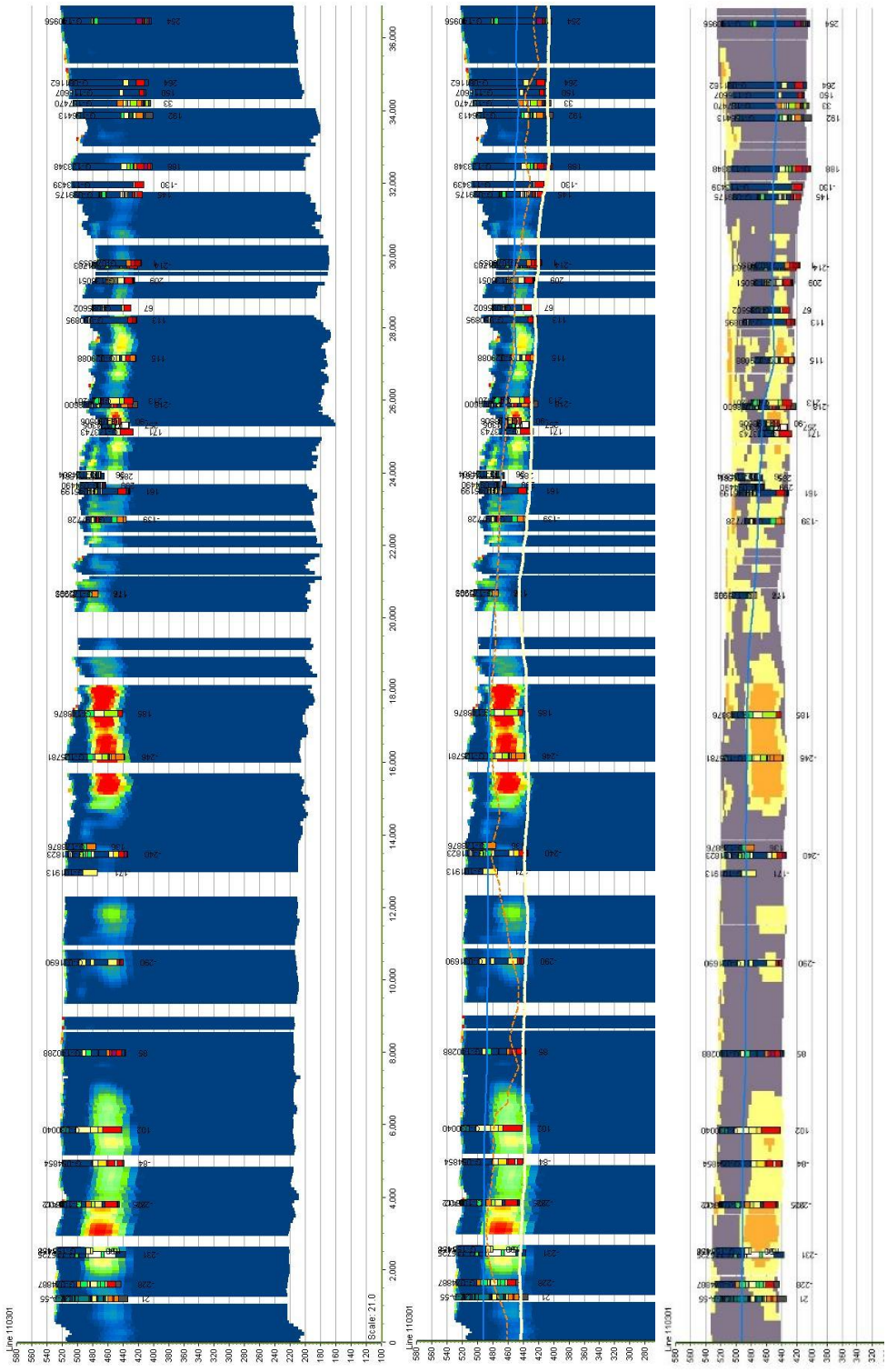

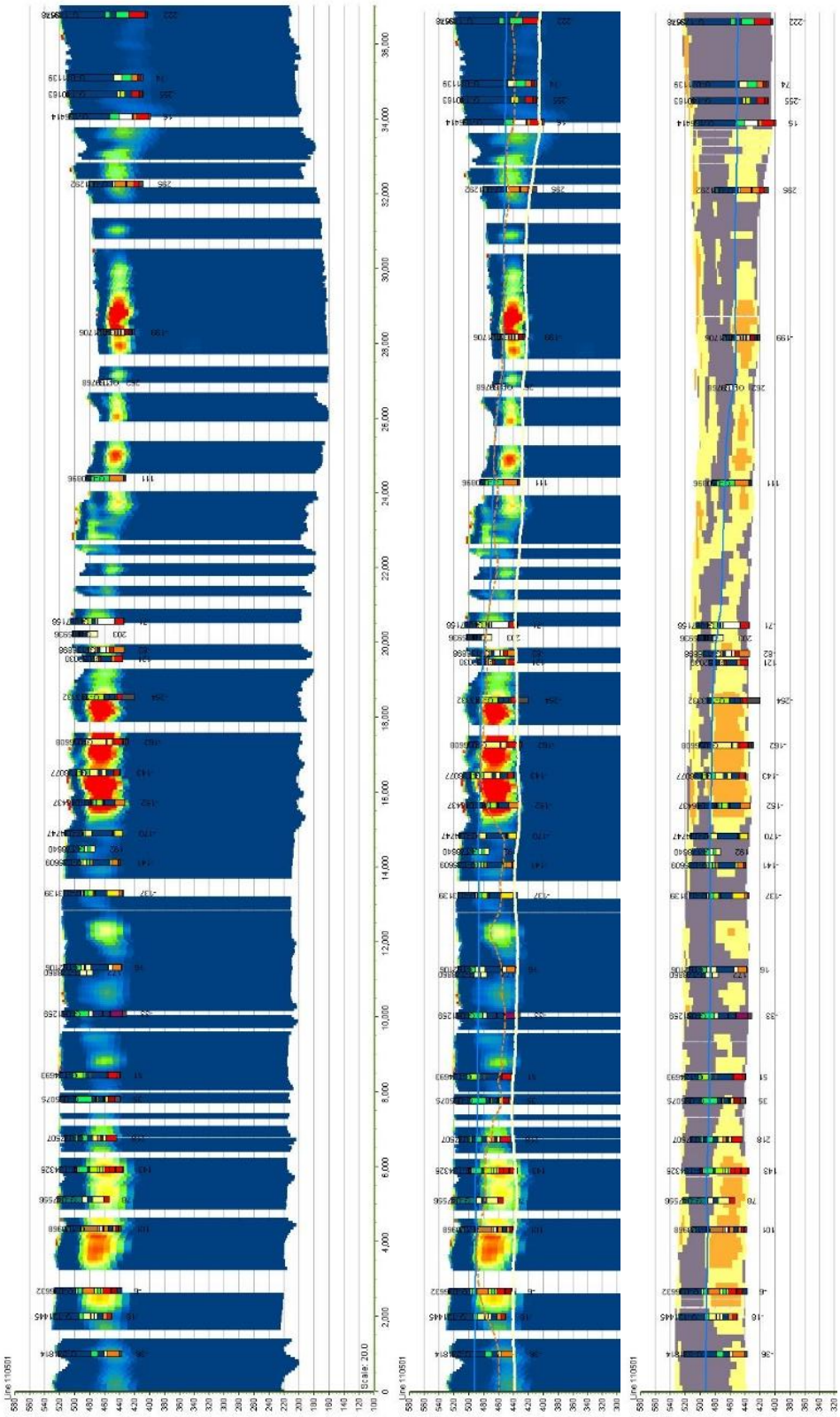

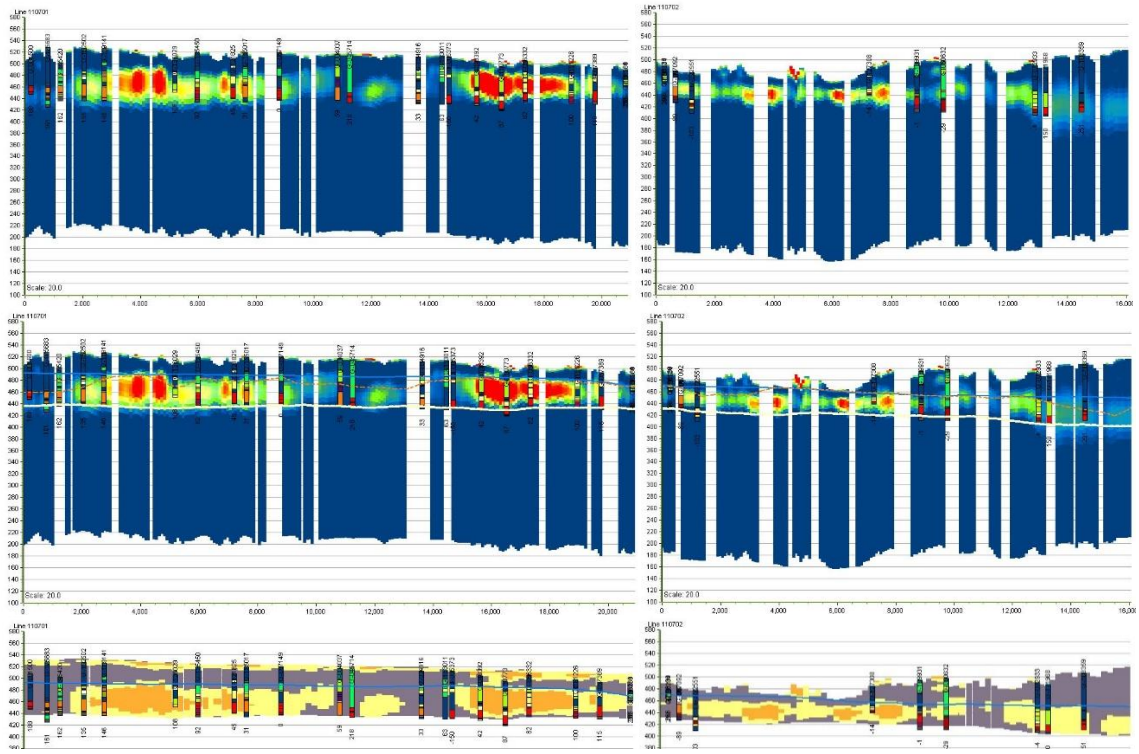

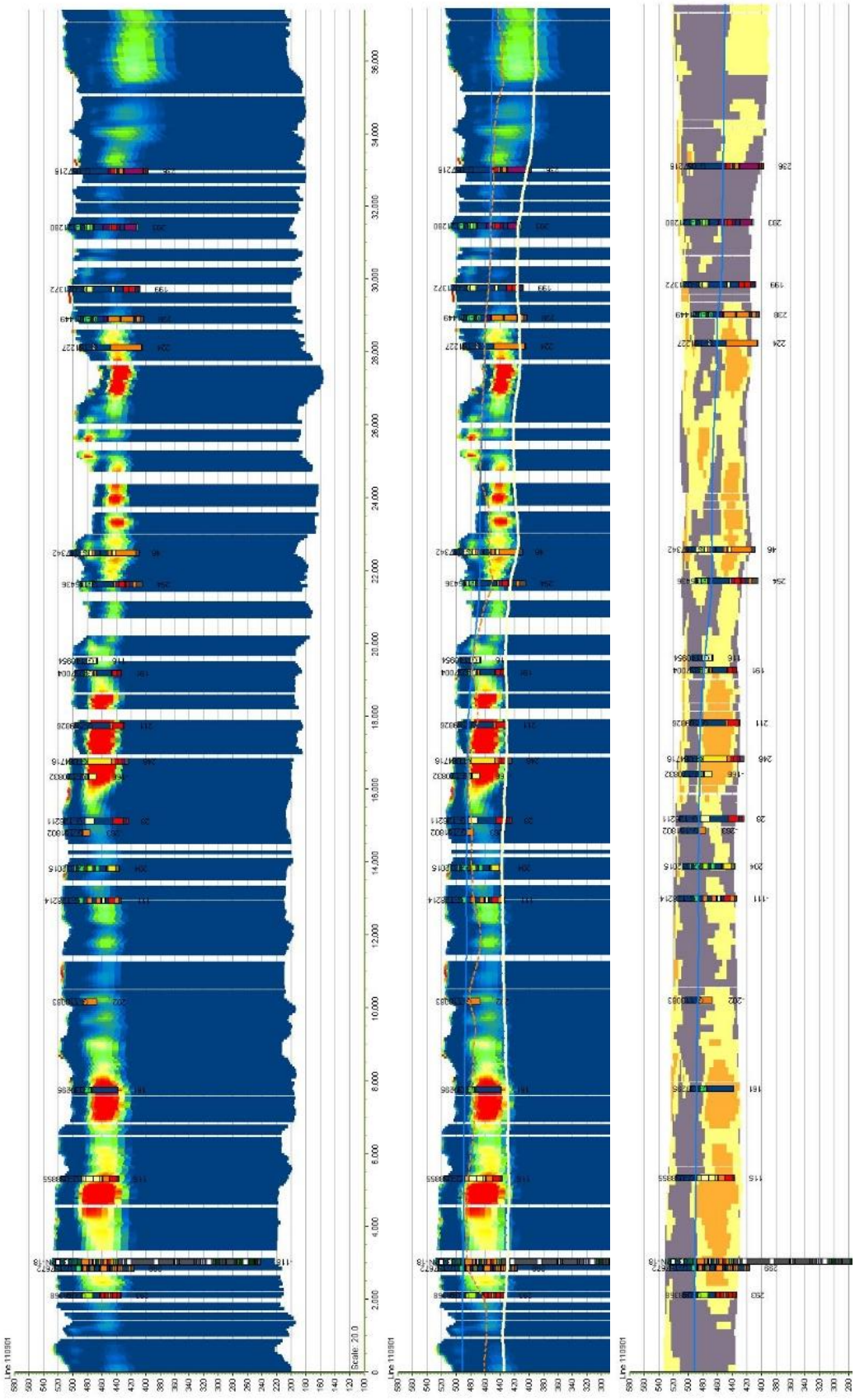

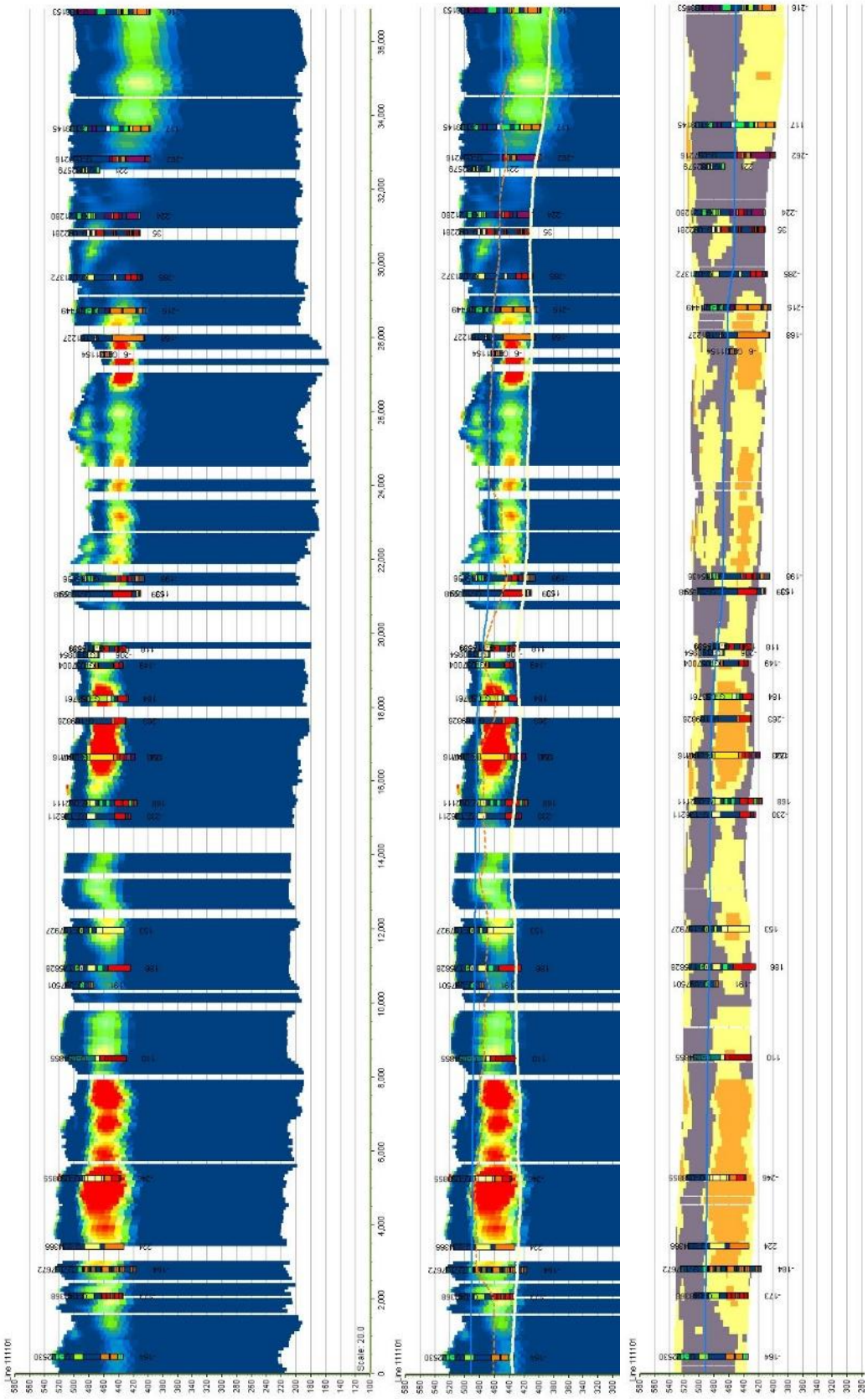

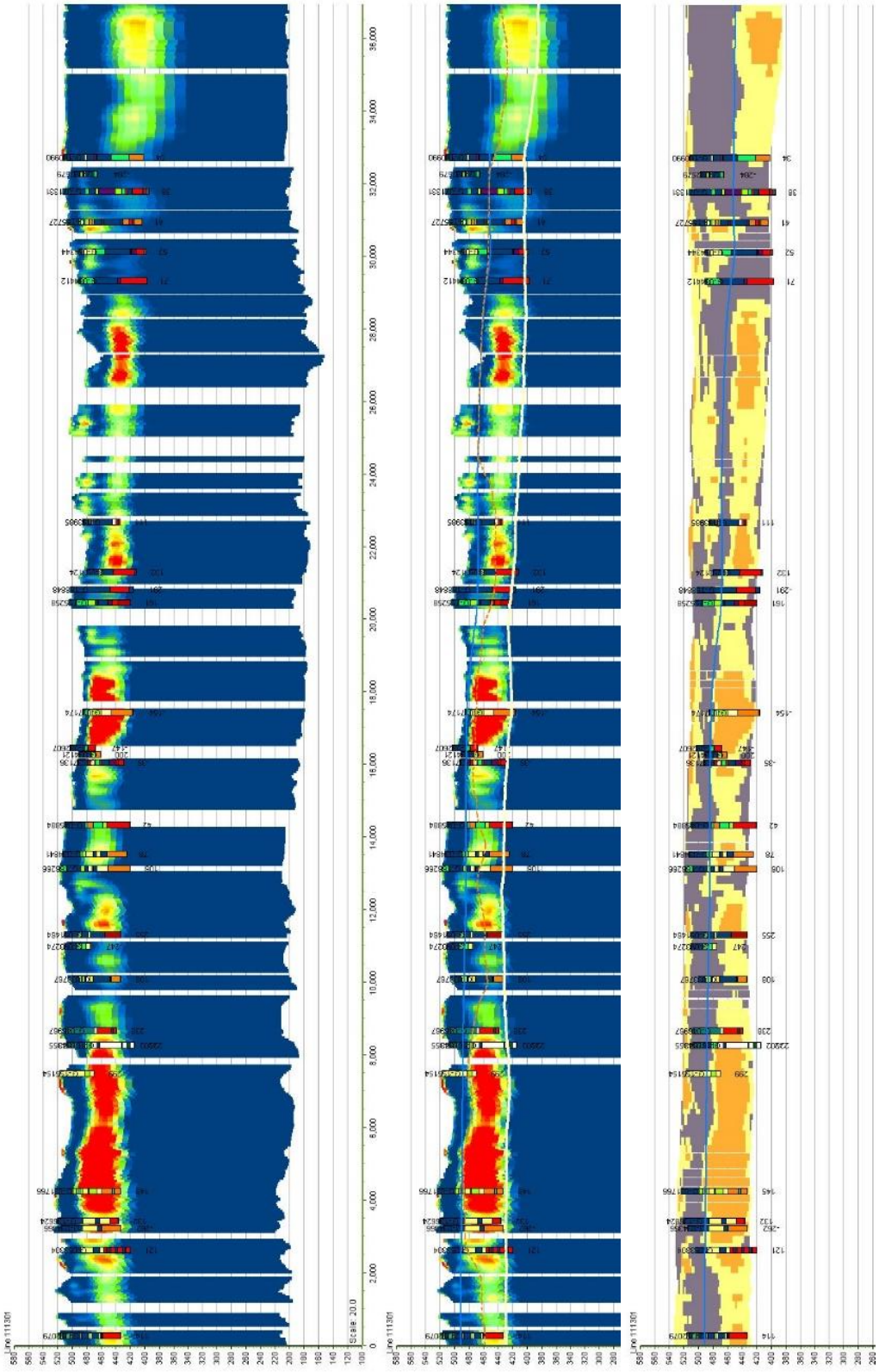

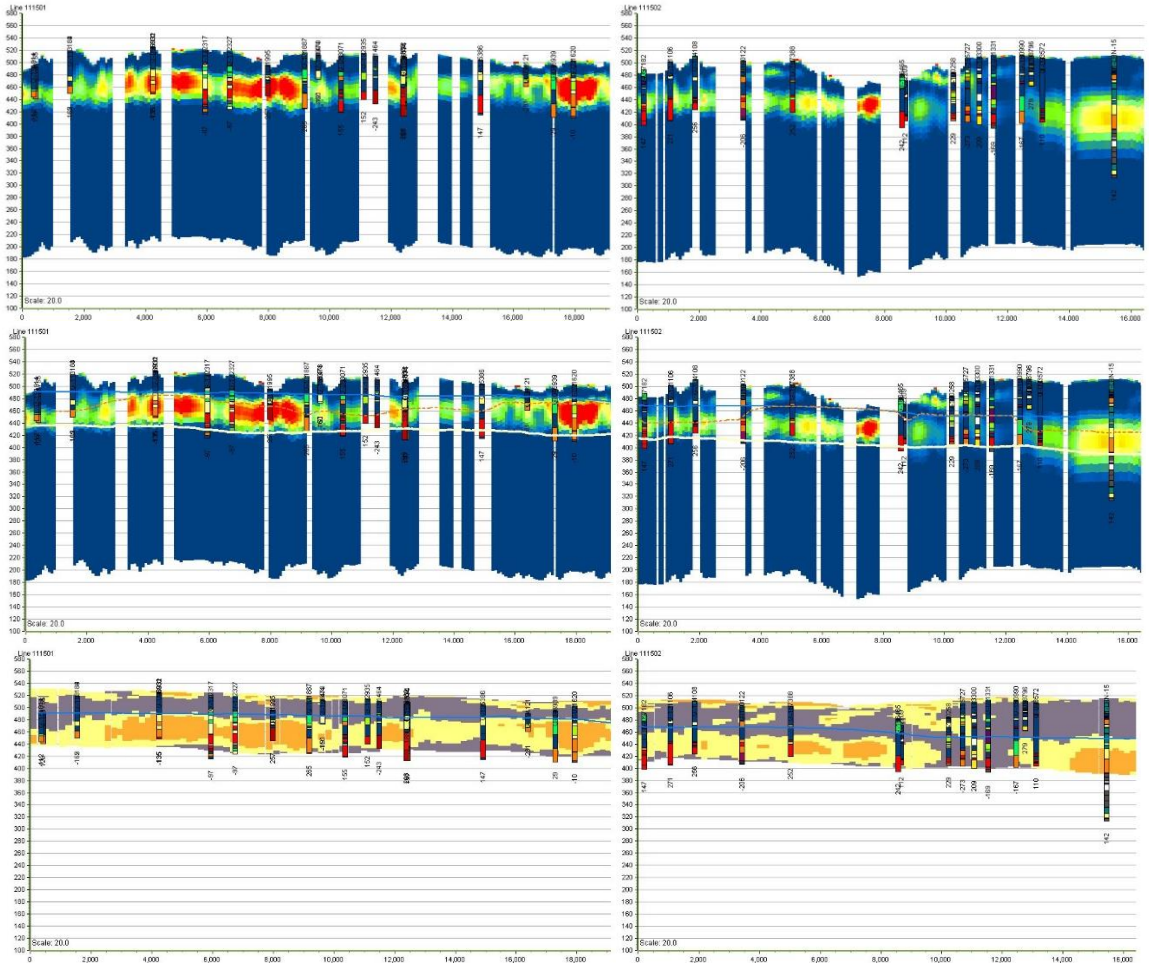
Line 111501
Line 111502
Scale: 20.0

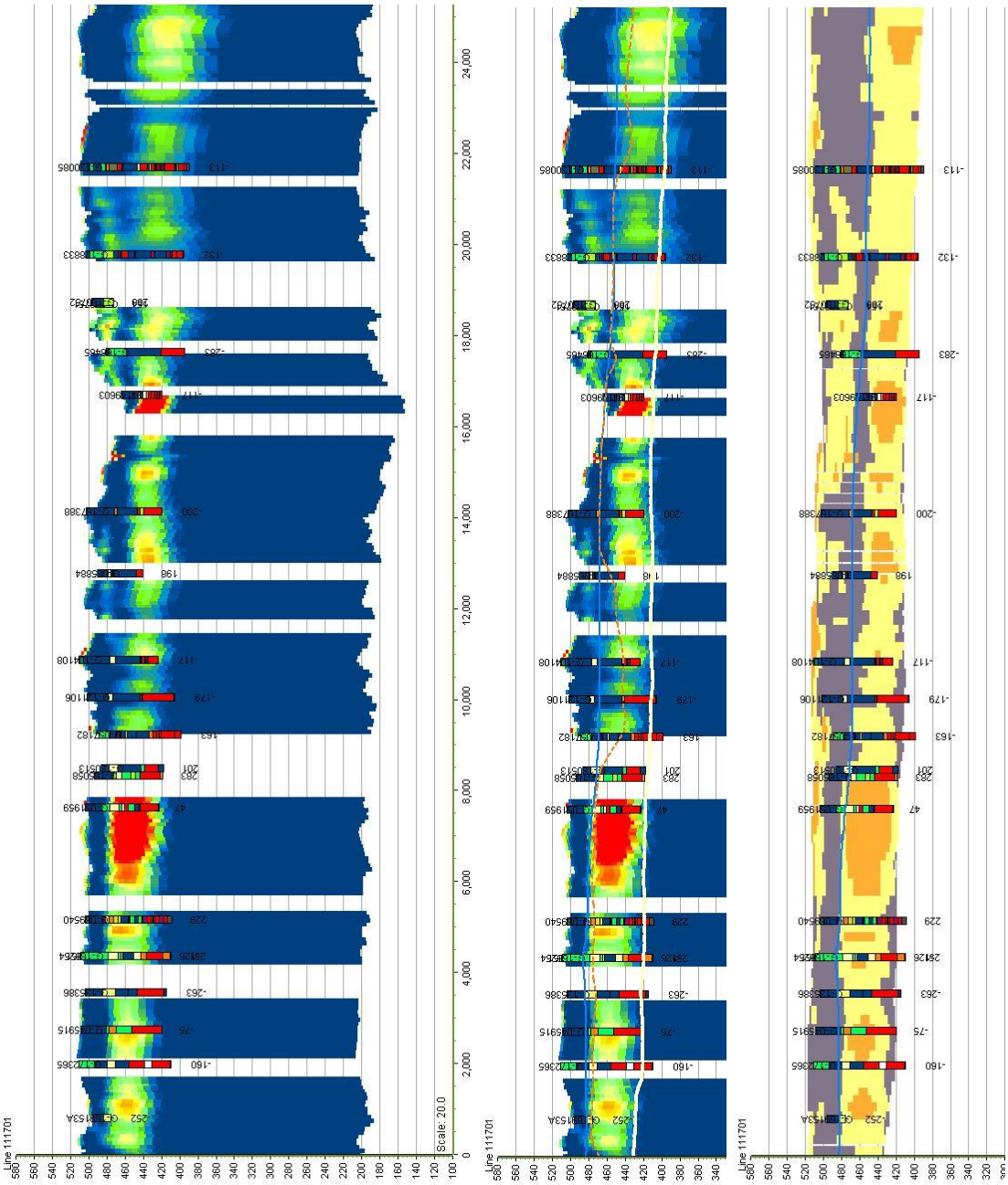

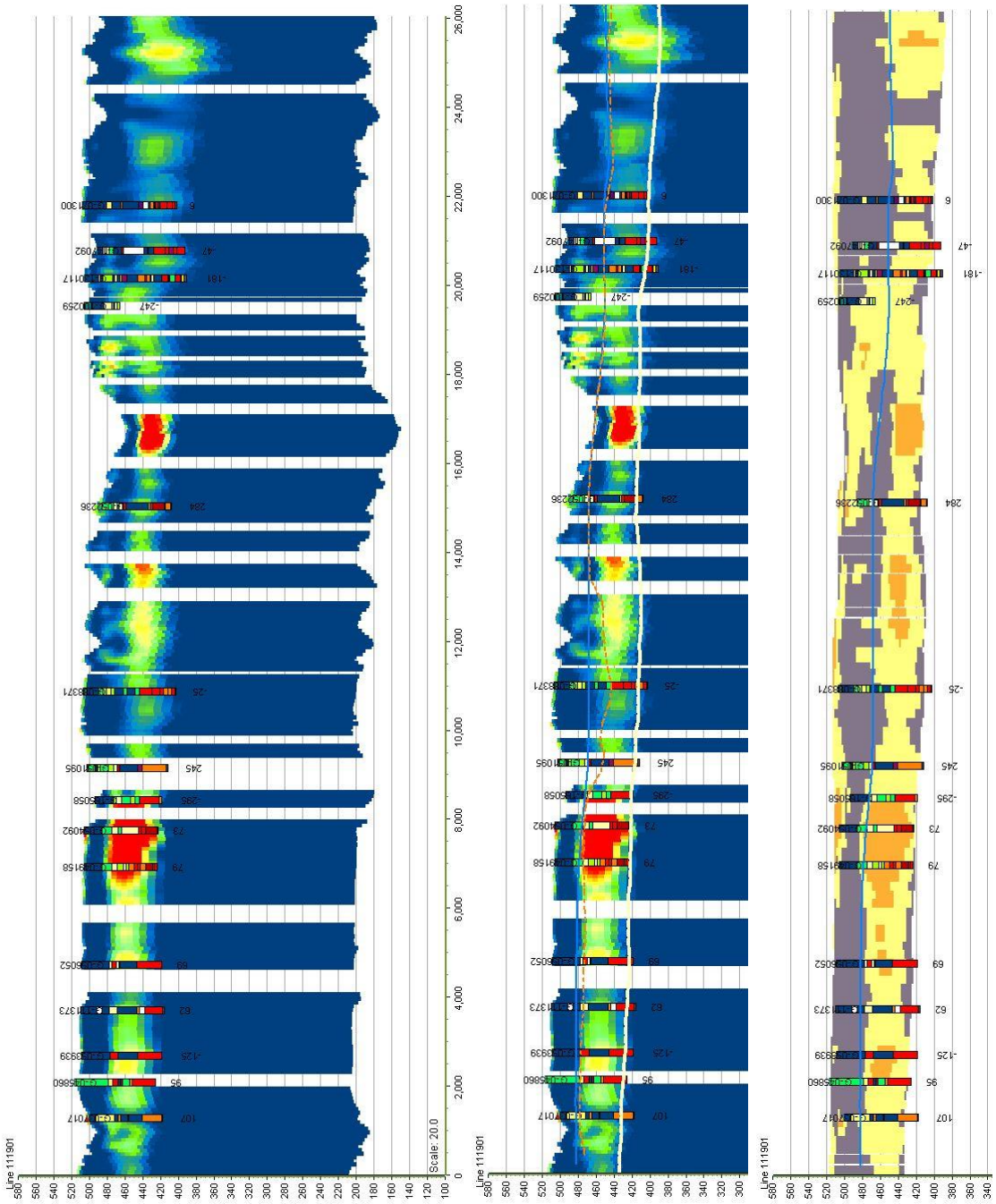

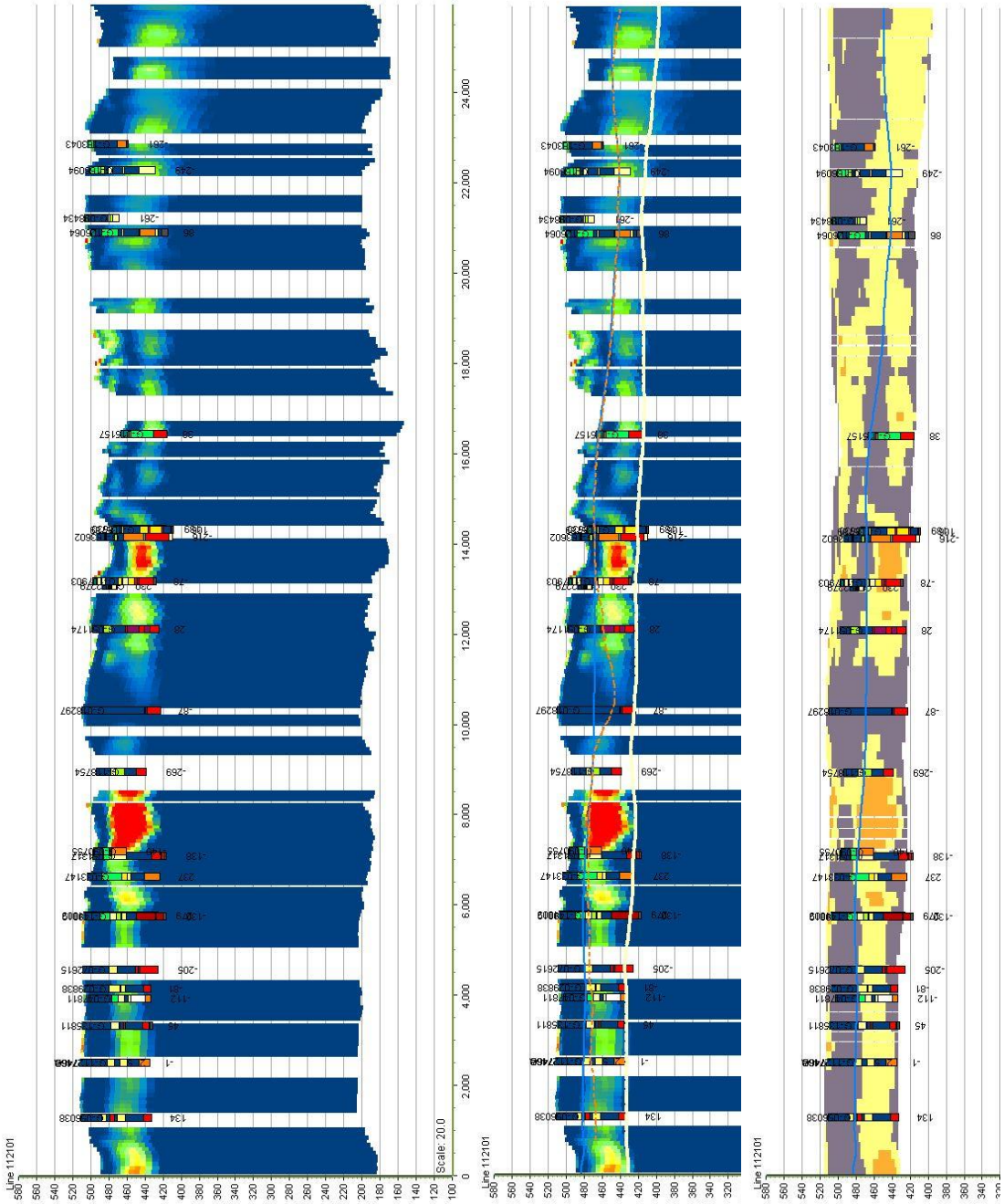
Line 112101
Scale: 20.0
Line 112101
Line 112101

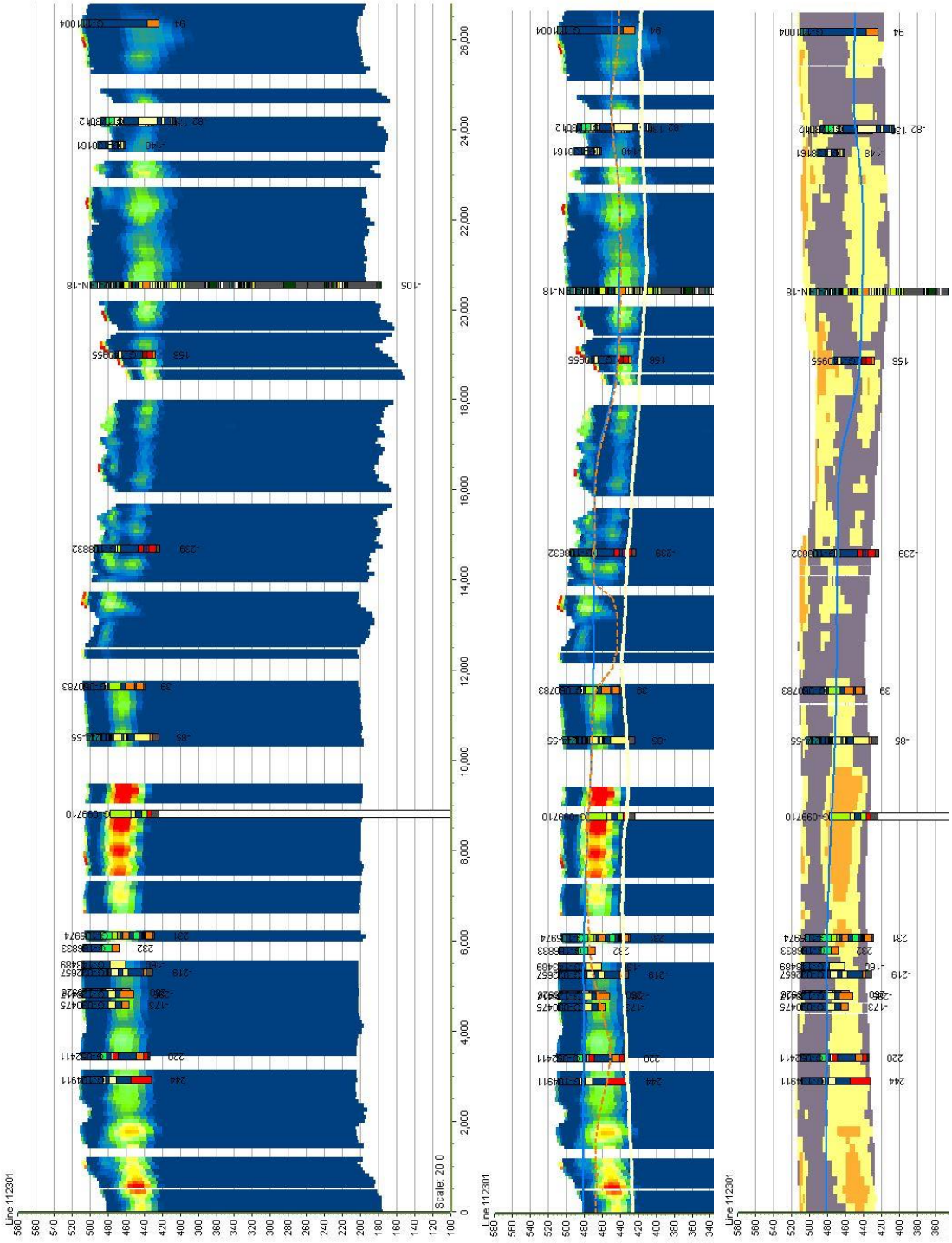
Line 112301
Scale: 20.0
26,000
24,000
22,000
20,000
18,000
16,000
14,000
12,000
10,000
8,000
6,000
4,000
2,000
0

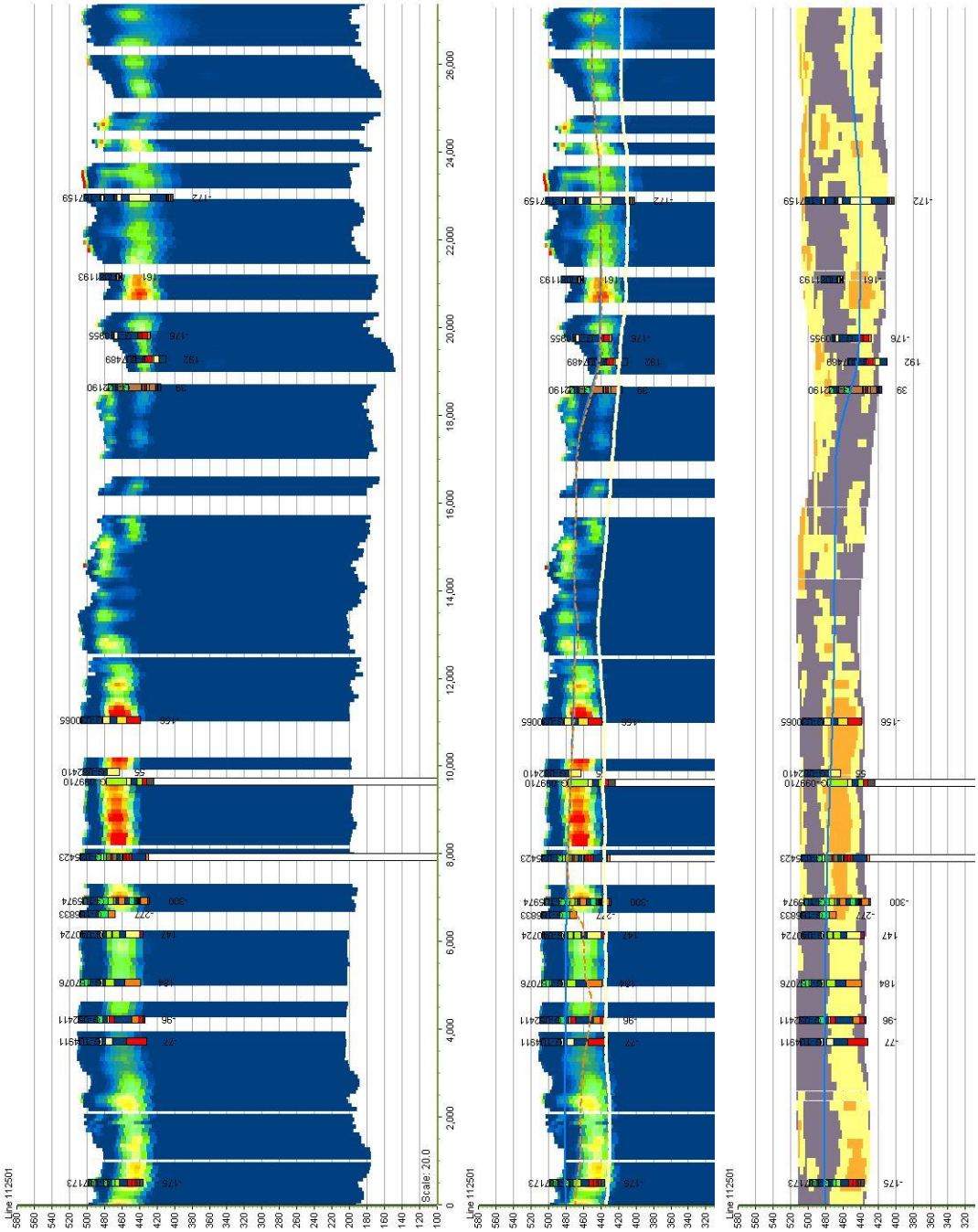
Line 112501
Scale: 20.0
26,000
24,000
22,000
20,000
18,000
16,000
14,000
12,000
10,000
8,000
6,000
4,000
2,000
0
580
560
540
520
500
480
460
440
420
400
380
360
340
320
300
280
260
240
220
200
180
160
140
120
100

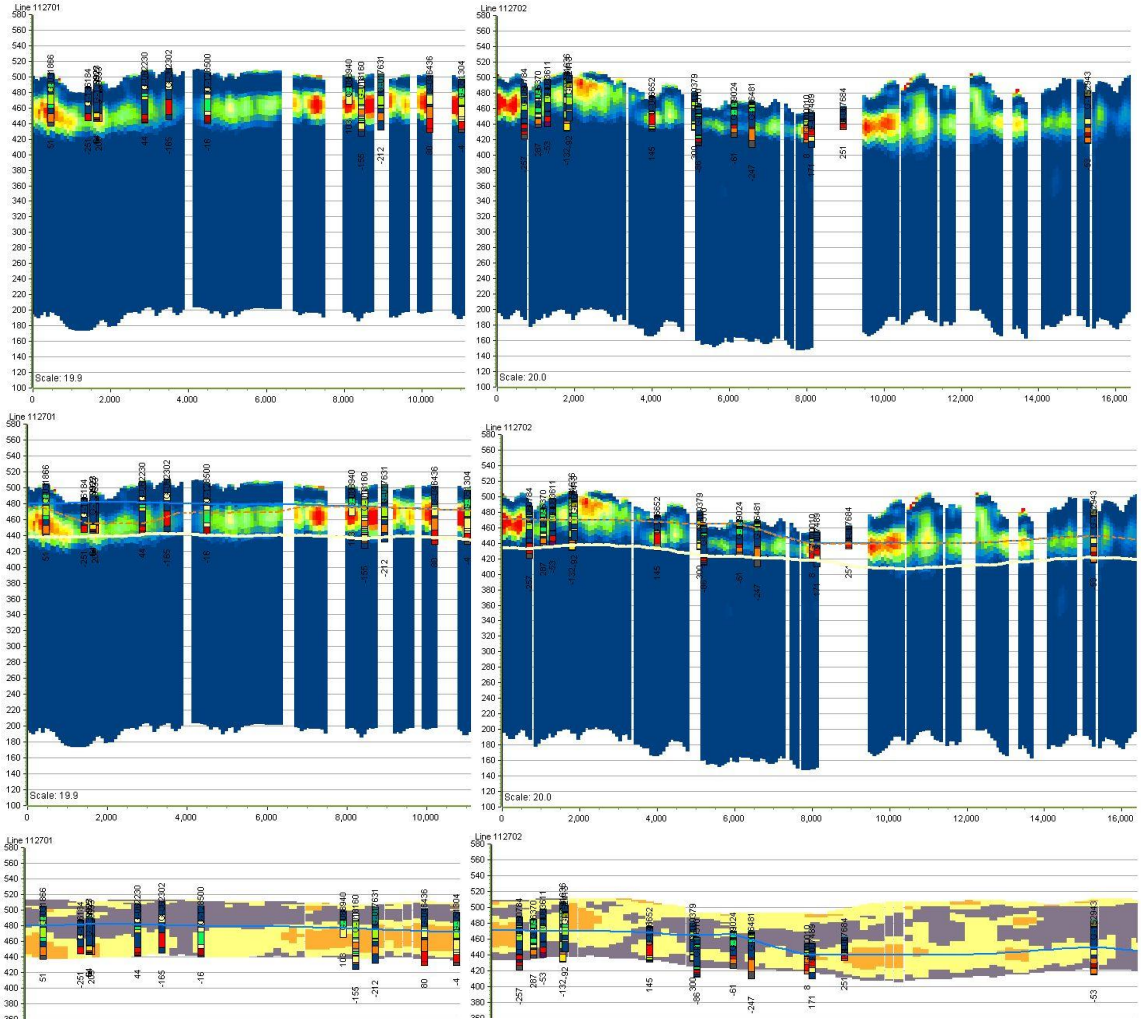
Line 112701
Scale: 19.9
Line 112702
Scale: 20.0
Line 112701
Scale: 19.9
Line 112702
Scale: 20.0
Line 112701
Line 112702

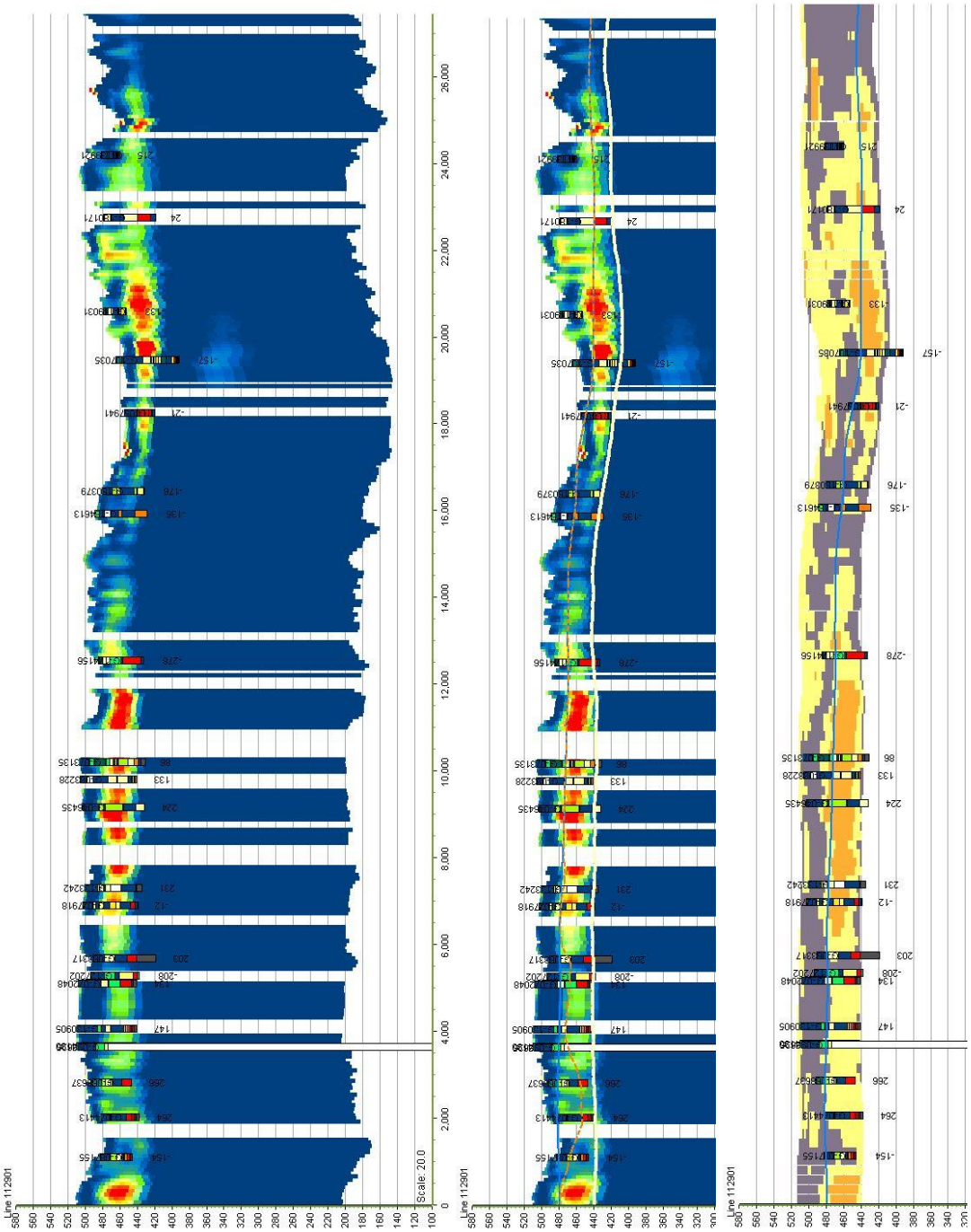
Line 112901
Scale: 20.0

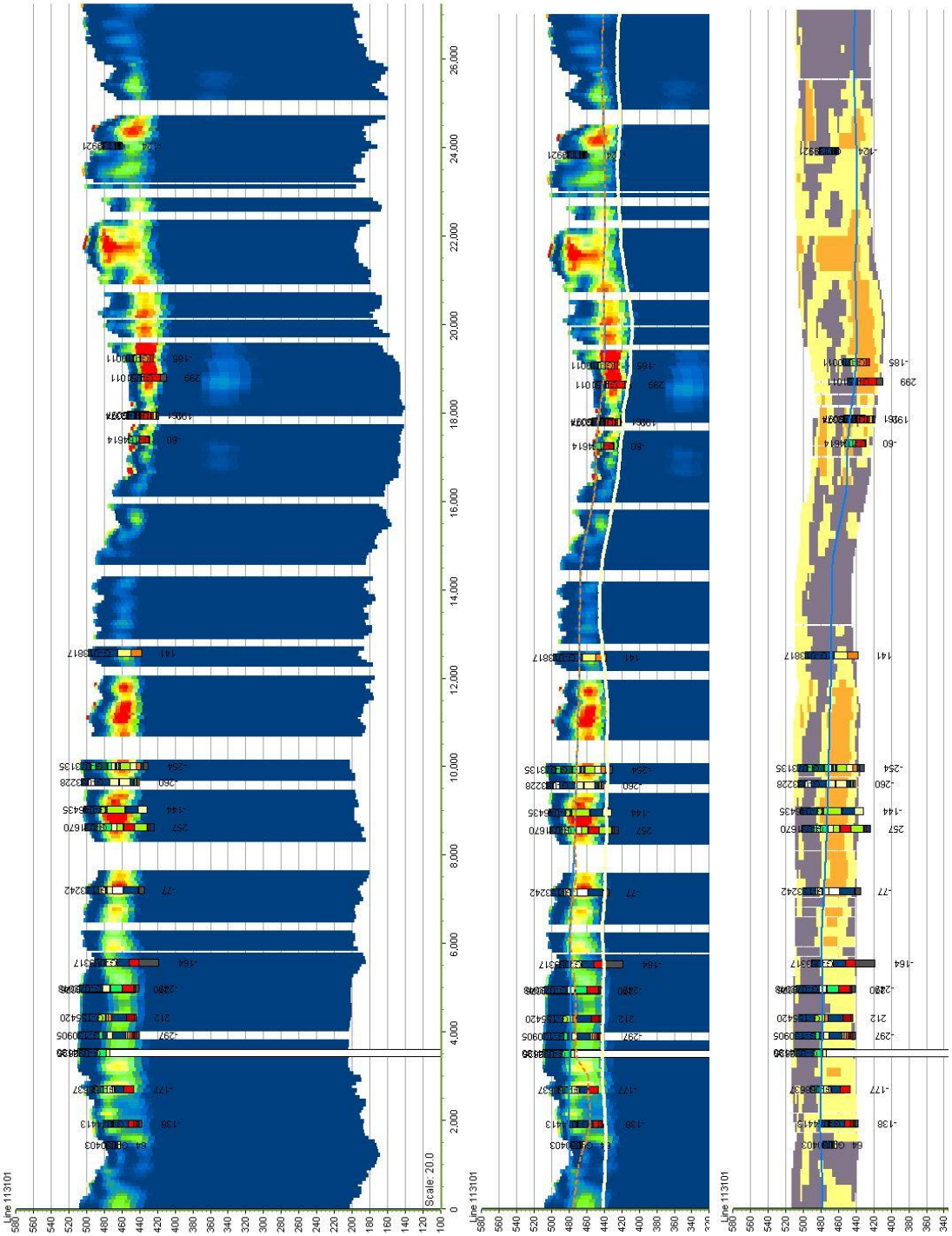
Line 113101
Scale: 20.0
Line 113101
Line 113101

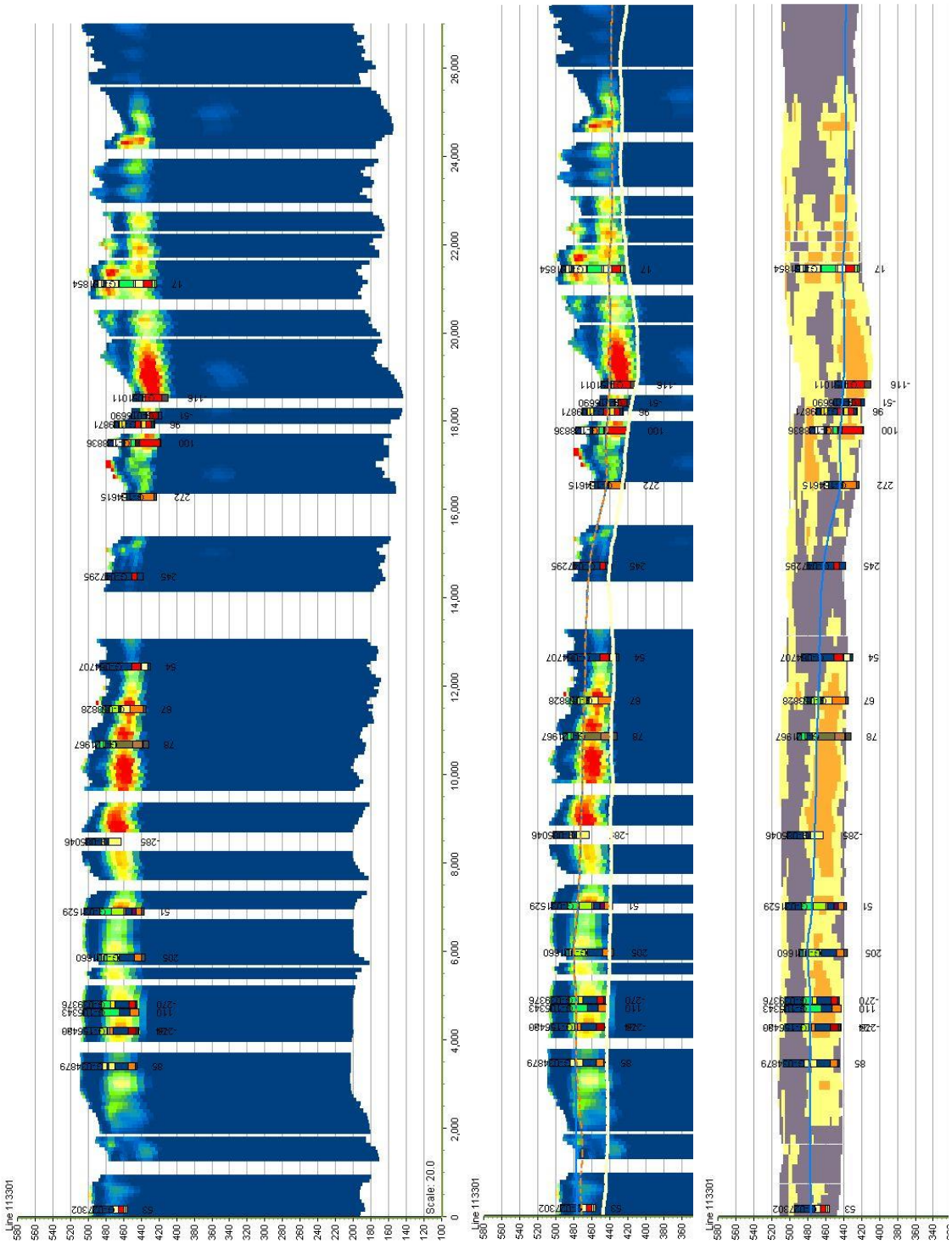
Line 113301
Scale: 20.0
Line 113301
Line 113301

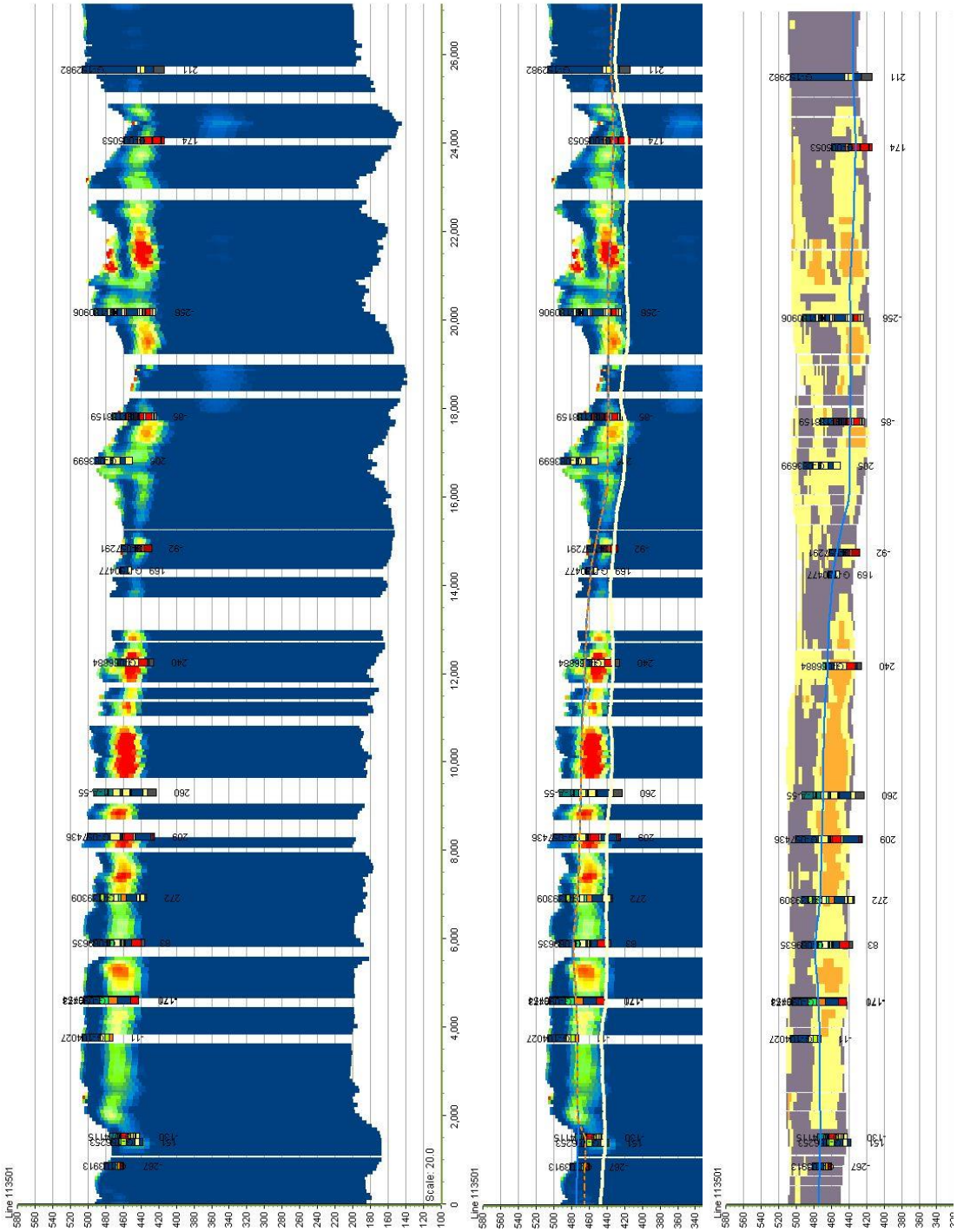
Line 113501
Scale: 20.0

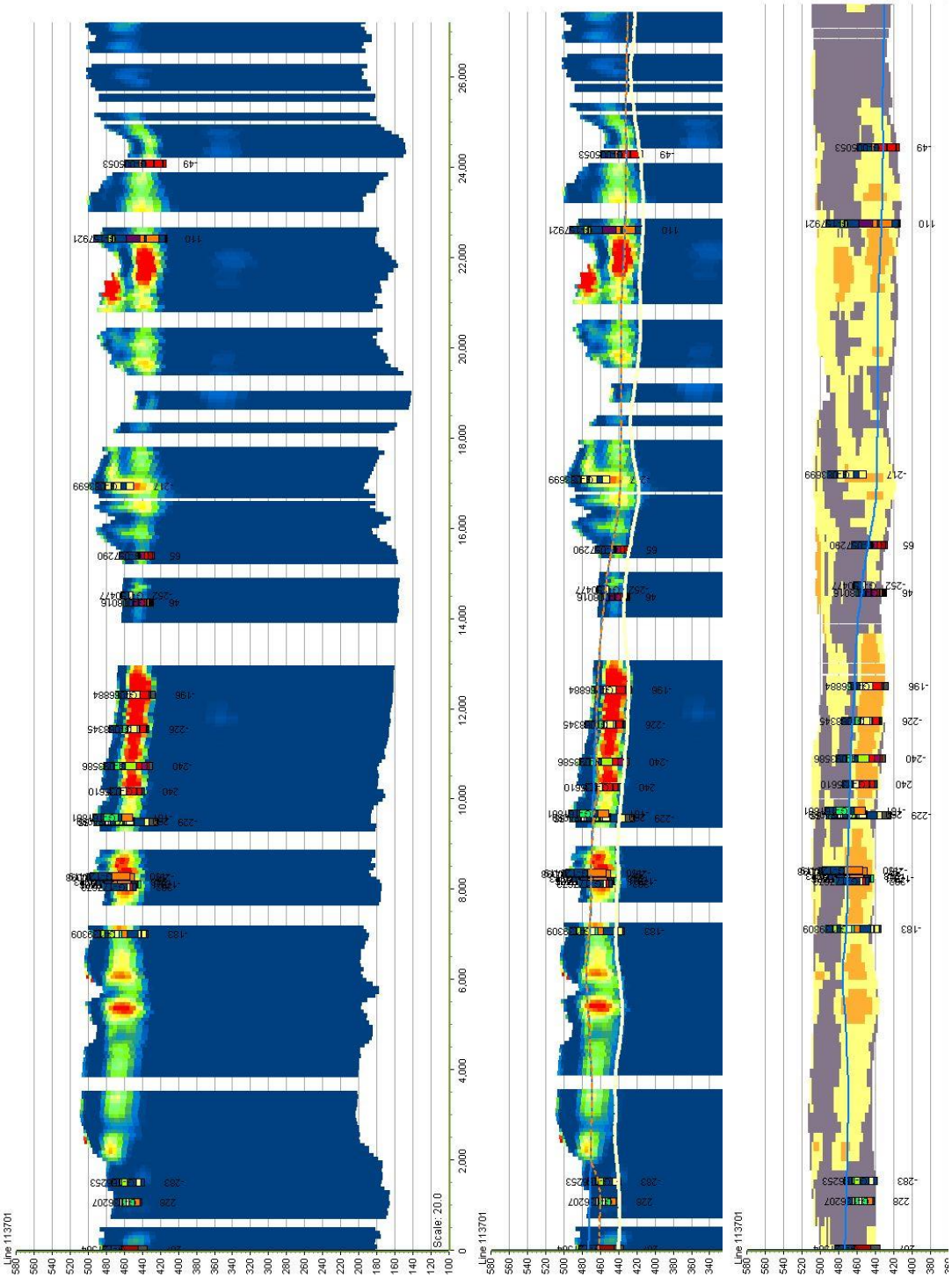
Line 113701
Scale: 20.0
Line 113701
Line 113701

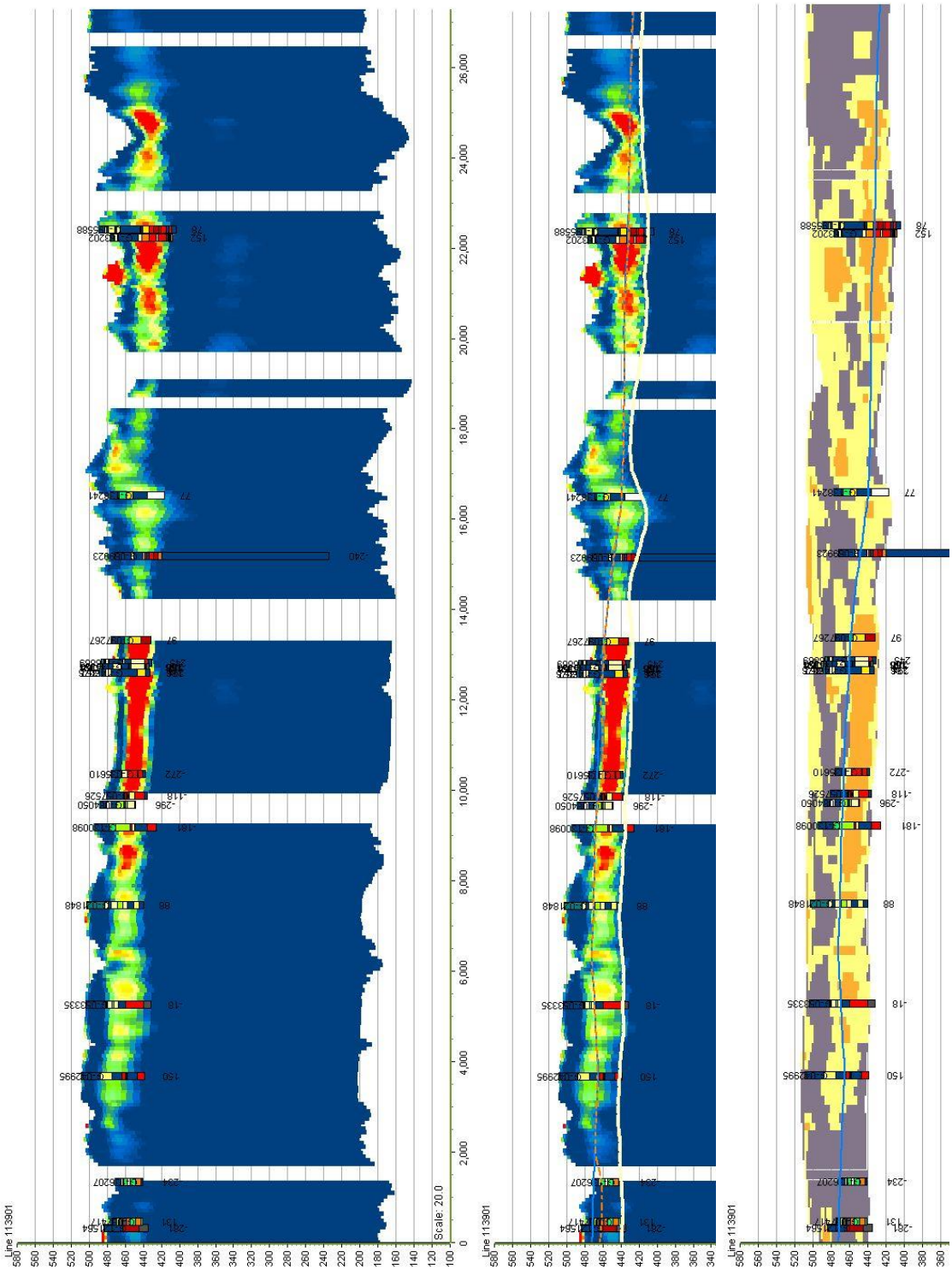
Line 113901
Scale: 20.0
Line 113901
Line 113901

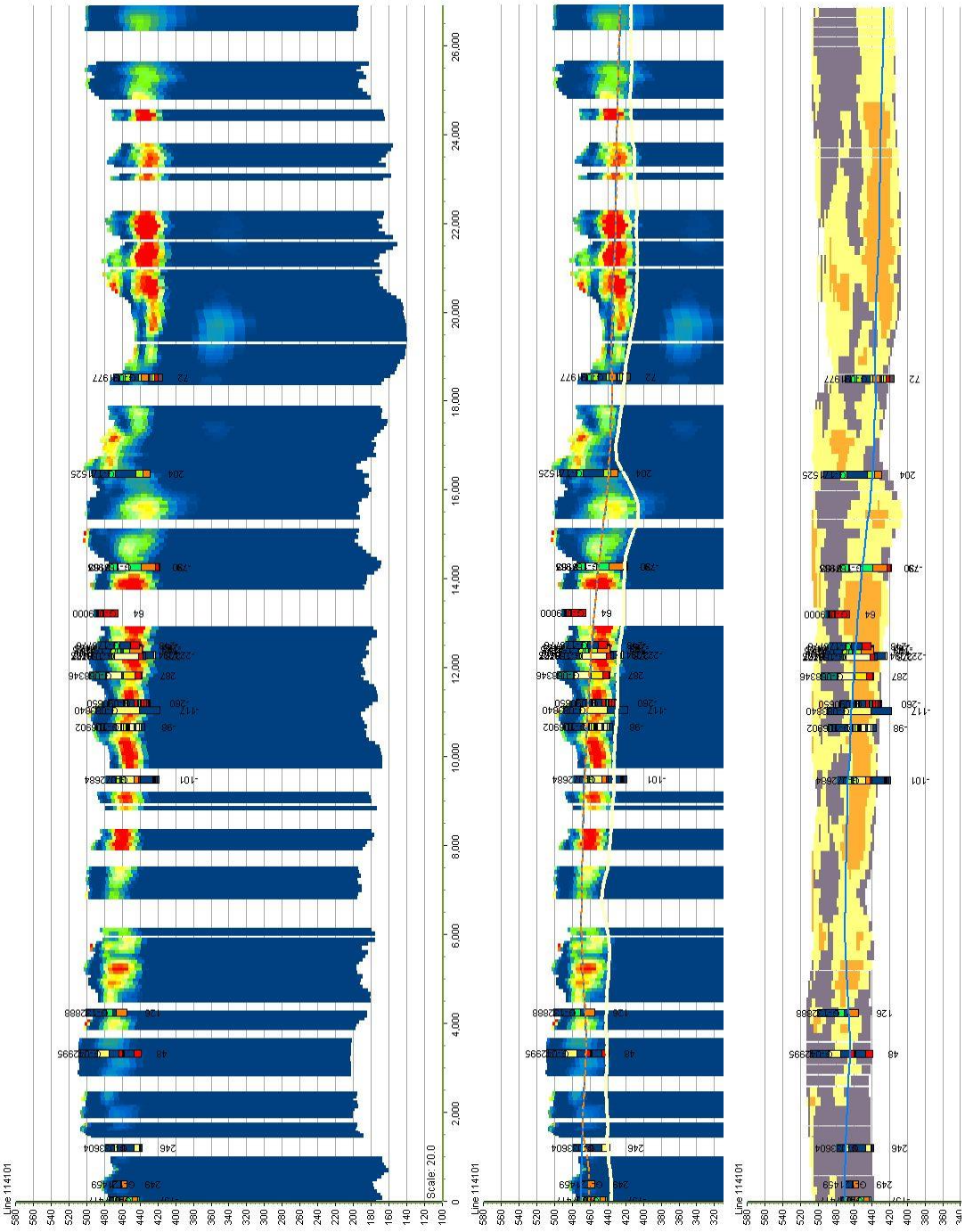
Line 114101
Scale: 20.0
Line 114101
Line 114101

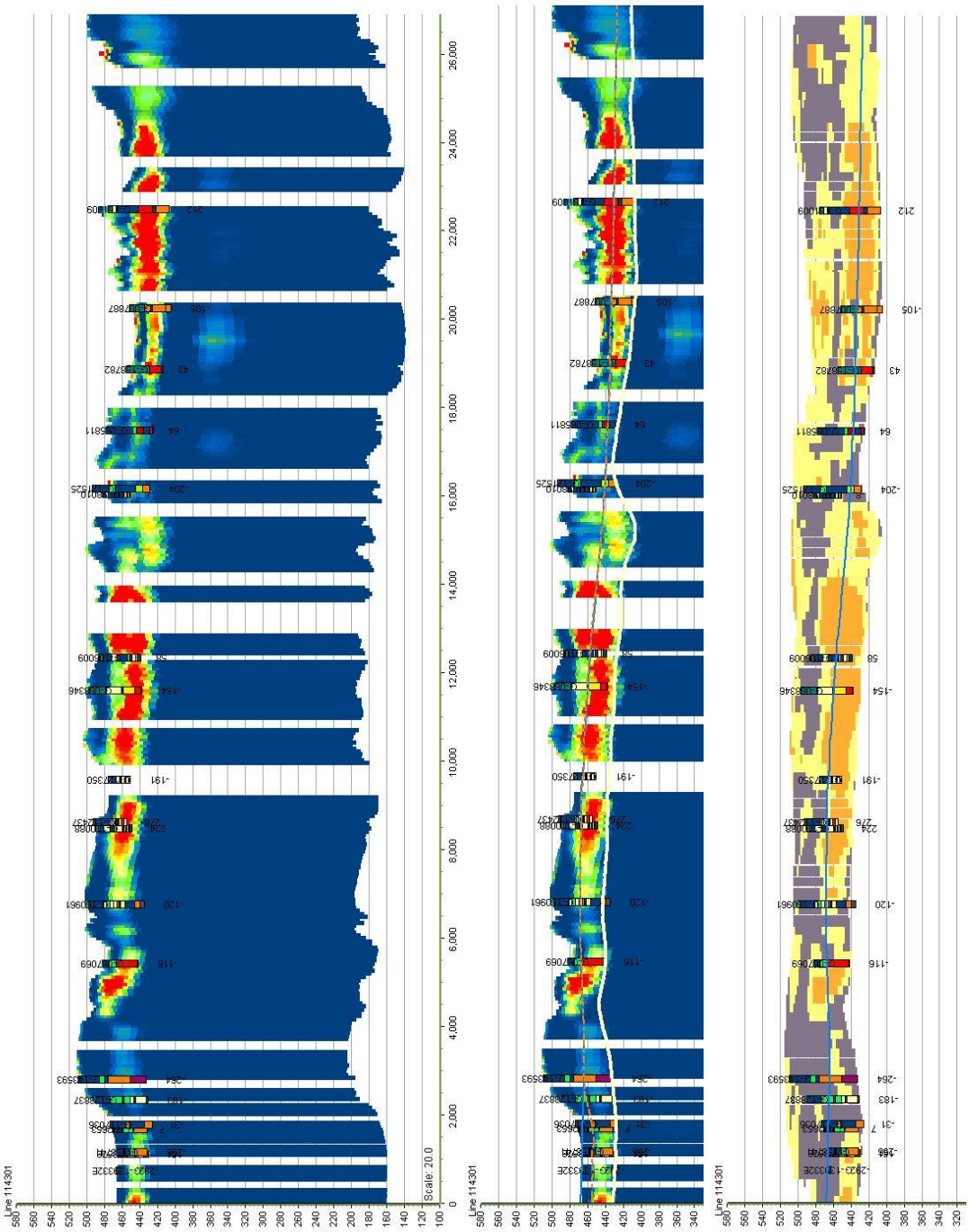

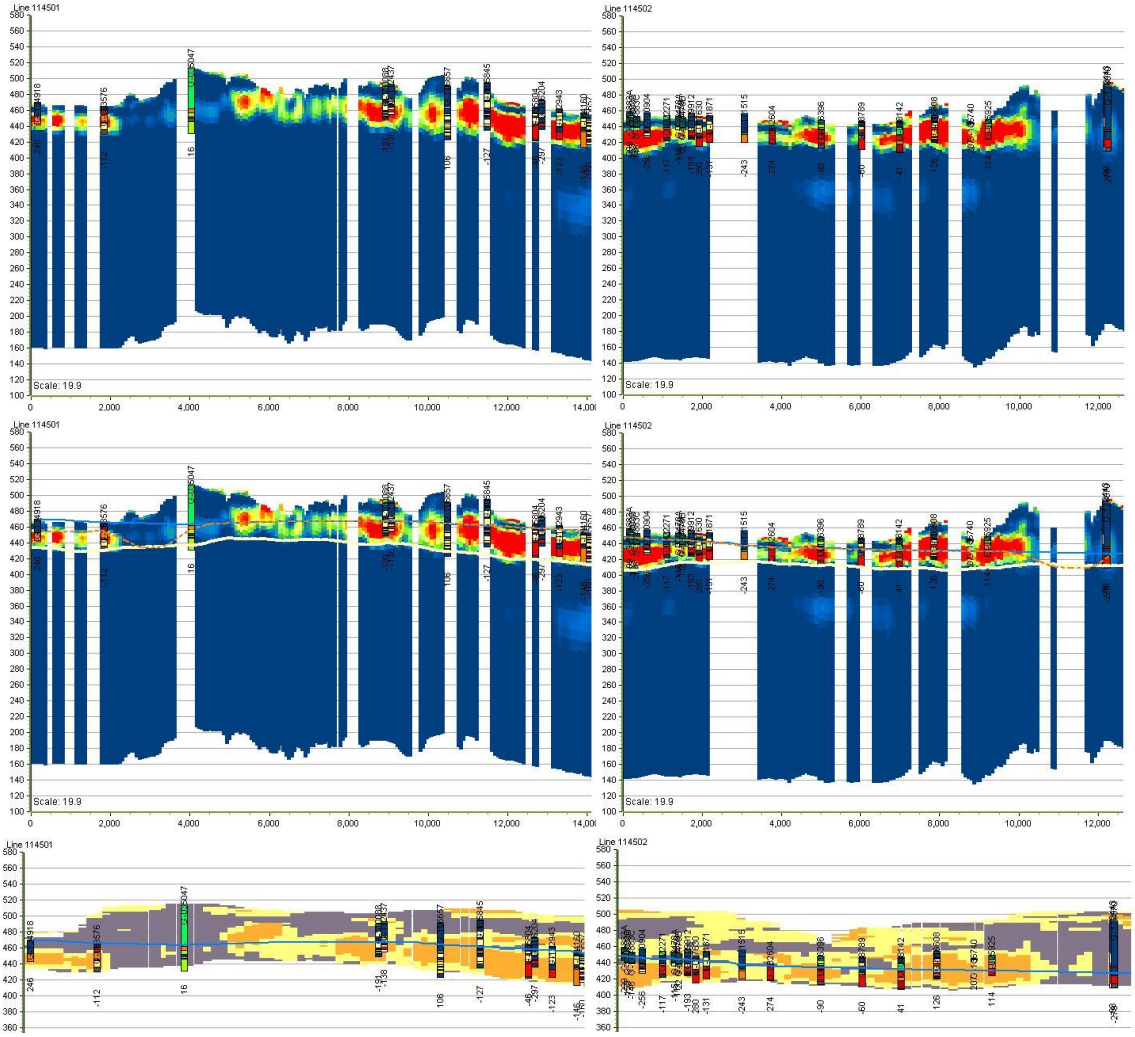
Line 114501
Line 114502
Scale: 19.9

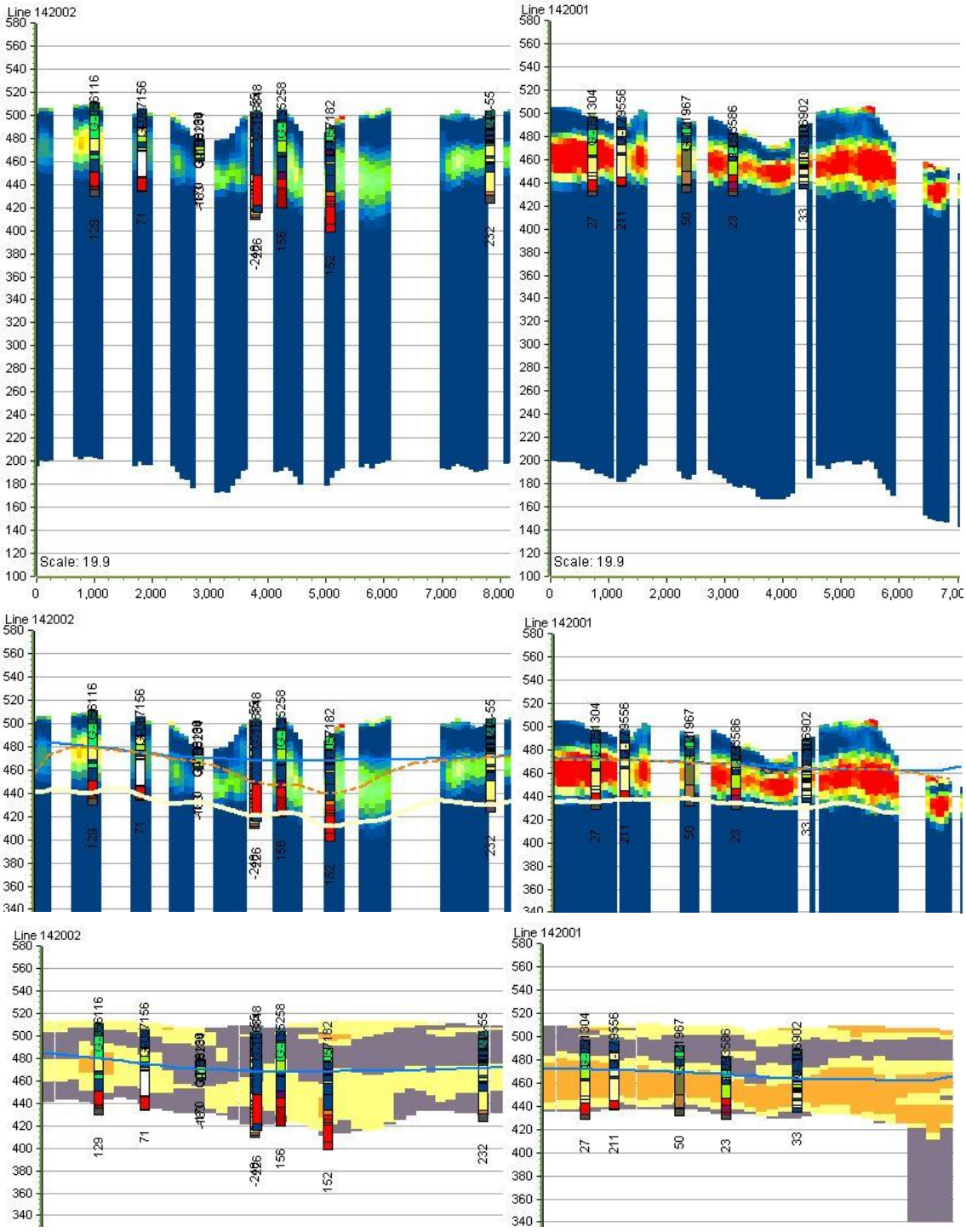
Line 142002
Scale: 19.9
Line 142001
Scale: 19.9
Line 142002
Line 142001
Line 142002
Line 142001

APPENDIX C: FULL HYDROGRAPH FOR EACH WELL SITE

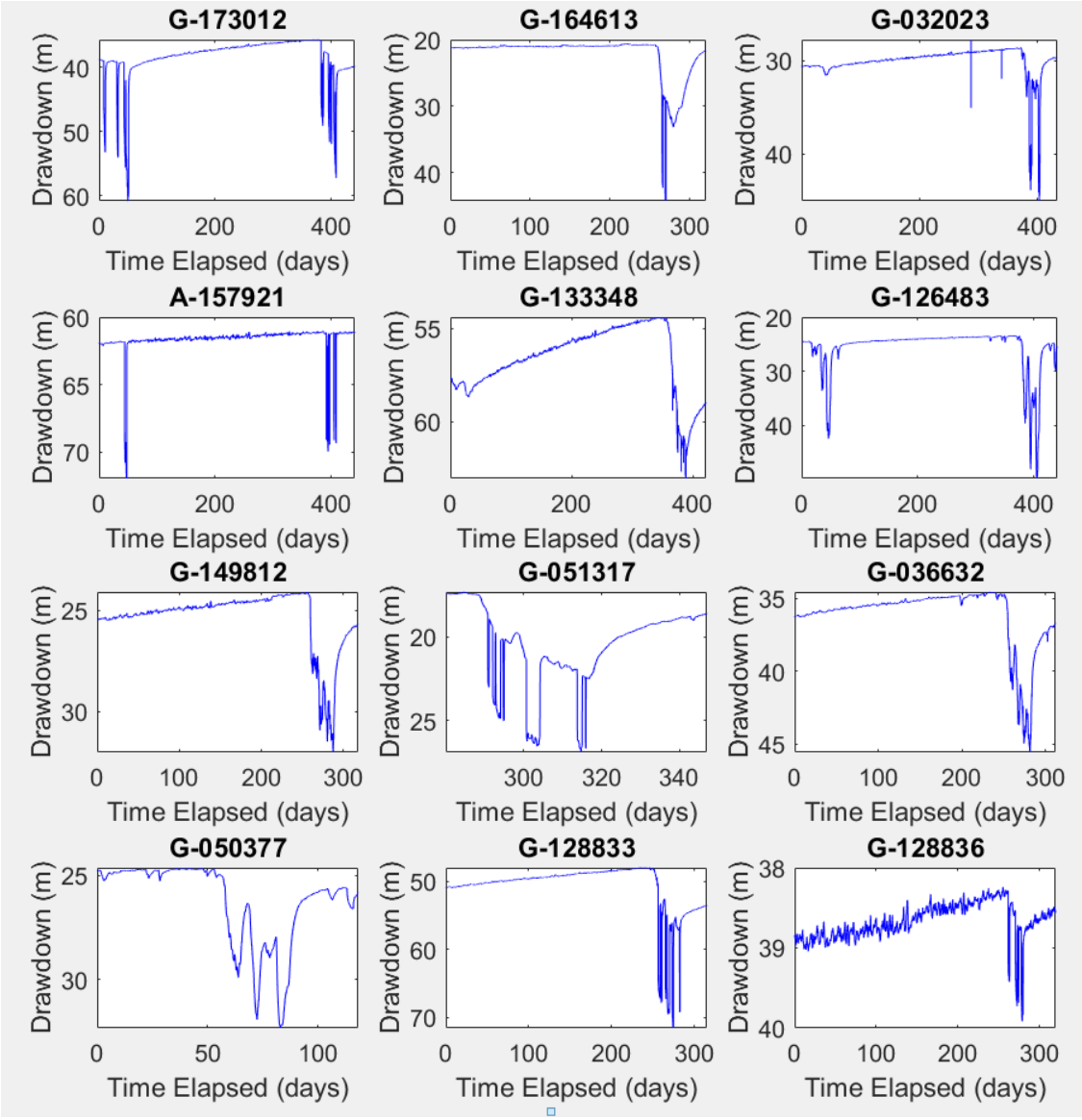

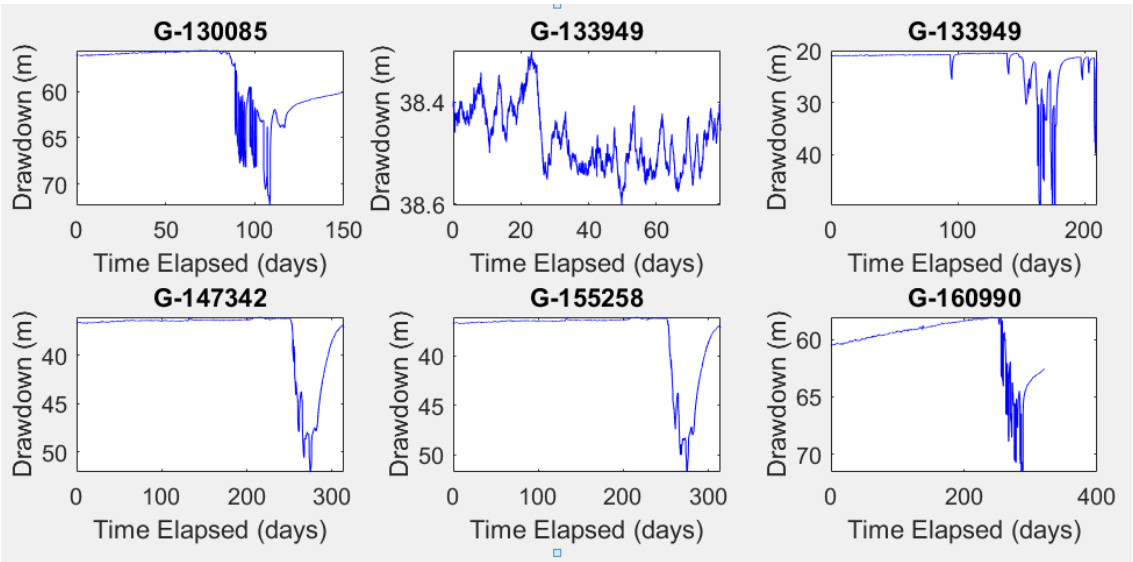
G-130085
Drawdown (m)
60
65
70
0
50
100
150
Time Elapsed (days)
G-133949
Drawdown (m)
38.4
38.6
0
20
40
60
Time Elapsed (days)
G-133949
Drawdown (m)
20
30
40
0
100
200
Time Elapsed (days)
G-147342
Drawdown (m)
40
45
50
0
100
200
300
Time Elapsed (days)
G-155258
Drawdown (m)
40
45
50
0
100
200
300
Time Elapsed (days)
G-160990
Drawdown (m)
60
65
70
0
200
400
Time Elapsed (days)

BIBLIOGRAPHY

Abraham, J. D., Minsley, B. J., Bedrosian, P. A., Smith, B. D., & Cannia, J. C. (2019). Airborne Electromagnetic Surveys for Groundwater Characterization. *ASEG Extended Abstracts*, *2012*(1), 1–4. https://doi.org/10.1071/aseg2012ab246

Aeschbach-Hertig, W., & Gleeson, T. (2012). Regional strategies for the accelerating global problem of groundwater depletion. *Nature Geoscience*, *5*(12), 853–861. https://doi.org/10.1038/ngeo1617

Alley, W., Reilly, T., & Franke, O. (1999). *Sustainability of Ground-Water Resources*.

Anderson, M. P. (1989). *Hydrogeologic fades models to delineate large-scale spatial trends in glacial and glaciofluvial sediments*. Retrieved from https://pubs.geoscienceworld.org/gsa/gsabulletin/article-pdf/101/4/501/3380524/i0016-7606-101-4-501.pdf

Aqua Geo Frameworks. (2017). *Hydrogeologic Framework of Selected Areas in the Lower Platte North Natural Resources District , Nebraska*.

Auken, E., Boesen, T., & Christiansen, A. V. (2017). A Review of Airborne Electromagnetic Methods With Focus on Geotechnical and Hydrological Applications From 2007 to 2017. In *Advances in Geophysics* (Vol. 58, pp. 47–93). https://doi.org/10.1016/bs.agph.2017.10.002

Balleau, W. P. (1988). Water appropriation and transfer in a general hydrogeologic system. *Natural Resources Journal*, *28*(2), 269–291.

Barfod, A. A. S., Vilhelmsen, T., Jorgensen, F., Christiansen, A., Hoyer, A.-S., Straubhaar, J., & Moller, I. (2018). Contributions to uncertainty related to hydrostratigraphic modeling using multiple-point statistics. *Hydrology and Earth System Sciences*, *22*, 5485–5508.

Benn, D., & Evans, D. J. (2014). *Glaciers and Glaciation*. New York, NY, Routlege.

Bettis, E. A. I. (1990). *Holocene Alluvial Stratigraphy and Selected Aspects of the Quaternary History of Western Iowa*.

Brunner, P., Hendricks Franssen, H. J., Kgotlhang, L., Bauer-Gottwein, P., & Kinzelbach, W. (2007). How can remote sensing contribute in groundwater modeling? *Hydrogeology Journal*, *15*(1), 5–18. https://doi.org/10.1007/s10040-006-0127-z

Butler, J. J., Stotler, R. L., Whittemore, D. O., & Reboulet, E. C. (2013). Interpretation of Water Level Changes in the High Plains Aquifer in Western Kansas. *GroundWater*, *51*(2), 180–190. https://doi.org/10.1111/j.1745-6584.2012.00988.x

Carney, C. P., Abraham, J. D., Cannia, J. C., & Steele, G. V. (2015). *Final Report on Airborne Electromagnetic Geophysical Surveys and Hydrogeologic Framework Development for the Eastern Nebraska Water Resources Assessment-Volume I, Including the Lewis and Clark, Lower Elkhorn, and Papio-Missouri River Natural Resources Dis*.

Christensen, N.K., Minsley, B. J., & Christensen, S. (2017). Generation of 3-D hydrostratigraphic zones from dense airborne electromagnetic data to assess groundwater model prediction error. *AGU Publications*, 1019–1038. https://doi.org/10.1111/j.1752-1688.1969.tb04897.x

Christensen, Nikolaj Kruse, Ferre, T. P. A., Fiandaca, G., & Christensen, S. (2017). Voxel inversion of airborne electromagnetic data for improved groundwater model construction and prediction accuracy. *Hydrology and Earth System Sciences*, *21*(2), 1321–1337. https://doi.org/10.5194/hess-21-1321-2017

Cresswell, R.G., Cresswell, R. G., Dent, D. L., Jones, G. L., & Galloway, D. S. (2004). Three-dimensional mapping of salt stores in the southeast Murray–Darling Basin, Australia. 1. Steps in calibration of airborne electromagnetic surveys. *Soil Use and Management*, *20*(2), 133–143. https://doi.org/10.1079/sum2004260

Cresswell, Richard G., Mullen, I. C., Kingham, R., Kellett, J., Dent, D. L., & Jones, G. L. (2007). Airborne electromagnetics supporting salinity and natural resource management decisions at the field scale in Australia. *International Journal of Applied Earth Observation and Geoinformation*, *9*(2), 91–102. https://doi.org/10.1016/j.jag.2006.05.005

Dawson, K. J., & Istok, J. D. (2002). *Aquifer Testing: Design and Analysis of Pumping and Slug Tests*. Lewis Publishers.

de Marsily, G., Delay, F., Gonçalvès, J., Renard, P., Teles, V., & Violette, S. (2005). Dealing with spatial heterogeneity. *Hydrogeology Journal*, *13*(1), 161–183. https://doi.org/10.1007/s10040-004-0432-3

Dent, D. (2007). Environmental geophysics mapping salinity and water resources. *International Journal of Applied Earth Observation and Geoinformation*, *9*(2), 130–136. https://doi.org/10.1016/j.jag.2006.09.005

Divine, D. P., & Korus, J. T. (2012). , *Three-dimensional hydrostratigraphy of the Sprague, Nebraska area: Results from Helicopter Electromagnetic (HEM) mapping in the Eastern Nebraska Water Resources Assessment (ENWRA), Geological Survey Bulletin: Lincoln, NE, Conservation and Survey Divisio* (p. 32). p. 32.

Divine, D., & Sibray, S. S. (2017). *An Overview of Secondary Aquifers in Nebraska*.

Domenico, P. A., & Schwartz, F. W. (1998). *Physical and Chemical Hydrogeology* (Second). John Wiley & Sons, Inc.

Dreeszen, V., & Burchett, R. (1971). *Buried valleys in the lower part of the Missouri River Basin* (pp. 21–25). pp. 21–25. : Kansas Geological Survey Special Distribution.

Driscoll, F. G. (1986). *Groundwater and Wells* (Second). St. Paul, Minnesota: Johnson Division.

Eyles, C. H., & Eyles, N. (2010). *Glacial Deposits, in James, N.P., and Dalrymple, R.W., eds., Facies Models 4, Geological Association of Canada*.

Famiglietti, J. S. (2014). The global groundwater crisis. *Nature Climate Change*, *4*(11), 945–948. https://doi.org/10.1038/nclimate2425

Fienen, M. N., & Arshad, M. (2016). The International Scale of the Groundwater Issue. In *Integrated Groundwater Management: Concepts, Approaches and Challenges* (pp. 21–48). https://doi.org/10.1007/978-3-319-23576-9_26

Foged, N., Marker, P.A., Christiansen, A.V., Bauer-Gottwein, P., Jørgensen, F., Høyer, A.S., And Auken, E., 2014, Large-scale 3-D modeling by integration of resistivity models and borehole data through inversion: Hydrology and Earth System Sciences, v. 18, p. 4349-4362.

Foster, S. S. D., & Chilton, P. J. (2003). Groundwater: The processes and global significance of aquifer degradation. *Philosophical Transactions of the Royal Society B: Biological Sciences*, *358*(1440), 1957–1972. https://doi.org/10.1098/rstb.2003.1380

Foster, T., Brozović, N., & Butler, A. P. (2015). Analysis of the impacts of well yield and groundwater depth on irrigated agriculture. *Journal of Hydrology*, *523*, 86–96. https://doi.org/10.1016/j.jhydrol.2015.01.032

Gondwe, B. R. N., Ottowitz, D., Supper, R., Motschka, K., Merediz-alonso, G., & Bauer-gottwein, P. (2012). Regional-scale airborne electromagnetic surveying of the Yucatan karst aquifer (Mexico): geological and hydrogeological interpretation. *Hydrogeology Journal*, 1407–1425. https://doi.org/10.1007/s10040-012-0877-8

Gosselin, D., Harvey, E., & Frost, C. (2001). Geochemical Evolution of Ground Water in the Great Plains (Dakota) Aquifer of Nebraska: Implications for the Management of a Regional Aquifer System. *Groundwater*, *39*.

Hall, S. H. (1993). Single Well Tracer Tests in Aquifer Characterization. *Groundwater Monitoring & Remediation*, *13*(2), 118–124. https://doi.org/10.1111/j.1745-6592.1993.tb00443.x

Hanson, P. R., Korus, J. T., & Divine, D. P. (2012). Three-dimensional hydrostratigraphy of the Platte River Valley near Ashland, Nebraska: Results from Helicopter Electromagnetic (HEM) mapping in the Eastern Nebraska Water Resources Assessment (ENWRA). In *Conservation Bulletin no.2 (New Series)* (Vol. 2). Retrieved from http://www.enwra.org/media/Ashland_ENWRA_Bull_2_2012_small.pdf

He, X. L., Koch, J., Sonnenborg, T. O., Jørgensen, F., Schamper, C., & Refsgaard, J. C. (2014). The emergence of hydrogeophysics for improved understanding of subsurface processes over multiple scales. *Water Resources Research*, 3147–3169. https://doi.org/10.1002/2013WR014593.Received

Heim, G., & Howe, W. (1963). *Pleistocene Drainage and Depositional History in Northwestern Missouri*. *66*(3), 378–392.

Høyer, A. S., Jørgensen, F., Sandersen, P. B. E., Viezzoli, A., & Møller, I. (2015). 3D geological modelling of a complex buried-valley network delineated from borehole and AEM data. *Journal of Applied Geophysics*, *122*, 94–102. https://doi.org/10.1016/j.jappgeo.2015.09.004

Isaaks, E. H., & Srivastava, R. . (1989). *An Introduction to Applied Geostatistics*. New York: Oxford University Press.

Jørgensen, F., Høyer, A. S., Sandersen, P. B. E., He, X., & Foged, N. (2015). Combining 3D geological modelling techniques to address variations in geology, data type and density - An example from Southern Denmark. *Computers and Geosciences*, *81*, 53–63. https://doi.org/10.1016/j.cageo.2015.04.010

Jørgensen, F., Møller, R. R., Nebel, L., Jensen, N. P., Christiansen, A. V., & Sandersen, P. B. E. (2013). A method for cognitive 3D geological voxel modelling of AEM data. *Bulletin of Engineering Geology and the Environment*, *72*(3–4), 421–432. https://doi.org/10.1007/s10064-013-0487-2

Kaufman, A., Cohen, D., & Yagel, R. (1993). Volume Graphics. *Computer*, *26*(7), 51–64. https://doi.org/10.1109/MC.1993.274942

Knight, R., Smith, R., Asch, T., Abraham, J., Cannia, J., Viezzoli, A., & Fogg, G. (2018). Mapping Aquifer Systems with Airborne Electromagnetics in the Central Valley of California. *Groundwater*, *56*(6), 893–908. https://doi.org/10.1111/gwat.12656

Koltermann, C. E., & Gorelick, S. M. (1996). Heterogeneity in sedimentary deposits: A review of structure-imitating, process-imitating, and descriptive approaches. *Water Resources Research*, Vol. 32, pp. 2617–2658. https://doi.org/10.1029/96WR00025

Korus, J. (2018). Combining hydraulic head analysis with airborne electromagnetics to detect and map impermeable aquifer boundaries. *Water (Switzerland)*, *10*(8). https://doi.org/10.3390/w10080975

Korus, J.T., Joeckel, R. M., & Divine, D. P. (2013). , *Three-dimensional hydrostratigraphy of the Firth, Nebraska area: Results from Helicopter Electromagnetic (HEM) mapping in the Eastern Nebraska Water Resources Assessment (ENWRA), in Larson, D.R., ed., Geological Survey Bulletin: Lincoln, NE, Conservatio*. 100.

Korus, Jesse T., Howard, L. M., Young, A. R., Divine, D. P., Burbach, M. E., Jess, J. M., & Hallum, D. R. (2013). *The Groundwater Atlas of Nebraska* (Third (rev).

Korus, Jesse T., Joeckel, R. M., Divine, D. P., & Abraham, J. D. (2016). Three-dimensional architecture and hydrostratigraphy of cross-cutting buried valleys using airborne electromagnetics, glaciated Central Lowlands, Nebraska, USA. *Sedimentology*, *64*(2), 553–581. https://doi.org/10.1111/sed.12314

Kruse Christensen, N., Christensen, S., & Ferre, T. P. A. (2016). Testing alternative uses of electromagnetic data to reduce the prediction error of groundwater models. *Hydrology and Earth System Sciences*, *20*(5), 1925–1946. https://doi.org/10.5194/hess-20-1925-2016

LPNNRD. (n.d.). Water Quantity-Lower Platte North Natural Resources District. Retrieved August 10, 2019, from https://lpnnrd.org/projects-and-programs/water-management/water-quantity/

Macfarlane, P. A. (1998). Is Sustainability a Viable Concept in the Management of Confined Aquifers in Kansas? In *BULLETIN-kANSAS GEOLOGICAL SURVEY* (pp. 97–116).

Marker, P. A., Vilhelmsen, T. N., Foged, N., Wernberg, T., Auken, E., & Bauer-Gottwein, P. (2017). Probabilistic predictions using a groundwater model informed with airborne EM data. *Advances in Water Resources*, *103*, 86–98. https://doi.org/10.1016/j.advwatres.2017.03.002

Matheron, G. (1963). Principles of Geostatistics. *Economic Geology*, *58*, 1246–1266.

McGuire, V. (2019). High Plains aquifer water-level changes, predevelopment to 2015. Retrieved from USGS website: https://www.usgs.gov/media/images/high-plains-aquifer-water-level-changes-predevelopment-2015

Moon, S. K., Woo, N. C., & Lee, K. S. (2004). Statistical analysis of hydrographs and water-table fluctuation to estimate groundwater recharge. *Journal of Hydrology*, *292*(1–4), 198–209. https://doi.org/10.1016/j.jhydrol.2003.12.030

Morgan, S. E., Allen, D. M., Kirste, D., & Salas, C. J. (2019). Investigating the hydraulic role of a large buried valley network on regional groundwater flow. *Hydrogeology Journal*, 2377–2397. https://doi.org/10.1007/s10040-019-01995-0

Neuman, S. P. (1975a). Analysis of pumping test data from anisotropic unconfined aquifers considering delayed gravity response. *Water Resources Research*, *11*(2), 329–342. https://doi.org/10.1029/WR011i002p00329

Neuman, S. P. (1975b). Analysis of pumping test data from anisotropic unconfined aquifers considering delayed gravity response. *Water Resources Research*, *11*(2), 329–342. https://doi.org/10.1029/WR011i002p00329

Obuobie, E., Diekkrueger, B., Agyekum, W., & Agodzo, S. (2012). Groundwater level monitoring and recharge estimation in the White Volta River basin of Ghana. *Journal of African Earth Sciences*, *71–72*, 80–86. https://doi.org/10.1016/j.jafrearsci.2012.06.005

Oldenborger, G. A., Pugin, A. J.-M., & Pullan, S. E. (2013). Airborne time-domain electromagnetics, electrical resistivity and seismic reflection for regional three-dimensional mapping and characterization of the Spiritwood Valley Aquifer, Manitoba, Canada. *Near Surface Geophysics*, *11*, 63–74.

Paillet, F. L., & Reese, R. S. (2000). Integrating Borehole Logs and Aquifer Tests in Aquifer Characterization. *Groundwater*, *38*(5), 713–725.

Palacky, G. (1988). Resistivity Characteristics of Geologic Targets. In *Electromagnetic methods in applied geophysics: Theory* (pp. 53–129). Tulsa, Oklahoma: Society of Exploration Geophysics.

Palamara, D. R., Rodriguez, V. B., Kellett, J., & Macaulay, S. (2010). Salt mapping in the Lower Macquarie area, Australia, using airborne electromagnetic data. *Environmental Earth Sciences*, *61*(3), 613–623. https://doi.org/10.1007/s12665-009-0375-z

Paul, R., Raper, P., Simons, J. A., Stainer, G., George, R. J., & Paul, G. (2011). *Weaber Plain aquifer test results*. Retrieved from http://researchlibrary.agric.wa.gov.au/rmtr

Ritter, D. F., Kochel, R. C., & Miller, J. R. (2011). *Process Geomorphology* (Fifth). Long Grove, Illinois: Wavelend Press, Inc.

Robinson, D., Binley, A., Crook, N., Day-Lewis, F., Ferre, T., Grauch, V., … Slater, L. (2008). Advancing process-based watershed hydrological research using near-surface geophysics: a vision for, and a review of, electrical and magnetic geophysical methods. *Hydrological Processes*, *22*(March), 3604–3635. https://doi.org/10.1002/hyp

Roy, M., Clark, P. U., Barendregt, R. W., Glasmann, J. R., & Enkin, R. J. (2004). Glacial stratigraphy and paleomagnetism of late Cenozoic deposits of the north-central United States. *Bulletin of the Geological Society of America*, *116*(1–2), 30–41. https://doi.org/10.1130/B25325.1

Royse, K. R. (2010). Combining numerical and cognitive 3D modelling approaches in order to determine the structure of the Chalk in the London Basin. *Computers and Geosciences*, *36*(4), 500–511. https://doi.org/10.1016/j.cageo.2009.10.001

Sanders, L. L. (1998). *A Manual of Field Hydrogeology* (R. A. McConnin & K. Schiaparelli, Eds.). Upper Saddle River, NJ: Prentice-Hall, Inc.

Sapia, V., Oldenborger, G. A., Jørgensen, F., Pugin, A. J.-M., Marchetti, M., & Viezzoli, A. (2015). 3D modeling of buried valley geology using airborne electromagnetic data. *Interpretation*, *3*(4), SAC9–SAC22. https://doi.org/10.1190/int-2015-0083.1

Scanlon, B. R., Faunt, C. C., Longuevergne, L., Reedy, R. C., Alley, W. M., McGuire, V. L., & McMahon, P. B. (2012). Groundwater depletion and sustainability of irrigation in the US High Plains and Central Valley. *Proceedings of the National Academy of Sciences*, *109*(24), 9320–9325. https://doi.org/10.1073/pnas.1200311109

Scanlon, Bridget R., Jolly, I., Sophocleous, M., & Zhang, L. (2007). Global impacts of conversions from natural to agricultural ecosystems on water resources: Quantity versus quality. *Water Resources Research*, *43*(3). https://doi.org/10.1029/2006WR005486

Scharling, P. B., Rasmussen, E. S., Sonnenborg, T. O., Engesgaard, P., & Hinsby, K. (2009). Three-dimensional regional-scale hydrostratigraphic modeling based on sequence stratigraphic methods: A case study of the Miocene succession in Denmark. *Hydrogeology Journal*, *17*(8), 1913–1933. https://doi.org/10.1007/s10040-009-0475-6

Sharpe, D., Pugin, A., Pullan, S., & Gorrell, G. (2003). Application of seismic stratigraphy and sedimentology to regional hydrogeological investigations: an example from Oak Ridges Moraine, southern Onterio, Canada. *Canadian Geotechnical Journal*, *40*(4), 711–730.

Siebert, S., Burke, J., Faures, J. M., Frenken, K., Hoogeveen, J., Döll, P., & Portmann, F. T. (2010). Groundwater use for irrigation - A global inventory. *Hydrology and Earth System Sciences*, *14*(10), 1863–1880. https://doi.org/10.5194/hess-14-1863-2010

Soller, D. R. (1997). *Map showing the thickness and character of quaternary sediments in the glaciated United States east of the Rocky Mountains--Northern and Central Plains states*. U.S. Geological Survey.

Sørense, K. I., & Auken, E. (2004). SkyTEM ? a new high-resolution helicopter transient electromagnetic system. *Exploration Geophysics*, *35*(3), 194–202. https://doi.org/10.1071/EG04194

Srinivasan, V., Lambin, E. F., Gorelick, S. M., Thompson, B. H., & Rozelle, S. (2012). The nature and causes of the global water crisis: Syndromes from a meta-analysis of coupled human-water studies. *Water Resources Research*, *48*(10), 1–16. https://doi.org/10.1029/2011WR011087

Steward, D. R., Bruss, P. J., Yang, X., Staggenborg, S. A., Welch, S. M., & Apley, M. D. (2013). Tapping unsustainable groundwater stores for agricultural production in the High Plains Aquifer of Kansas, projections to 2110. *Proceedings of the National Academy of Sciences*, *110*(37), E3477–E3486. https://doi.org/10.1073/pnas.1220351110

Summerside, S., Olafsen-Lackey, S., Goeke, J., & Myers, W. (2005). *Mapping of aquifer properties-transmissivity and specific yield-for selected river basins in central and eastern Nebraska*.

Supper, R., Motschka, K., Ahi, A., Bauer-Gottwein, P., Gondwe, B., Alonso, G. M., … Kinzelbach, W. (2009). Spatial mapping of submerged cave systems by means of airborne electromagnetics: An emerging technology to support protection of endangered karst aquifers. *Near Surface Geophysics*, *7*(5–6), 613–627. https://doi.org/10.3997/1873-0604.2009008

Theis, C. V. (1935). THE RELATION BETWEEN THE LOWERING OF THE PIEZOMETRIC SURFACE AND THE RATE AND DURATION OF DISCHARGE OF A WELL USING GROUND-WATER STORAGE. In *REPORTS AND PAPERS.*

Vereecken, H., Kemna, A., Munch, H., Tillmann, A., & Verweerd, A. (2005). Aquifer Characterization by Geophysical. *Groundwater*, 2265–2283.

Viezzoli, A., Christiansen, A. V., Auken, E., & Sørensen, K. (2008). *Constrained Inversion*. *73*(3).

Vilhelmsen, T., Marker, P., Foged, N., Wernberg, T., Auken, E., Christiansen, A. V., … Hoyer, A.-S. J. W. R. M. (2019). A Regional Scale Hydrostratigraphy Generated from Geophysical Data of Varying Age, Type, and Quality. *Water Resources Management*, *33*, 539–553.